AMERICAN UNIVERSITY OF BEIRUT

# MATERIALS ENGINEERING OF ZR-METAL-ORGANIC FRAMEWORK CATALYSTS FOR THE OPTIMIZED PRODUCTION OF BIOFUEL ADDITIVES

by
ASMAA BILAL JRAD

A dissertation
submitted in partial fulfillment of the requirements
for the degree of Doctor of Philosophy
to the Department of Mechanical Engineering
of the Maroun Semaan Faculty of Engineering and Architecture
at the American University of Beirut

Beirut, Lebanon
January 2021

AMERICAN UNIVERSITY OF BEIRUT

# MATERIALS ENGINEERING OF ZR-METAL-ORGANIC FRAMEWORK CATALYSTS FOR THE OPTIMIZED PRODUCTION OF BIOFUEL ADDITIVES

by

ASMAA BILAL JRAD

Approved by:

Prof. Mohammad Ahmad, Ph.D., Professor — Advisor
Department of Chemical Engineering & Advanced Energy, AUB

Prof. Mohamad Hmadeh, Ph.D., Associate Professor — Co-Advisor
Department of Chemistry, AUB

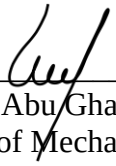

Prof. Kamel Abu Ghali, Ph.D., Professor — Member of Committee
Department of Mechanical Engineering, AUB

Prof. Cassia Boyadjian, Ph.D., Assistant Professor — Member of Committee
Department of Chemical Engineering & Advanced Energy, AUB

Prof. Michael Zaworotko, Ph.D., Professor — Member of Committee
Bernal Institute, Crystal Engineering, University of Limerick

Prof. Ioannis Economou, Ph.D., Professor — Member of Committee
Department of Chemical Engineering, Texas A&M University, Qatar

Date of thesis defense: January 25, 2021

# AMERICAN UNIVERSITY OF BEIRUT

# DISSERTATION RELEASE FORM

Student Name: ____ Jrad_____Asmaa_____ Bilal_____
Last First Middle

I authorize the American University of Beirut, to: (a) reproduce hard or electronic copies of my dissertation; (b) include such copies in the archives and digital repositories of the University; and (c) make freely available such copies to third parties for research or educational purposes:

☑ As of the date of submission

☐ One year from the date of submission of my dissertation.

☐ Two years from the date of submission of my dissertation.

☐ Three years from the date of submission of my dissertation.

07-02-2021

_____

Signature Date

(This form is signed & dated when submitting the dissertation to the University Libraries ScholarWorks)

# ACKNOWLEDGMENTS

First, I would like to express my gratitude to my advisor Prof. Mohammad N. Ahmad, and co-adviser Prof. Mohamad Hmadeh for their guidance and support throughout my Ph.D. program. I was lucky to have the chance to benefit from their research experience and critical thinking. Additionally, I would like to thank the dissertation committee members: Prof. Michael Zaworotko, Prof. Ioannis Economou, Prof. Kamel Ghali, Dr. Cassia Boyadjian, for their valuable revisions and suggestions. My gratitude extends to the faculty members and staff of the Mechanical Engineering, Chemical Engineering, and Chemistry Departments, as well as the managers and engineers at Kamal Shair CSRL lab at the American University of Beirut for their help in the achievement of this work. Furthermore, I would also like to thank my colleagues Eng. Ghadir Awada and Eng. Ranim Chakleh for their support and contribution to this work.

I am also very thankful to my dear colleagues and friends at the American University of Beirut, who supported and motivated me to achieve my goals: Douaa Al Assaad, Jinane Charara, Rasha El Moussawi, Manar Younis, Dr. Nicolas Aramouni, Hady Hashem, Dr. Hussein Sammoury, Ahmad Harb, Hussein Kassem, Haytham Dbouk, Rasha Seblany, Farah Mneimneh, Safaa Khalil, Elvire Katramize, Hussein Daoud, Walid Abou Hweij, Ghewa El Sabeh, Mahmoud El Cheikh, Rawan El Natour, Zainab Nizam, Zahraa Yaghi, and Patrick Damacet.

I am forever grateful to my family; my parents: Bilal & Fida, my sisters: Rayan & Aisha, and my brother: Saeed. Your presence has always been a source of joy and inspiration in my life. Words cannot express how appreciative I am for your love and care. Mom and Dad, you taught me my very first words and loved me through every hardship until this day, thank you for always being by my side, and thank you for all the sacrifices that you have made for my siblings and me.

Most importantly, my deepest gratitude is dedicated to the source of existence, love, and all good, the dearest to my heart and closest to me of all, my support and shelter with every breath I take. To you, I will never be thankful enough.

# ABSTRACT
# OF THE DISSERTATION OF

Asmaa Bilal Jrad for Doctor of Philosophy
Major: Mechanical Engineering

Title: Materials engineering of Zr-metal-organic frameworks catalysts for the optimized production of biofuel additives

The development of novel fuel additives from sustainable biomass feedstock is one of the common paths in the global transportation sector to mitigate the environmental drawbacks of the excessive dependence on fossil fuels. In order to boost the competitiveness of these green fuel additives, the use of an efficient catalyst becomes critical to obtain a satisfactory overall conversion to the product of interest in a short time. Metal-Organic frameworks (MOFs) have recently emerged as an important candidate to become the next generation of catalysts for biofuel production. The reason behind this interest in MOF catalysts originates from different features such as their permanent porosities, very high surface areas, and, most importantly, the flexibility by which their characteristics could be altered for a specific application. MOFs have thus opened a vast door to materials engineering in the catalysis field. In our study, we focus on the optimization of Zr-based MOFs' characteristics by selectively engrafting active functional groups onto their organic linkers, by the intentional introduction of structural defects on their metal cluster, and by using a mixed-linker approach. The obtained samples are fully characterized and subsequently serve as acid catalysts in the esterification reaction of butyric acid in the presence of butanol for the efficient production of butyl butyrate, a novel green biofuel. We investigate the effect of the different characteristics of the MOFs catalysts such as their surface area, particle size, linker deficiency, acidity, and porosity on the mechanism and conversion in the catalytic reaction. Based on all the data obtained, a linear regression model is developed to determine the relative significance of each characteristic of the MOF structure in dictating its catalytic activity and to predict the final yield to butyl butyrate based on these characteristics. With the knowledge obtained, the catalytic activity of MOFs can be engineered from a laboratory prototype and optimized to serve as effective catalysts for the production of fine chemicals such as biofuels.

TABLE OF CONTENTS

# ILLUSTRATIONS

Figure

# TABLES

Table

# CHAPTER I

# INTRODUCTION

The global demand for energy is ever-expanding, and the limitations of conventional fossil fuels in terms of being non-renewable and environmentally harmful pushes the energy mix towards renewables [4]. The technical advancement and environmental concerns are the drivers of the shift towards a more sustainable and renewable energy system that meets the growing demand while reducing carbon emissions [5].

Liquid biofuels gained a lot of interest in the research field of renewables as they constitute a promising alternative for fossil fuels [1]. However, the challenge remains in boosting the competitiveness of biofuels by maximizing their production and lowering their cost [6].

Ethanol and butanol are some of the known biofuels, but another chemical compound recently gained interest in the field of biofuels and bio-additives for conventional fuels and it is butyl butyrate [7, 8]. Butyl butyrate is an ester that can be obtained by the esterification reaction of butyric acid and butanol, both of which can be obtained from biomass through fermentation processes. One of the reasons behind this interest in butyl butyrate is the fact that it's a flammable ester with an octane number similar to that of butanol [8, 9]. In addition, butyl butyrate has a cetane index similar to that of diesel, and a flash point lower than that of butanol which makes it safer to use. All these properties and many others put butyl butyrate under the classification of emerging biofuels [8, 9].

In esterification reactions, as in most chemical reactions, catalysts come at the heart of the production process. Catalysts facilitate the efficient making and breaking of chemical bonds which is the base for the production of new chemical compounds [10]. Catalysts needed for esterification reactions, in general, are of acidic nature, which is necessary for the efficient production of the desired ester [11].

Liquid homogeneous catalysts were commonly used in biofuel production such as sulfuric acid and hydrofluoric acid [2, 12]. However, many technical problems were encountered when these catalysts were used because of their corrosive nature [13]. In addition, the recovery of the catalyst and its separation from the reaction medium is hard as the catalyst is in one phase with the reaction mixture [14]. Moreover, the recovery of the catalyst requires the washing of the mixture with water which causes the loss of some of the biofuel and generates a lot of wastewater [15]. Thus, homogeneous catalysts are not easy to reuse or recycle which increases the biofuels production cost as a consequence of the increase in the catalyst amount purchased and consumed. For all the previously mentioned reasons, homogeneous acid catalysts are considered non-environmentally friendly and economically inefficient, and a lot of effort had been put to replace these with new green catalysts for the production of biofuels [16].

Recently, heterogeneous catalysts have been extensively used in industries because of their ability to be recycled without losses in the reaction yield [16]. Many types of these heterogeneous catalysts, such as zeolites, metal oxides, resins, and heterogeneous acid catalysts have been used for organic reactions [17, 18]. However, their use had one or more disadvantages regarding selectivity, safety, cost, and catalyst disposal [19].

A new class of porous materials that are being investigated in the catalysis field consists of the novel metal-organic frameworks (MOFs) [20]. MOFs are novel inorganic-organic materials that are mainly attractive because of their crystalline nature, very large surface area, and the significant variety of active groups that could be incorporated in their structure [21-24]. MOFs were originally used for several applications like gas storage, gas purification, drug delivery, and biomedicine [25]. Recently, MOFs have been gaining a lot of interest as a heterogeneous catalyst since their organic linker, their inorganic metal clusters, as well as their porous network, could be tuned to contribute to their catalytic activity [20]. MOFs make an interesting alternative to conventional catalysts since they showed a potential to bridge the gap between homogeneous and heterogeneous catalysis [26, 27]. In fact, although MOFs are heterogeneous solid catalysts, having a very high surface area and the ability to include a high density of active sites in their structure allows them to perform relatively similar to homogeneous catalysts in liquid reactions compared to other solid catalysts [26, 27].

In the specific case of esterification reactions, acidic active sites are required in the MOF structure. In fact, MOFs should provide functional groups which are, Brønsted or Lewis acids, in order for the esterification reaction to occur efficiently [11]. The acidic properties of the MOF were investigated given the great interest in developing heterogeneous acid catalysts and the relative ease of inducing acidity in the MOFs structures [28]. In most cases, the MOFs acid strength was evaluated by using them in reactions that required acidic sites and by assessing their relative catalytic activity in such reactions [29, 30]. However, the cases where MOFs were used for esterification reactions or were developed for the specific target of biofuel production, remain rare [29, 30].

While the industry of biofuel production is in great need to find green, recyclable, and efficient catalysts to boost the competitiveness of clean energy, the essential aim of this Ph.D. project is to design the structure of Zr-based MOFs for optimized production of butyl butyrate. The engineering of the MOFs' structure will be achieved using different techniques to fine-tune the characteristics and catalytic sites of the MOFs synthesized in order to maximize the production of the studied biofuel additive. The catalytic activity of the MOF to be developed will be boosted to perform better than conventional counterparts and, ultimately, to approach the performance of the homogeneous liquid catalyst where possible. One of the main outcomes of the research is to provide the catalysis field with deep knowledge on the effect of MOFs' characteristics on their catalytic activity and, consequently, the conversion to butyl butyrate. On the other hand, it is essential to understand the means by which these characteristics could be tuned through the synthesis procedure to obtain the required catalytic properties of the MOFs. For this reason, the effect of the different characteristics of the tested catalysts, such as specific surface area, pore size, active sites, functional groups, and metal nodes, on the reported performance of each catalyst will also be explored to obtain a deeper understanding of those materials emerging as new catalysts.

After the introduction, which is the 1$^{st}$ chapter in this dissertation, the upcoming sections are organized as follows:

- Chapter 2 provides research background and related work to the topics covered in this study, mainly, the definitions and characteristics of energy security, biofuels, homogeneous and heterogeneous catalysis, metal-organic frameworks, and esterification reactions. At the end of the chapter, the three main materials engineering

strategies adopted in this study are explained, namely linker functionalization, defects engineering, and multivariate (MTV) MOFs approach. The chapter is concluded by stating the objectives of this work.

- Chapter 3 presents and explains the research methodologies developed which are based on the three main materials engineering strategies employed in this Ph.D. work, namely, linker functionalization, defect engineering, and multivariate (MTV) or mixed-linker MOFs.

- Chapter 4 presents the results and discussion based on each MOFs' engineering strategy.

- Chapter 5 consists of a general conclusion of the work and suggested ideas to move forward with this research.

# CHAPTER II

# BACKGROUND

## A. GLOBAL SHIFT TO RENEWABLE ENERGY

### *1. World Energy Status*

The sustainable development and well-being of modern societies are tightly linked to access to energy [31]. From trivial activities like the daily ride to work to operating leading industries in the world, access to energy is vital [32]. The natural consequence of the previous is an increase in energy demand with the increase in the world population and the growth of human activity. Since the industrial revolution, the prosperity of the world had been accompanied by an increase in the demand for energy. Subsequently, energy demand is expected to grow by 30% between today and 2040 [33]. This has shed light on the importance of concepts such as energy security, which could be defined as the easy access to sustainable and affordable energy resources that meet the energy demand without causing detrimental effects on the global society [4]. Different energy sources have been used to meet this trend in energy demand, but the famous fossil fuels continue to have, by far, the largest share of the global energy mix [5]. Nowadays fossil fuels make up approximately 81% of the global energy mix, of which more than a quarter is consumed by the transport sector [34]. Looking from an energy security perspective, fossil fuels are still the most affordable energy source, but two important factors, which are sustainability and harmlessness, remain unfulfilled [35]. To begin with, fossil fuel sources are limited and their reservoirs will be depleted [36], this means that the global societies cannot rely persistently on fossil fuel reservoirs as these cannot be reproduced once depleted, which thus makes them non-sustainable.

On the other hand, the definition of energy security suggests that the use of energy sources should not harmful to human societies, but this is not the case for fossil fuels. Based on the Intergovernmental Panel on Climate Change (IPCC) 2014 report, fossil fuels and industrial processes have contributed to 78% of the total GHG emission since 1970 [37]. Some of the devastating effects that GHG contribute to include climate change, glaciers recession, rise in sea level, and loss of biodiversity [38].

Hence, the need to meet the growth in energy demand while reducing the dependency on fossil fuels for the above-mentioned reasons has diverted sights towards alternatives that must be renewable, sustainable, non-polluting, and cost-effective such as renewable energy sources [6, 39]. In this context, it was expected that renewables will account for more than 30% of the energy supply for power generation in 2040 as shown in **Figure 1** [1]. Renewable alternatives include biofuels, biomass, solar, wind, and geothermal energy, and their use is becoming more popular as significant global efforts are being invested to handle the environmental and sustainable constraints [40]. Moreover, biofuels and fuel bio-additives are considered an interesting substitute to petroleum-based transportation fuels, as they have shown conventional fuel properties in car engines alongside their sustainability, biodegradability, and low carbon-emission [41].

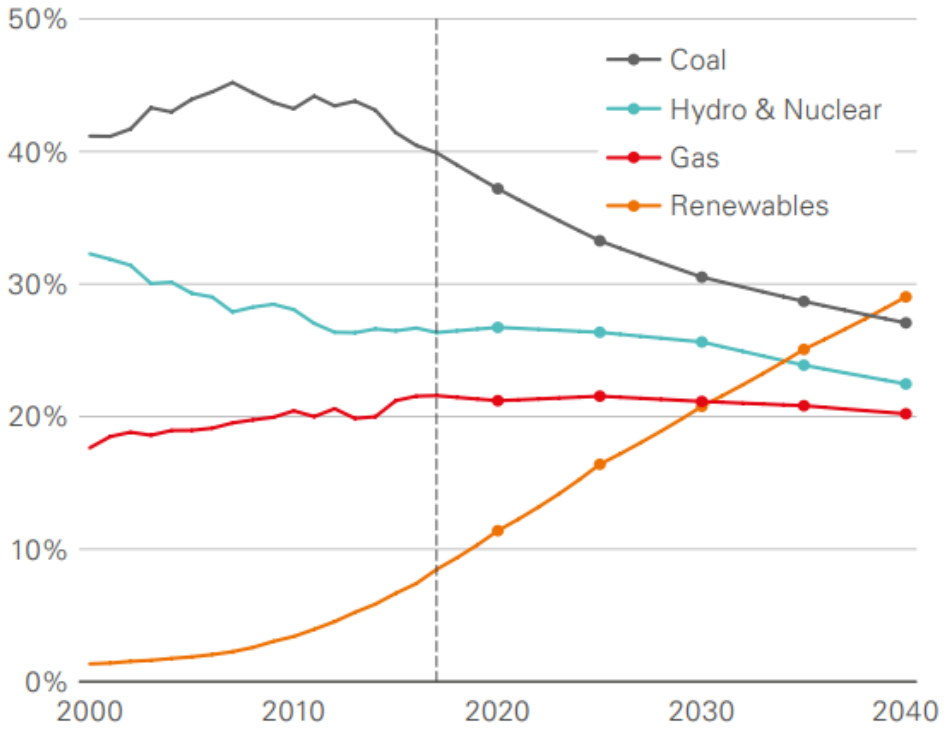


**Figure 1:** Fuel shares in power generation with projection till 2040 [1]

a. Liquid biofuel

By definition, bioenergy is a type of energy that is based on organic matter or what is known as biomass, this includes all materials that are biologically originated and that are not fossilized [42]. Bioenergy could be used in its original form, i.e. wood, as a fuel, or it could be refined to form solid, liquid, or gaseous fuels that could be used in modern systems such as power plants for electricity production, transportation engines, and in industrial processes [42].

Liquid biofuels, a bioenergy type, gained a lot of interest in the research field of renewables as they constitute a promising alternative for liquid fossil fuels. However, the challenge remains in boosting the competitiveness of biofuels by maximizing their production and lowering their cost.

The reason behind the interest in biofuels is based on the fact that biomass needs to take in carbon from the atmosphere to grow and emits it into the air when used for energy production. It is thus considered a carbon-neutral energy resource. Moreover, biomass could be grown over and over again which makes biofuels a sustainable energy source.

Fulfilling energy security as well as environmental protection are thus the main causes of bioenergy and biofuel sectors' growth in the last years. Based on a report from the International Renewable Energy Agency (IRENA), it is expected that 22% of transportation fuels will originate from biofuels and biogas in 2050 [43].

i. Bioethanol and biodiesel: Pros and Cons

Liquid biofuels could be used in their pure form or as additives to existing petroleum fuels as they have been shown to have similar properties to conventional fuels. These properties include heating value, octane number, viscosity, water content, and flash point [41]. Among these biofuels, ethanol, and biodiesel are the most commonly used [7].

Ethanol, resulting mainly from the fermentation of food crops, can be used as a substitution of gasoline to fuel a spark-ignition engine in its pure form (E100) or blended with gasoline [44]. Its use as an alternative source for conventional gasoline is preferable due to its high-octane number, hence it can be employed as an octane number booster. Ethanol also has a higher flash point and a lower heating value than existing gasoline [44]. In addition, ethanol is less toxic than gasoline and it is not carcinogenic [45]. Another common biofuel type is biodiesel which is characterized by low sulfur and aromatic content, and high biodegradability when compared to petroleum-based

diesel [41]. Studies showed that biodiesel engine performance is comparable to that of fossil diesel indicating that it can be used in its pure form as an engine fuel or as an additive with another fuel [46]. However, a number of key issues restrict the usage of these biofuels in the transport sector. One of these limitations is the large land area required to grow the feedstock needed for bioethanol and biodiesel production [8, 9], which may impact biodiversity. In addition, bioethanol suffers from poor energy density, and biodiesel shows an oxidative instability and an inefficient performance at low temperature [9]. In an attempt to overcome these issues, a new generation of renewable fuels is now being explored.

ii. Butyl Butyrate: A competent Biofuel

The focus of the research is now directed towards exploring new fossil fuel alternatives that could be derived from cellulosic sources or that could be collected from waste food, which are more abundant than food crops necessary for bioethanol production. For instance, butyl butyrate (BB) has been explored for this reason.

Butyl butyrate is an ester with a pear-pineapple like aroma. This colorless liquid has been used as a flavoring agent in the food industry, particularly in baked goods, soft candy, and chewing gum [47]. It could also be found naturally in apple juice, orange juice, and orange peel oil [47].

Jenkins et al. showed in their study on BB that it could be used as a potential biofuel in aviation as its flash point exceeds the minimum standards while exhibiting reliable low-temperature aviation fuel properties [9]. In the same study, it was shown that this ester appears as a promising candidate that can substitute gasoline as it has an octane number of 97.3 which is similar to that of conventional gasoline [9]. Moreover,

in recent research, Sjöblom et al. showed similar performance of a heavy-duty diesel engine running on pure diesel and on diesel mix blended with up to 30% BB which makes the latter an interesting diesel substitute/additive [8]. Also, BB is the product of the esterification reaction of butanol and butyric acid (BA), both of which could be derived from biomass through fermentation processes [48].

## *2. Biofuel Production Process: Acid-catalyzed Esterification reaction*

The esterification reaction is considered to be one of the most important organic reactions as it yields valuable intermediates for the synthesis of drugs, perfumes, pharmaceuticals, and plasticizers [2], in addition to its tremendous role in biofuel production. This reaction is usually catalyzed in liquid phase and it is known to yield low conversion if not occurring in the presence of catalyst [14]. For this reason, this reaction had long been performed with the use of catalysts such as enzymes [49, 50] and acid catalysts [10]. However, acid-catalyzed esterification is more common [11]. As in all chemical reactions, catalysis is considered essential in the production process, as it allows the efficient making and breaking of chemical bonds which is the base for the production of new chemical compounds [51]. Catalysts needed for esterification reactions are mainly active acid sites, Brønsted or Lewis acids, which are essential for the efficient production of the desired ester. The role of the addition of a Brønsted acid is to protonate the carbonyl carbon and allow for a nucleophilic attack by the alcohol (steps 1 and 2 in **Figure 2**) followed by the formation of a water molecule which is a superior leaving group (step 4 in **Figure 2**). In this context, different types of acid catalysts were investigated, tested, and briefly overviewed in this section.

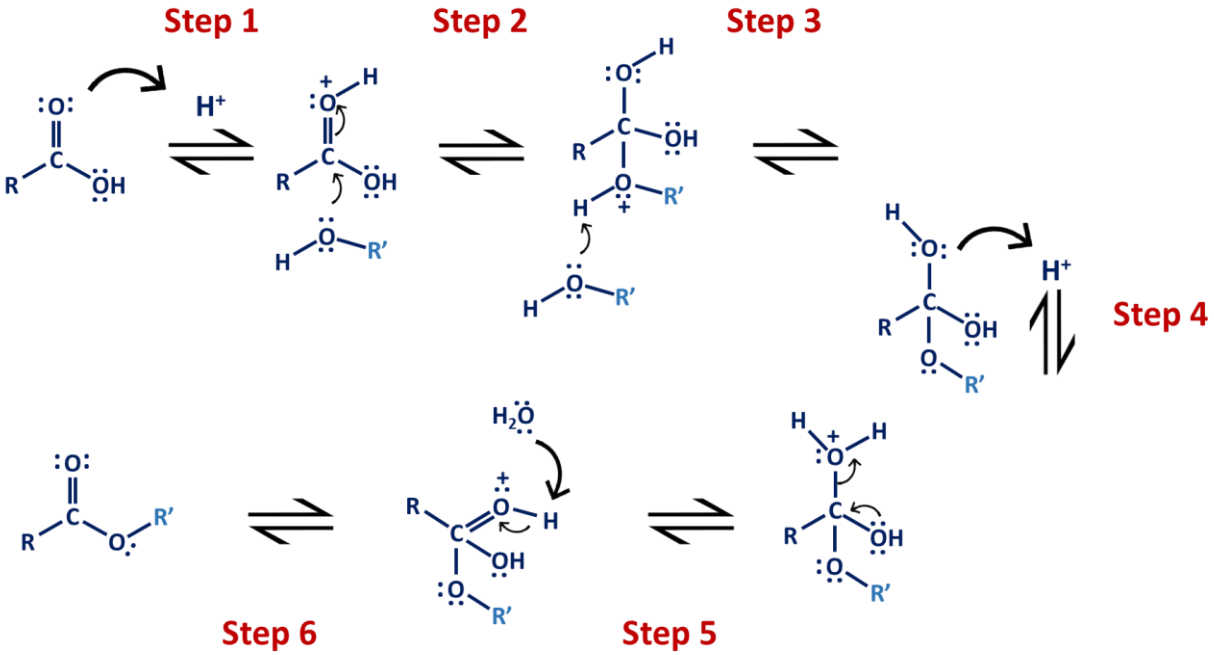


**Figure 2:** The mechanism of Fisher esterification acid-catalyzed reaction [2]

Another reaction mechanism that can take place in an esterification reaction is the dual acid-base mechanism, where the basic sites form hydrogen-bonded adducts increasing the nucleophilic character of the alcohol's O atom, and favoring its reaction with the carboxylic acid. [52, 53]

a. <u>Homogeneous mineral acid catalysts</u>

Inorganic acids such as $H_2SO_4$, HCl, HF, $AlCl_3$, and $H_3PO_4$ have been widely used for the catalysis of Fischer esterification reaction [2, 12]. These catalysts had shown significantly increased rates of conversion compared to other catalysts [14]. However, the use of these catalysts causes many technical problems in industrial facilities because of their corrosive nature [13]. Additionally, the homogenous catalysts form one phase with the reaction components, which makes the recovery of the catalyst and its

reusability a challenging process [14]. Moreover, the recovery of the product and its separation from the liquid acid catalyst requires washing the mixture with water which causes the loss of some of the biofuel and generates a lot of wastewater, increasing thus the production cost [15]. For all the previously mentioned reasons, homogeneous acid catalysts are considered harmful to the environment and economically inefficient. Therefore, a lot of effort had been devoted to finding new green heterogeneous catalysts for the production of biofuels.

b. Heterogeneous solid acid catalysts

Recently, heterogeneous catalysts have been extensively used in industries because of their ability to be easily separated from the reaction mixture without the need for sophisticated separation units and without any losses of the product yield [16]. In addition, heterogeneous acid catalysts are far less corrosive, or non-corrosive, compared with homogeneous catalysts. Moreover, some heterogeneous catalysts have the ability to be recycled without significant loss in their activity and could be reused for many cycles, which makes them, not only environmentally friendly but also cost-effective. However, the main challenge remains in finding heterogeneous solid catalysts with chemical activities comparable to their homogeneous counterparts [16].

Great progress has been achieved in the field of heterogeneous catalysis especially using crystalline porous materials such as zeolites [17, 18], Mesoporous silica [54], ion-exchange resins [55], and metal oxides [56]. All of these materials share common features making them an advancement in heterogeneous catalysis. However, these solid catalysts usually suffer from relatively low surface area resulting in low catalytic activity [19]. They also experience diffusion limitations [57] and, in some

cases, a decrease in their catalytic activity over recycling cycles had been reported due to the leaching of active sites in the reaction medium [57].

Considering a very efficient class of catalysts, zeolites, which are alumina-silicates porous structures that are known for their excellent thermal and chemical stability [58]. Zeolites are known to have a superior selectivity that is based on the design of their porous network where only reactants that fit can be activated to react or to be produced [59]. However, the micropores of zeolites could cause diffusion limitations when the targeted reaction is in liquid-phase with complex organic substrates involved. Additionally, the control of the pore size of the zeolites and the prediction of their crystalline structure prior to their synthesis remains challenging [60]. The previously stated disadvantages of zeolites have directed the attention towards finding a new class of materials that allows for easy engineering of their structure in order to control their characteristics. In catalysis applications, it is of great interest to be able to manipulate parameters such as the surface area, pore size, and density/type of active sites in a controlled manner to efficiently produce the desired product [61]. This flexibility in materials engineering allows narrowing down the efficiency gap between homogeneous and heterogeneous catalysis which would make a breakthrough in chemical reaction engineering [13]. The previously stated objectives have shed light on new materials in catalysis applications that are now being investigated for this purpose. In the following section, the novel metal-organic frameworks will be generally introduced, with a detailed emphasis on the reasons behind their suitability for catalysis applications.

### *3. Metal-Organic Frameworks (MOFs)*

a. MOFs: Introduction and Applications

In 1990, Hoskins and Robson's work on the formation of crystalline hybrid porous materials with efficient properties was considered the base for developing porous coordination polymers [62]. This work attracted the focus of scientists worldwide and launched the research in the field of metal organic frameworks (MOFs) [63]. In 1995, the term "Metal-Organic Frameworks" was foremost familiarized by Yaghi et al. [64], where he introduced the synthesis of a thermally stable layered Cobalt-trimesate MOF structure having reversible sorption properties. Two years later, Kitagawa et al. reported developing a 3D MOF displaying gas sorption properties [65]. Later on in 1999, two MOFs, MOF-5 [3] and HKUST-1 [66] were developed, and they are remain two of the most important and investigated structures due to their remarkable porosity and stability [60].

Following this brief historical background, MOFs will defined in detail. MOFs have emerged as a new class of hybrid crystalline materials with high surface area [21-24]. These highly porous materials are made of rigid inorganic clusters called secondary building units (SBUs) coordinated to multidentate organic linkers such as polycarboxylic acids [67]. The metals used in the synthesis of MOFs are alkali ($Li^{+}$…), alkaline earth ($Mg^{2+}$…), transition ($Hf^{4+}$, $Zr^{4+}$, $Cu^{2+}$…), post-transition metals ($Al^{3+}$…), or lanthanides ($Ce^{4+}$…) [68]. This wide variety of building blocks allows for the synthesis of a large range of MOFs with 1D, 2D, or 3D networks [69]. **Figure 3** is an illustration of the formation of a MOF structure from its main building blocks, while **Figure 4** shows a real Zn-based MOF where the yellow sphere indicates the pore of the structure.

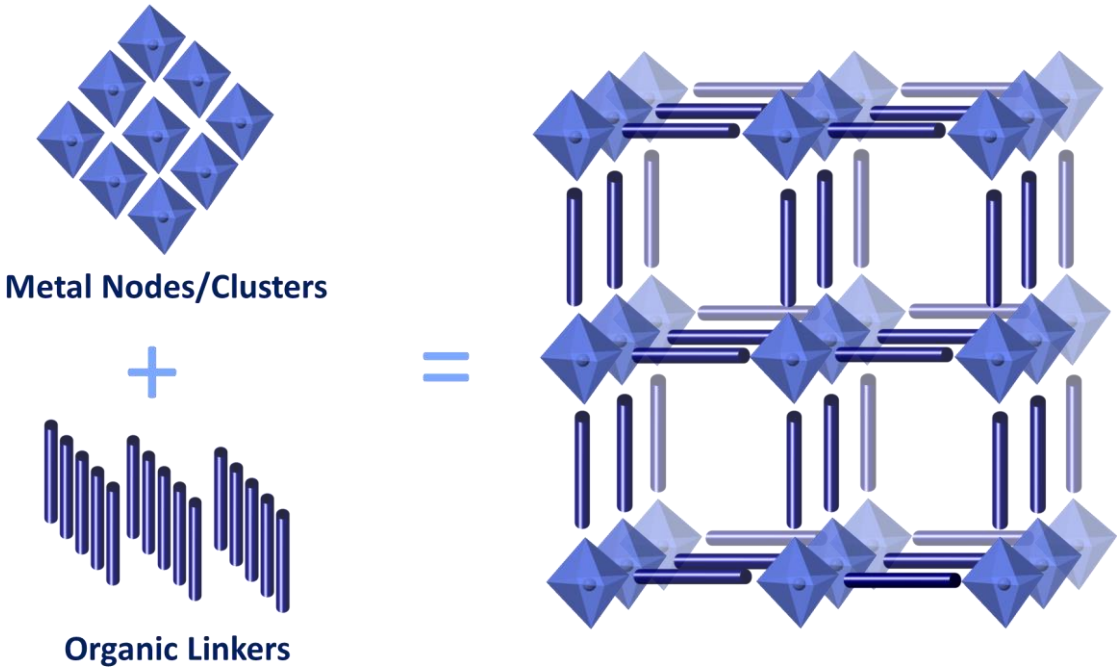


**Figure 3:** An illustration of MOFs' building blocks and corresponding final 3D structure

Given the hierarchical combination of inorganic metal nodes and organic linkers, robust materials are formed with tailorable topologies, tunable porosity, and adjustable functionalities, making them suitable for a wide range of applications [25]. MOFs are originally used for several applications like gas storage and separation [70], purification [71, 72], biomedicine, [73, 74] and chemical sensing [75].

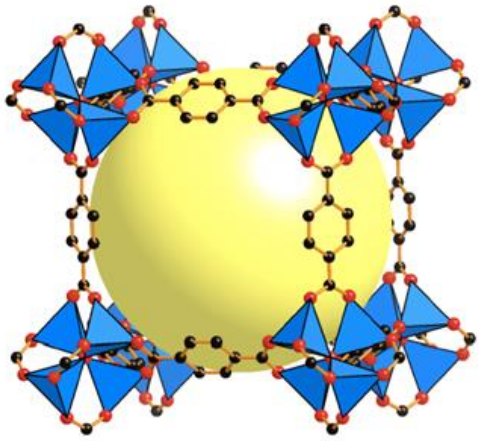

**Figure 4:** $Zn_4(O)(BDC)_3$ MOF-5 framework represented with eight clusters, where only seven are visible, constituting a unit cell that encloses a large cavity indicated by a yellow sphere of diameter 18.5 A. $Zn4(O)O_{12}C_6$ cluster (Zn, blue; O, green; C, grey) with the $ZnO_4$ tetrahedra indicated in blue [3].

In addition to the aforementioned applications, MOFs have been gaining a lot of interest as heterogeneous catalysts in the last two decades since active sites could be incorporated in their organic linkers, metal clusters, or as guest molecules that could be encapsulated within their porous networks [27, 76-78]. In other words, MOFs could be designed to have specific characteristics that boost their catalytic activity [79]. In addition to the wide range of MOFs that could be obtained by combining a certain metal cluster with different linker types, there is also a possibility to incorporate more than one linker having similar size but different functional groups [80]. This results in the formation of a single-phase material in which these two linkers are incorporated in a random manner and the number of active sites can be tuned by simply varying the ratio of these two linkers. Many terminologies describing these materials were found in the literature, such as multivariate Metal Organic-Frameworks (MTV-MOFs) based on Deng et al and [81] Mixed ligands Metal Organic-Frameworks (MIX-MOFs) as used by Kleist et al. [80].

b. MOFs: Opportunities for heterogeneous Catalysis

i. MOFs as Catalysts

In the last two decades, tens of thousands of MOFs have been developed, and many structures had been investigated in catalysis. The list includes: UiO-66/67, NU-1000 and MOF-808 (Zr-based metal nodes) MOF-5 (Zn-based metal nodes) MIL-101 (Cr or Al-based metal nodes), MIL-53 (Al or Fe-based metal nodes), MIL-100 (Al, Fe or Cr-based metal nodes), and ZIF-8 (Zn-based metal nodes) [20].

MOFs are considered attractive for catalytic applications because of their potential to bridge the gap between homogeneous and heterogeneous catalysis. This is due to their high porosities, very large surface area, ease of structural design, and the ability to significantly load the structure with active guest molecules accessible to the relevant reactants [26, 27]. Moreover, MOFs represent a number of advantages over other porous materials such as zeolites and mesoporous silica. Indeed, the maximum surface area and pore size recorded in the case of zeolites were 700 $m^2/g$ and 1 nm respectively [27], while Farha et al. succeeded in synthesizing Nu-109SP with a surface area exceeding 7500 $m^2/g$ [67] and Deng et al. synthesized MOF-74 with pore size greater than 9.8 nm [82]. These features make MOFs suitable for a wide range of applications that involve the use of bulky substrates such as the catalysis of liquid-phase reactions. Moreover, this high level of surface area and the sophisticated porous network also results in materials with a higher concentration of active sites per unit mass [27].

Given the previously stated features, MOFs have shown great catalytic activity in many chemical reactions. This can be attributed to the different components of the MOF structure where active sites could exist or could be engrafted. Indeed, it was found

that the active sites could be included in: (i) the metal nodes acting as Lewis acid when uncoordinated [83], (ii) the organic linker when functionalized with active groups such as Brønsted acidic groups [25] and basic groups [84], (iii) the porous network by encapsulating active guest species [28] (**Figure 5**).

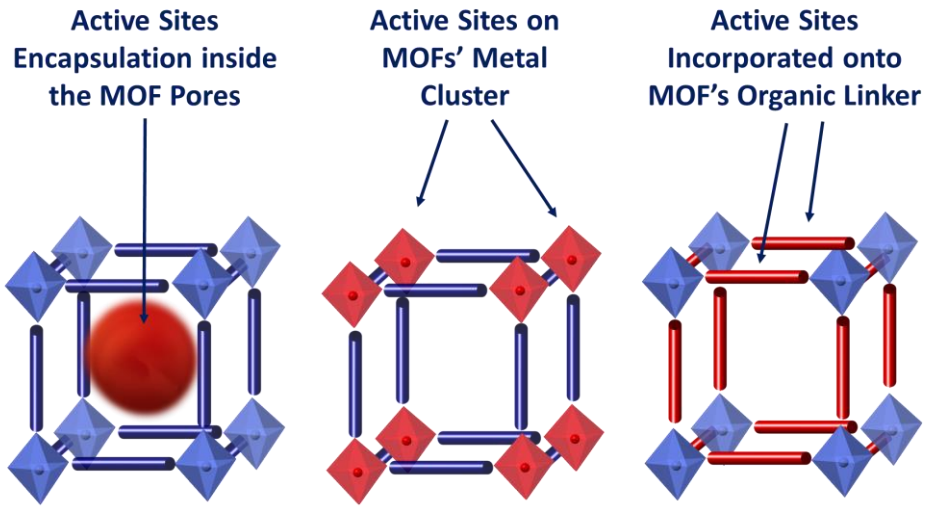


**Figure 5:** An illustration of the approaches that could be used to include active sites (represented in red) in the MOF structure

Another factor that boosts the activity of MOFs is the presence of structural defects in their framework. In fact, the formation of flawless crystals is almost unachievable since these structural defects, caused by a missing cluster or a missing linker, are practically inevitable (**Figure 6)**.

However, defective MOFs have appeared as a subject of curiosity for many researchers who have sought to intentionally introduce these defects into the framework [79]. The reason behind this is the fact that defected MOFs manifested an increased level of catalytic activity, porosity, and surface area compared with the ideal structure where the catalytic activity is hindered by the fully- coordinated metal cluster [79, 85]. For this reason, modulated synthesis was developed and first tested by Schaate et al.[86], which consists of adding mono-dentate ligands (modulators) having the same

chemical functionality of the linker. The role of the modulator is to compete with the linker to either control the nucleation [86-88] (promoting or inhibiting it), crystallinity, morphology of MOFs, or to generate defects in the structure [89]. For instance, acetic acid [79], di and tri-fluoroacetic acid [79], benzoic acid [86, 90], and formic acid [79, 88] have been used as modulators in the synthesis of different MOFs. These monocarboxylate ligands can be then removed leaving behind new open active sites for enhanced catalytic performance which drastically enhances the catalytic activity levels.

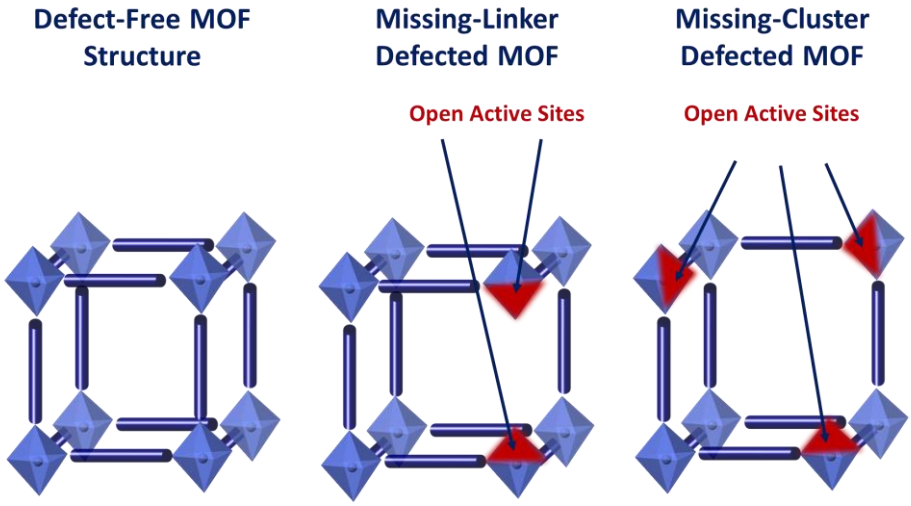


**Figure 6:** An illustration of the defects types that could exist in MOFs

Despite the tremendous advantages of MOFs previously presented, their applicability has been hindered by drawbacks such as their relatively low thermal, mechanical, and chemical stability making their usage limited to reactions requiring mild conditions [91, 92]. Additionally, there is a significant number of dormant catalytically active sites in MOFs because, in most of the cases, the metal nodes are fully blocked by the organic ligands which hinders the activation of substrates [85]. For this reason, all sights have been diverted towards catalytically active and highly stable sub-classes of MOFs such as Zr-based MOF.

The discovery of UiO-66 (**Figure 7**), UiO-67 and UiO-68 (where UiO refers to Universitetet i Oslo, or the University of Oslo) by Cavka et al. in 2008 could be considered as a milestone in MOFs development [92]. These MOFs are made of $[Zr_6O_4(OH)_4]^{12+}$ coordinated to 12 $BDC^{2-}$ (benzene dicarboxylate), $BPDC^{2-}$ (4,4'-biphenildicarboxylate), and $TPDC^{2-}$ (4,4'-triphenyl dicarboxylate) respectively. This coordination is behind the high thermal stability (up to 540°C) of these MOFs [93]. In addition to their thermal stability, these MOFs have shown an outstanding chemical and hydrothermal stability [94] as tested by Decost et al. The stability tests included stability of the MOFs in different organic solvents (methanol, isopropanol, acetone, chloroform, and pyridine), basic solution of NaOH, acidic solution of HCl, and in water.

Thus, the catalytic application of MOFs has been widely expanding so that different MOFs have been developed and used in cyanosilylation [95], hydrogenation [96], oxidation [97], isomerization [98], and esterification [52, 99].

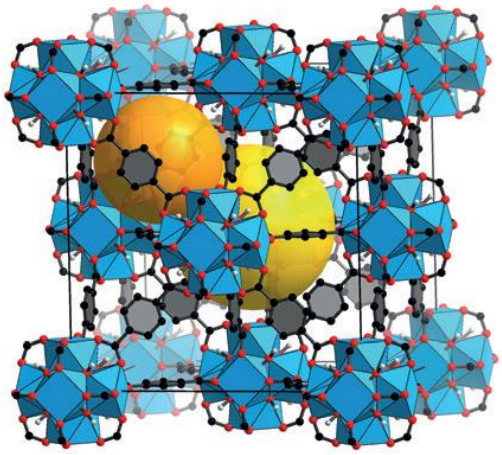

**Figure 7:** UiO-66 made up of $[Zr_6O_4(OH)_4]$ clusters with 1,4-benzodicarboxylic acid struts. The yellow sphere shows the primary pore size and the orange sphere shows the secondary pore size, both of which could be accessed. (Zr blue; C black; O red; H white)

ii. MOFs: Catalysts for esterification reactions

Recent studies have reported the use of MOFs for the catalysis of esterification reaction which seemed to be an efficient approach given the many ways to acidify the MOF framework.

As previously noted, Brønsted or Lewis acidity could be mainly incorporated into the MOF structure by three techniques [100]. The first technique consists of encapsulating the acid molecules inside the pores of the frameworks. The second way of introducing acidity is coordinating acid groups such as hydroxyl to the metal cluster. The third way consists of bonding an acid functional group to the ligand [100].

Additionally, Brønsted acidity could be incorporated in the MOF structures through the transformation of Lewis acid sites on the cluster to Brønsted acid sites [100]. In fact, it often happens that one or more of the coordinative positions around the metallic nodes is occupied by solvent molecules, water molecules, or even uncoordinated ligands usually present during the synthesis of MOFs. Some of these MOFs can be activated by heating under vacuum leading to the evacuation of these positions without the collapse of the framework [101]. This favors the interaction between metal nodes and substrates. In this case, coordination unsaturated sites (CUS) or open metal sites (OMS) with low coordination number are formed in metal nodes to act as a Lewis acid catalyst [102]. These open Lewis sites are then transformed into Brønsted acid sites via the adsorption of water or alcohol molecules [79], which could potentially act as activation sites in esterification reactions.

Besides their acidic nature, Zr-MOFs have been attractive as catalysts for the esterification reaction because of their hydrothermal stability which is required for the esterification reaction involving water generation [103].

The acidity, hydrothermal stability, and intriguing catalytic activity make MOFs a remarkable choice for esterification reaction.

## B. MOFS ENGINEERING TECHNIQUES

Despite the recent work in this area, the opportunities for enhancing the synthesis and performance of these materials remain vast. The following three sections will focus on the materials engineering strategies that are covered in this work and that are believed to be still not well explored in the application of biofuel production.

### *1. Linker Functionalization*

The effect of MOFs' active sites on the catalytic activity in esterification reactions has been previously reported in the literature [52, 53, 99, 104]. Up to this point, the activity of MOFs was in most cases attributed to the effect and role of the metal cluster [76], and specifically to coordination vacancies caused by a missing linker and/or cluster defects in the framework [52, 79, 89, 102]. Catalytic activity was also attributed to the post-synthetic modification of the MOF such as sulfation [30, 99] and the incorporation of polyoxometalates in the MOFs structure [29]. Although some reports focus on the role of the organic linker in the activity of MOFs in esterification reactions [52, 53, 105], these reports mainly focus on the use of the amino-functionalized UiO-66, UiO-66($NH_2$), which does not offer additional acid active sites to optimize the reaction conversion. To this end, the aim of choosing this MOFs' engineering strategy is to shed light on the importance of the proper choice of the organic linkers for a specific application and to provide a deeper understanding of their

role in order to optimize the design of MOF catalysts for efficient production of valuable chemicals such as butyl butyrate.

### *2. Defects Engineering*

Recent studies showed that the presence of structural defects on the SBU created additional Lewis acid sites that have proved to be beneficial to the catalytic properties of MOFs [106, 107]. Given the defects' benefit of increasing the density of active sites, many studies have developed methods to systematically introduce defects into the MOFs structures [106]. Specifically, a lot of research was focused on Zr-based MOFs, such as UiO-66 which is based on $Zr_6O_4(OH)_4(CO_2)_{12}$ cluster, that has been proven to retain its relatively high chemical and thermal stability even in the presence of a significant number of structural defects [102, 108].

A simple method for the systematic introduction of defects into the MOFs structure is the "modulated synthesis", which is becoming very popular. It is not until recently that the modulation synthesis was linked to the formation of structural defects in the MOFs structure, which was proven to have a direct impact on the stability, porosity, and, most importantly, the catalytic activity of MOFs [79, 102, 106, 109]. However, the functional groups that could be attached to the organic ligand could also offer extremely interesting options for the control of the MOFs' catalytic properties. This could be done by the introduction of catalytic centers that offer locations for reactants' adsorption and activation, or that could be incorporated in dual activation mechanism, or by increasing the affinity of the MOFs' catalytic activity towards a specific reactant [20]. In most of the recent reports, the main focus is usually on the standard UiO-66 and the sole effect of the defects in the cluster [79, 104, 108-112].

Furthermore, reports that focus on the role of changing the functional group attached to the organic linker in the MOF to enhance its properties rarely include the effect of the structural defects, and their subsequent benefit from enhancing porosity to the increase in the density of active sites on the cluster [52, 106, 113]. To the best of our knowledge, there haven't been any reports that present a detailed investigation on the effect of modulated synthesis, or defects engineering, in functionalized UiO-66 MOFs. This means that tuning the catalytic properties of these Zr-based MOFs by the combined control of structural defects on the cluster and the functional groups attached to the linker is still not investigated.

### *3. Multivariate (MTV-MOFs) or Mixed-ligand (MIX-MOFs) approach*

Although the functional groups attached to the organic linkers add up to the active sites density in the structure, they have their drawbacks as well. Many studies have reported that the functionalization of the UiO-66 structures is always accompanied by a significant decrease in the surface area of the structure and its pore volume. [52, 53, 103, 114] Most importantly, some studies raised the issue of internal diffusion limitations that seemed to be encountered in functionalized structures relative to the open non-functionalized UiO-66 framework. [52] Furthermore, the aim of this technique is to maximize the catalytic activity of the synthesized structures by benefiting from the added active sites of functionalized linkers while maintaining high levels of surface areas and pores accessibility. This had shifted our attention to assessing the use of a multivariate MOFs approach, MTV-MOFs, which is based on mixing linkers incorporating different functionalities within the same topology. [81, 115] We were specifically interested in trying the isostructural mixed linkers approach,

being relatively a simple way of introducing two or more organic linkers into the MOF structure. [116, 117] In the specific case of UiO-66, MTV-MOFs would incorporate two or more terephthalic acid derivatives as means to tune the properties of the structure especially in terms of surface area, porosity, and reactivity. [118, 119] The change in the MTV-UiO-66 properties will depend on the ratio between the different linkers incorporated within the MOF crystals. This level of incorporation will have to be determined by $^{1}$H-NMR spectroscopy [120]. While most reports focus on the importance of the cluster reactivity to boost the catalytic activity of the MOF catalysts, [79, 104, 108-112] fewer reports focus on the combination of the cluster activity with the linker functionalization [121]. Furthermore, and to the best of our knowledge, there haven't been any reports that focus on the optimization of the MOF catalytic activity for esterification reactions by combining the MTV-MOFs approach and the intentional introduction of defects into the cluster.

## C. OBJECTIVES OF THIS WORK

As mentioned in the previous sections, the exploration of the catalytic activity of MOFs for biofuel production is still not well explored especially using the materials engineering techniques chosen in this research project. These techniques consist of the organic linker functionalization, the cluster defects engineering, and the MTV-MOFs approach. To this end, the main purpose of this research project is to optimize the design of Zr-based MOFs for the efficient production of butyl butyrate based on the aforementioned materials engineering techniques. These techniques are meant to fine-tune the properties and active sites of the MOFs synthesized in order to maximize the

production of the relevant biofuel additive (**Figure 8**). The performance of the MOFs to be synthesized will be enhanced to overcome that of conventional catalysts and, ultimately, to mimic that of the homogeneous catalyst as much as possible. One of the main outcomes of the research is to provide the catalysis field with deep knowledge on the effect of MOFs characteristics on their catalytic activity and, consequently, the conversion to butyl butyrate. On the other hand, it is essential to understand the mechanisms by which these characteristics could be tuned through the synthesis procedure to obtain the required catalytic properties of the MOFs.

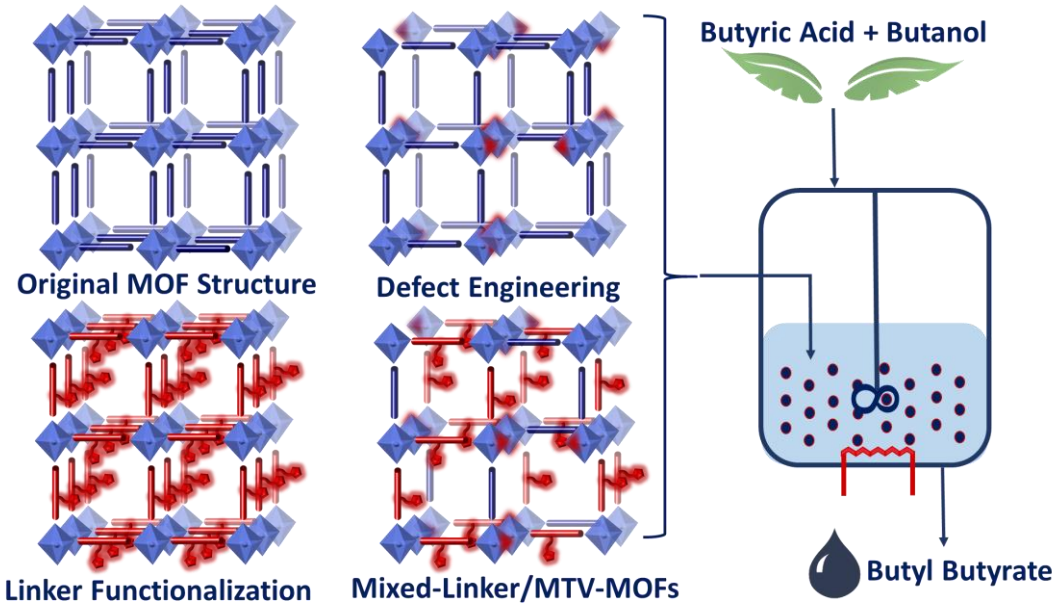


**Figure 8:** An illustration of the three MOF's engineering techniques used, namely linker functionalization, defect engineering, and MTV-MOFs, for the development of active catalysts in the production of butyl butyrate

# CHAPTER III

# MATERIALS AND METHODOLOGIES

In view of the interesting properties of MOFs for catalysis applications on one hand, and the insufficient investigation of their capacities for biofuel production on the other, the overall objective of this research is the development of efficient catalysts based on MOFs for butyl butyrate production as a biofuel additive. These catalysts will be synthesized, characterized, and tested to enhance the production rates of butyl butyrate. The effect of the characteristics of the MOFs' structures on the conversion to butyl butyrate will be investigated, and the findings will be used as feedback for further enhancement of the MOF structure in order to boost its catalytic activity. The previous suggests that the project be divided into sections based on the materials engineering method used to boost the performance of the relevant MOF, and use the findings from one section as a starting point of the other until satisfying results are obtained. The research starts with a detailed review of the literature in order to choose a class of MOFs suitable for the relevant application. The choice was on the Zr-based MOFs, UiO-66, given their higher chemical and thermal stability which is needed in the chemical reaction of interest. The MOFs chosen were never used for the intended application and thus their activity was first to be assessed using synthesis procedures similar to those in the literature. The results obtained were then the base to start optimizing their structure and tuning their properties to enhance their performance. To this end, the overall methodology, as shown in **Figure 9**, starts with an in-depth integrative literature review that feeds into the first stages of each of the three displayed research studies. These studies include the main steps followed to achieve the intended

objective. That is, the overall methodology includes four steps: (1) Synthesis of the catalysts taking into account the literature review and the feedback from our previous studies, (2) characterization of the catalysts to obtain a detailed description of their properties such as surface area, particle size, pore volume, active sites density, and other relevant properties, (3) test the fully characterized MOF catalysts in the esterification reaction of butyric acid to obtain butyl butyrate and (4) track the change in conversion to butyl butyrate with respect to the change in MOF properties and decide on the next optimization step based on the conclusions. These conclusions mainly include the effects of each MOF characteristic and other parameters on their catalytic activity. In the following subsections, the common experimental procedures are first introduced and explained.

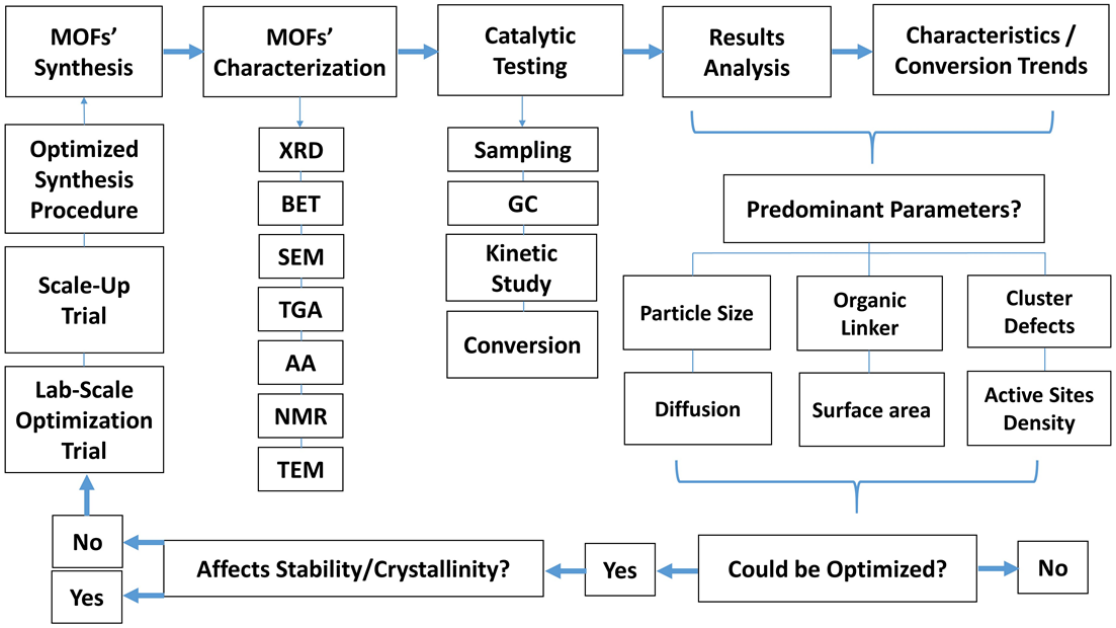


**Figure 9:** General research methodology followed in the experimental work

## A. MAIN MATERIALS ENGINEERING STRATEGIES

### *1. Linker Functionalization*

As previously mentioned in the introduction, the functionalization of the linker is still rarely explored as a strategy to increase the density of active sites and thus the catalytic activities of Zr-MOFs, especially for biofuel production. Furthermore, focusing on this strategy first aims at shedding light on the importance of exploring the effect of adding a functional group to the MOF structure on the yield to butyl butyrate. To this end, three isostructural UiO-66-based MOFs incorporating different organic linkers are synthesized using the same procedure, characterized and used as catalysts in the esterification reaction of butyric acid in presence of butanol to produce butyl butyrate (**Figure 10**). The effect of the different properties of the synthesized MOFs such as the number of defects, surface area, pore size, and their acid active sites on their catalytic activity is explored in light of the different functional groups incorporated in the structure of the MOFs. Furthermore, the study includes the effects of the reaction time, catalyst loading, the recovery, and reusability of the MOFs on the conversion to butyl butyrate. Since zeolites such as H-Beta and H-USY have been previously reported as potential catalysts for other esterification reactions [122], they were thus used in this study to compare their catalytic activity with that of the synthesized MOFs.

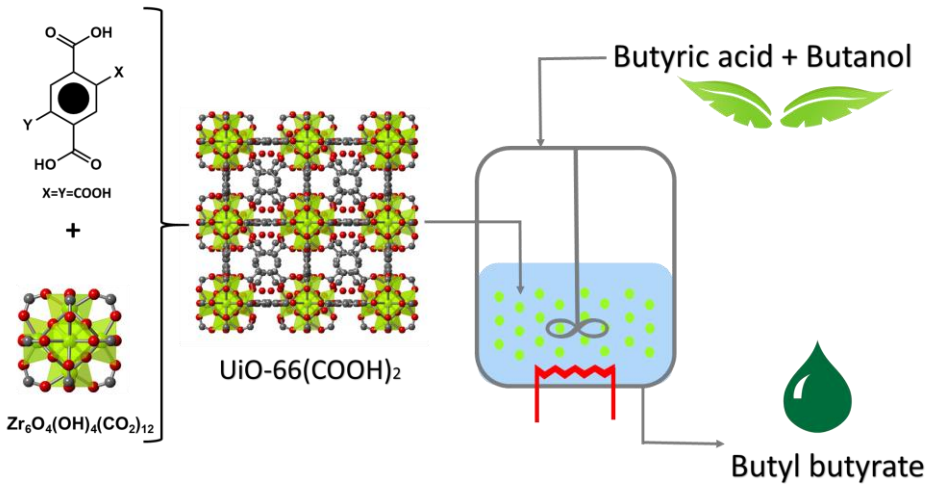


**Figure 10:** Schematic representation of the first approach used, linker functionalization, to boost the catalytic activity of MOFs using linker functionalization. The scheme shows the cluster and the linker used on the left. The represented MOF structure is UiO-66$(COOH)_2$ for x=y=COOH in the linker shown. The MOF is used as catalyst in the esterification reaction of butyric acid in presence of butanol for butyl butyrate production.

### *2. Defects Engineering*

As indicated in the introduction, no reports had researched the effect of linker functionalization combined with a systematic study on defects engineering, it thus was suggested that the two strategies would be joined in the second investigation to further boost the catalytic activity of the MOFs synthesized. This inspired us to perform a systematic study in which 15 different UiO-66 and functionalized UiO-66 samples are synthesized based on different modulation synthesis conditions. The main objective of the work was to engineer the MOFs' structural defects through modulated synthesis combined with organic linker functionalization for enhanced production of butyl butyrate (**Figure 11**). Additionally, the work aims to investigate the relative effect of active sites of the linker and the cluster on the MOFs properties, catalytic conversion, and reaction mechanism. For this reason, 5 different samples of each of UiO-66, UiO-

66(COOH)$_2$, and UiO-66(NH$_2$) were synthesized, where each sample differed from the other by the concentration or the strength of the acid modulator used. The synthesized structures were thoroughly characterized using powder X-ray diffraction (PXRD), thermogravimetric analysis (TGA), $N_2$ sorption-desorption, and scanning electron microscopy (SEM). The studied MOFs were then tested as catalysts for the production of butyl butyrate, and the catalytic conversion was monitored using Gas Chromatography (GC). To rationalize the results obtained following the esterification reaction, the effect of the change in the different properties of the MOFs on their catalytic activity and the conversion to butyl butyrate was thoroughly discussed, including the effect of the number of defects, particle size, surface area, internal mass transfer resistance, and many more.

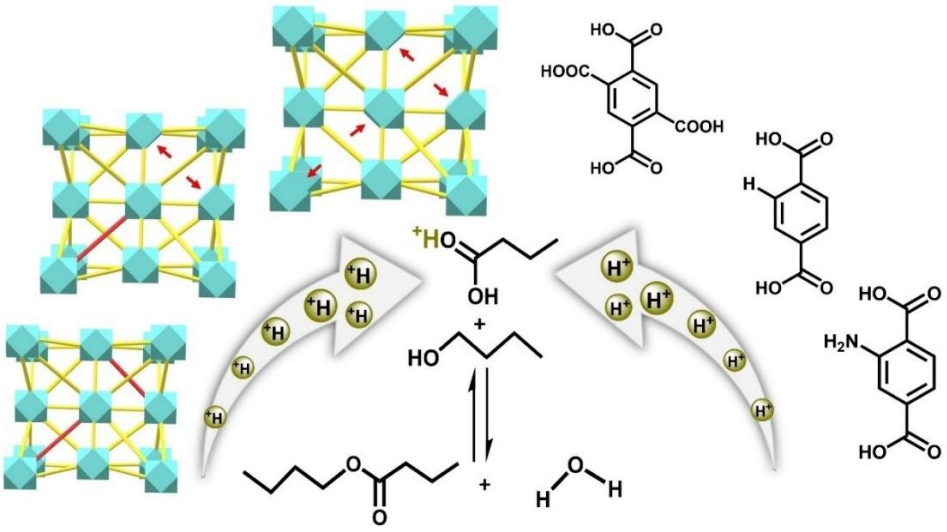


**Figure 11:** Schematic representation of the second approach used, defect engineering to boost the catalytic activity of MOFs using defect engineering (left) coupled with linker functionalization (right). The linkers shown in red in the MOF structures to the left are the missing linkers that leave behind open active sites on the cluster, which are pointed out with red arrows. The arrows with H+ protons in the middle show the increase in the acidity of the structure with the incorporation of more acidic linkers as shown to the right, and with the increase in the number of defects as shown to the left.

### *3. Mixed-linker approach*

As the full functionalization of the MOFs structure might compromise the internal diffusion of reactants and thus the catalytic activity of MOFs, this investigation focused on implementing the partial functionalization of the UiO-66 structures using the MTV-MOFs approach which is explained in details in the introduction. In this study, the linkers of UiO-66 are partially functionalized in a controlled manner through the synthesis of MTV-MOFs. In addition to terephthalic acid, either 1, 2, 4, 5-benzenetetracarboxylic acid (MTV-UiO-66$(COOH)_2$) or 2,5-Dihydroxyterephthalic acid (MTV-UiO-66$(OH)_2$) is added to the reaction mixture. The modulation synthesis condition used for all synthesized structures is set to the optimal obtained in our previous study to ensure maximized defectiveness and, thus, activity on the Zr-cluster [121]. The ratio between the two linkers in each structure is varied to study its effect on the structural properties of the MOFs and their catalytic activity. After their synthesis, all MOF structures are fully characterized using powder X-ray diffraction (PXRD), $N_2$ sorption-desorption, thermogravimetric analysis (TGA), proton nuclear magnetic resonance ($^1$H-NMR), and scanning electron microscopy (SEM). The synthesized MOFs are then tested as catalysts for the esterification reaction of butyric acid in presence of butanol for butyl butyrate production (**Figure 12**). This study will thus provide basic knowledge and guidelines for the materials engineering tools required to maximize the potential of the emerging MOF catalysts for biofuel additives production through esterification reactions.

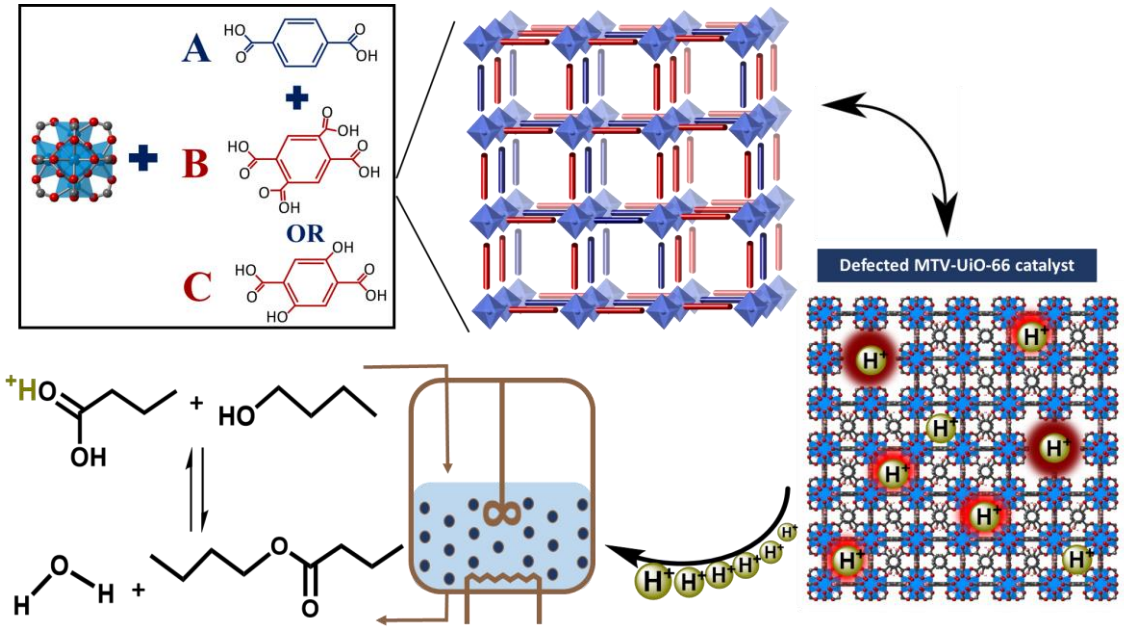


**Figure 12:** Schematic representation of the third approach used, MTV-MOFs, to boost the catalytic activity of MOFs by incorporating two different linkers in the same structure. The functionalized linkers with OH or COOH groups are shown in blue in the structure in the middle, while non-functionalized linkers are shown in blue. The MOF structure to the right highlights the presence of active sites through defects on the cluster and functional groups on the linker. These active sites serve in the catalysis of the esterification reaction for butyl butyrate production.

## B. MOFS SYNTHESIS

The Zr-based MOFs were synthesized using the solvothermal method, which is one of the most used for the synthesis of MOFs. In brief, an equimolar ratio of the metal salt to be used, which is $ZrCl_4$ in our case, and an organic linker of choice, are dissolved in N,N-dimethylformamide (DMF) using a sonicator. Additionally, an organic acid, chosen based on the required synthesis procedure and, in some cases, water, are added to the mixture. The whole mixture is placed in a sealed bottle that is placed in a preheated oven at 120°C for 21 hours. The obtained precipitate is the MOF to be collected and washed. The mixture containing mainly the MOF and the solvent is

moved to a falcon tube and placed in the centrifuge to collect the MOF. The obtained MOF powder is washed with DMF for three consecutive times over three days to remove remaining unreacted materials in its porous network. In each wash, the MOF/solvent mixture is centrifuged to remove the used solvent, then a new solvent is added and the mixture is agitated using the sonicator for around 30 minutes then left to settle for at least two hours. The MOF crystals are then washed to remove DMF using a low boiling point solvent, which is in our case dichloromethane (DCM). The purpose of the second wash is to allow for a solvent exchange inside the porous network of the MOFs, where the second solvent is easier to evacuate in the next steps. The same washing procedure is used for another three times using DCM. The MOF crystals are then dried in a vacuum oven at around 140 °C to remove the solvent and make the pores accessible. The following sections summarize the details of synthesis procedures for the three materials engineering techniques used.

### *1. Linker Functionalization: MOFs Synthesis Procedure*

In this study, three MOFs (**Figure 13**) were synthesized using the solvothermal procedure as detailed below.

UiO-66 was synthesized under conditions similar to those reported in the literature with a few modifications [93]. In brief, $ZrCl_4$ (0.795 g, 3.411 mmol) and terephthalic acid (0.566 g, 3.411 mmol) were dissolved in 250 mL of DMF by sonication at room temperature. 15 mL of acetic acid was added to the obtained mixture that was put in a 500 mL autoclavable reagent bottle and placed in a pre-heated oven at 120°C for 21 hours.

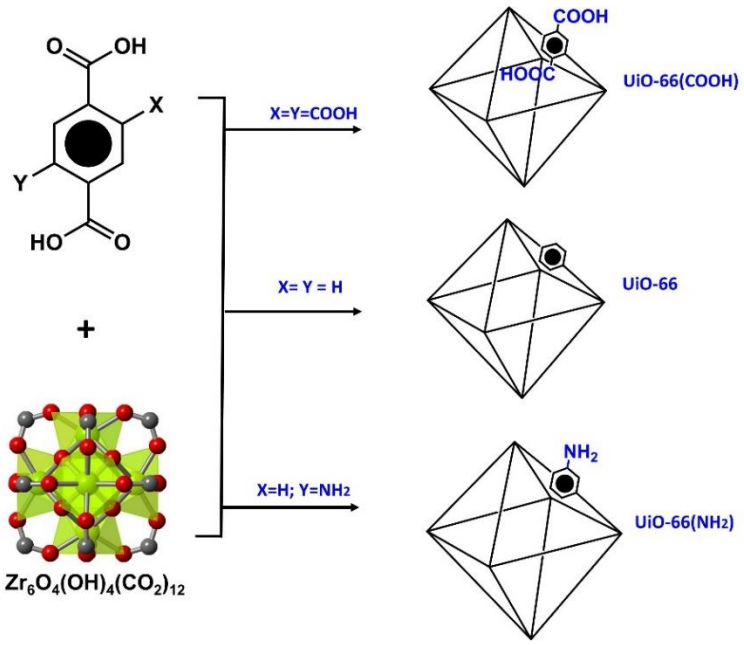


**Figure 13:** Schematic representation of the synthesis of UiO-66, UiO-66$(COOH)_2$ and UiO-66$(NH_2)$

The obtained white precipitate was collected by centrifugation and washed three times with around 50 mL of DMF and then three times with 50 mL of DCM. In the first two washes in each solvent, MOFs were allowed to settle for 3 hours, whereas in the last wash, MOFs were soaked in the fresh solvent overnight. UiO-66 was then dried in a vacuum oven at 140°C overnight. The synthesis of UiO-66$(COOH)_2$ and UiO-66$(NH_2)$ was done in the same manner but by replacing the terephthalic acid with 1, 2, 4, 5-benzenetetracarboxylic acid (0.866 g, 3.411 mmol) and 2-aminoterphthalic acid (0.617 g, 3.411 mmol) as the linker respectively. The details of the synthesis procedure are shown in **Table 1**.

**Table 1**: Details of the synthesis conditions of the MOF catalysts UiO-66, UiO-66(COOH)$_2$ and UiO-66(NH$_2$)

| Sample name | Molar equivalents (with respect to 3.411 mmol of $ZrCl_4$) | | | | | | |
|---|---|---|---|---|---|---|---|
| | $ZrCl_4$ | DMF | DI water | Terephthalic Acid | 1,2,4,5 Benzenetetra-carboxylic Acid | 2-Amino Terephthalic Acid | Acetic Acid |
| **UiO-66** | 1 | 350 | 4 | 1 | 0 | 0 | 80 |
| **UiO-66(COOH)$_2$** | 1 | 350 | 4 | 0 | 1 | 0 | 80 |
| **UiO-66(NH$_2$)** | 1 | 350 | 4 | 0 | 0 | 1 | 80 |

### 2. *Defects Engineering: MOFs Synthesis Procedure*

Fifteen different MOFs based on the three structures in the previous study were synthesized using a similar synthesis procedure (**Figure 14**).

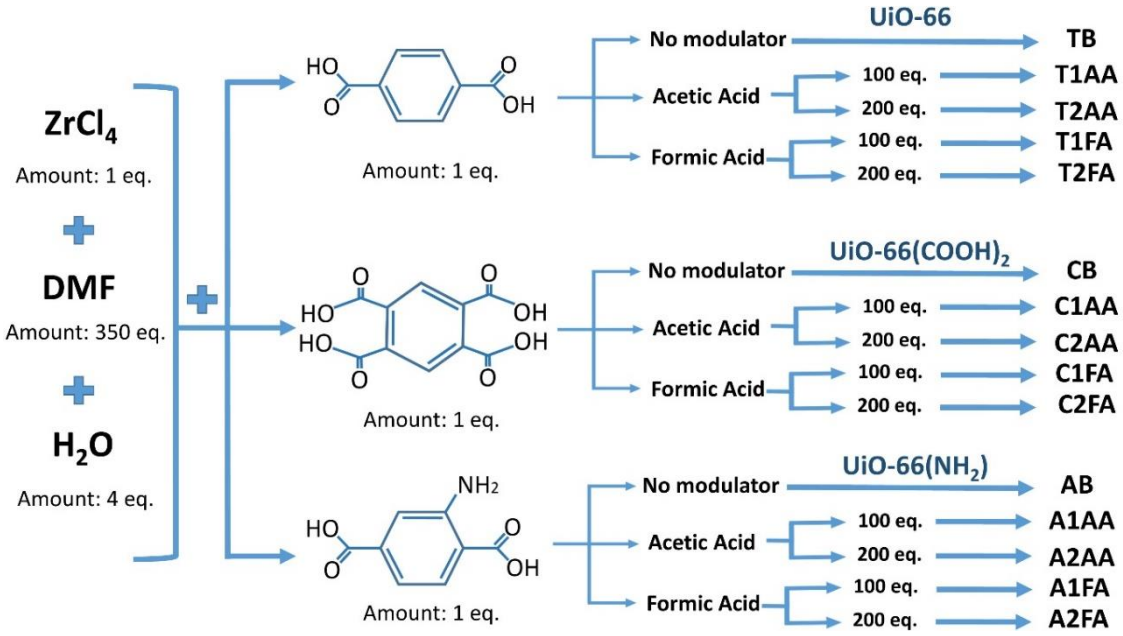


**Figure 14**: Schematic representation of the synthesis conditions of the 15 tested MOF catalysts for the defect engineering study (eq. is mole equivalent with respect to $ZrCl_4$)

UiO-66 was synthesized by dissolving 344 mg of ZrCl4 (1.48 mmol) and 245 mg of terephthalic acid (1.48 mmol) in 40 mL of DMF (516.74 mmol) and 0.1 mL of DI water (5.91 mmol). A modulator with the appropriate type and amount was then added to the mixture (**Table 2**), and the mixture was put in a 100 mL sealed vial before being placed in a sonicator. After complete homogenization of the mixture components, the vial was placed in a preheated oven at 120 $^{o}$C for 21 hours. The same procedure was used to synthesize UiO-66(COOH)$_2$ and UiO-66($NH_2$) by respectively using 1,2,4,5-benzenetetracarboxylic acid and 2-aminoterephthalic acid as the organic linker instead of the terephthalic acid used in the case of UiO-66.

After 21 hours, the vial is removed from the oven and is left to cool to room temperature. The content of the vial is then moved to a falcon tube and the white precipitate, or pale yellow precipitate in case of UiO-66($NH_2$), is collected by centrifugation. The obtained MOF crystals are washed using fresh DMF for three consecutive times for three days, followed by washing with DCM for another three consecutive times. After completing the last wash, DCM is removed by centrifugation and the washed MOF crystals are placed in a vacuum oven at 170$^{o}$C for thermal activation. The characterization of the MOFs was all done after thermal activation.

For every given linker, the MOF was synthesized without using a modulator, using 100 equivalents (5.56 mL) and 200 equivalents (11.13 mL) of formic acid, or using 100 (8.43 mL) and 200 equivalents (16.87 mL) of acetic acid. This means that every MOF structure was synthesized in 5 different modulation conditions, yielding the total of 15 MOFs being studied. Details about the synthesis procedure are given in **Table 2**. The synthesis procedure showing the 15 MOFs used in the study with their

names, which will be used throughout the paper for simplicity, and compositions are given in **Figure 14.**

**Table 2:** Details of the synthesis conditions of the 15 tested MOF catalysts for the defect engineering study

| Sample name | Molar equivalents (with respect to 3.411 $ZrCl_4$) | | | | | | | |
|---|---|---|---|---|---|---|---|---|
| | $ZrCl_4$ | DMF | DI water | Terephthalic Acid | 1,2,4,5 Benzenetetra-carboxylic Acid | 2-Amino Terephthalic Acid | Acetic Acid | Formic Acid |
| **TB** | 1 | 350 | 4 | 1 | 0 | 0 | 0 | 0 |
| **T100AA** | 1 | 350 | 4 | 1 | 0 | 0 | 100 | 0 |
| **T200AA** | 1 | 350 | 4 | 1 | 0 | 0 | 200 | 0 |
| **T100FA** | 1 | 350 | 4 | 1 | 0 | 0 | 0 | 100 |
| **T200FA** | 1 | 350 | 4 | 1 | 0 | 0 | 0 | 200 |
| **CB** | 1 | 350 | 4 | 0 | 1 | 0 | 0 | 0 |
| **C100AA** | 1 | 350 | 4 | 0 | 1 | 0 | 100 | 0 |
| **C200AA** | 1 | 350 | 4 | 0 | 1 | 0 | 200 | 0 |
| **C100FA** | 1 | 350 | 4 | 0 | 1 | 0 | 0 | 100 |
| **C200FA** | 1 | 350 | 4 | 0 | 1 | 0 | 0 | 200 |
| **AB** | 1 | 350 | 4 | 0 | 0 | 1 | 0 | 0 |
| **A100AA** | 1 | 350 | 4 | 0 | 0 | 1 | 100 | 0 |
| **A200AA** | 1 | 350 | 4 | 0 | 0 | 1 | 200 | 0 |
| **A100FA** | 1 | 350 | 4 | 0 | 0 | 1 | 0 | 100 |
| **A200FA** | 1 | 350 | 4 | 0 | 0 | 1 | 0 | 200 |

### *3. MTVMOFs: MOFs Synthesis Procedure*

Nine different MOF catalysts incorporating single or mixed linkers were synthesized by a solvothermal modulated method using N,N-dimethylformamide as a solvent and formic acid as modulator at 120 °C. The synthesis of the nine MOF samples is summarized in **Figure 15**.

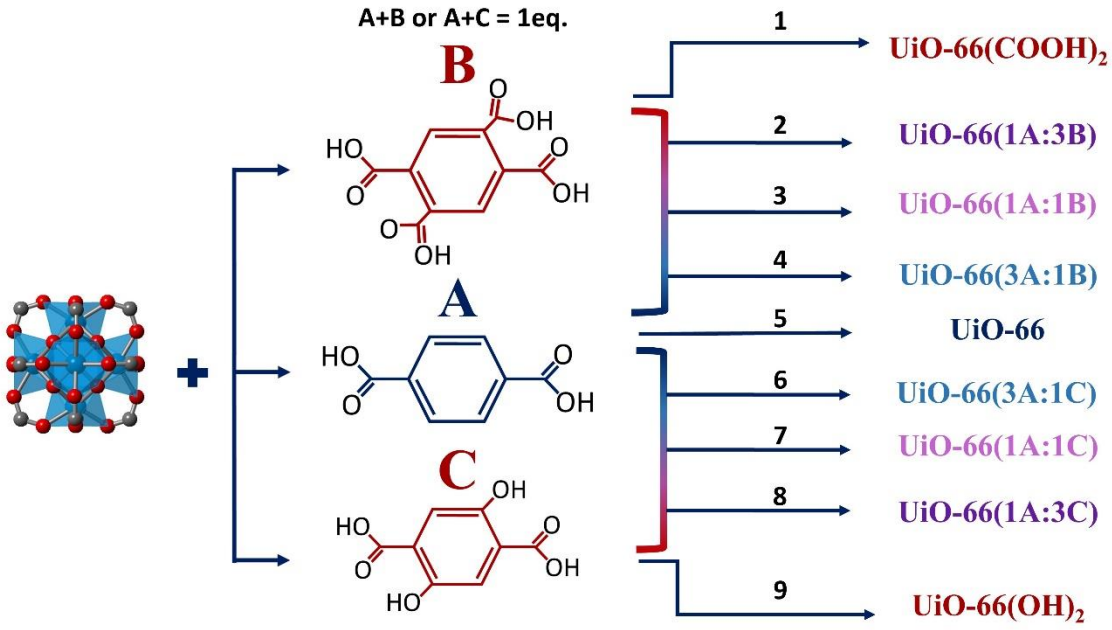


**Figure 15:** Schematic illustration of the synthesis details of the 9 tested MOF catalysts for the MTV-MOFs study (1 eq. is one molar equivalent with respect to $ZrCl_4$ in the synthesis mixture).

The single linker MOFs synthesized are UiO-66, UiO-66$(COOH)_2$, and UiO-66$(OH)_2$. For the synthesis of UiO-66, 344 mg of $ZrCL_4$ (1.48 mmol) were dissolved in 40 mL of DMF (516.74 mmol) along with 245 mg of terephthalic acid (1.48 mmol). 11 mL of formic acid were then added to the mixture which was placed in a 100 mL vial, and the mixture was agitated in the sonicator for around 10 minutes. The homogenized mixture was then placed in a preheated oven at 120 °C for 21 hours. After 21 hours in the oven, the vials are removed, allowed to cool to room temperature, and the precipitated powder is collected from the synthesis solution by centrifugation. The obtained as-synthesized MOF is washed with DMF three consecutive times, allowing it to settle for at least 2 hours in between, and it is then similarly washed with DCM. After separating MOF from DCM following the last wash, MOFs are moved to a glass vial and is placed in a vacuum oven at 170 °C overnight for thermal activation. Full characterization of MOF then takes place.

The synthesis of UiO-66$(COOH)_2$ and UiO-66$(OH)_2$ occurred in the same manner by replacing the terephthalic acid in the synthesis mixture with 376 mg (1.48 mmol) of 1, 2, 4, 5-benzenetetracarboxylic acid and 293 mg (1.48 mmol) of 2,5-dihydroxyterephthalic acid respectively. Six MOFs were synthesized using MTV approach, with three catalysts incorporating both terephthalic acid and 1, 2, 4, 5-benzenetetracarboxylic acid, and the other three incorporating both terephthalic acid and 2,5-Dihydroxyterephthalic acid. The starting molar ratio of the two linkers was changed between 3:1, 1:1, and 1:3 with the total number of mole of both linkers being equivalent to 1 with respect to the number of moles of $ZrCl_4$ in the synthesis mixture. More details on the synthesis procedures of the MTV-MOFs can be found in the supporting information file in **Table 3**. **Figure 15** is an illustration of the MOFs synthesis conditions and it displays the corresponding MOF nomenclature that will be adopted throughout the paper.

**Table 3:** Details on the synthesis conditions of the 9 MOF catalysts synthesized for the MTV-MOFs study

| **Sample name** | **Molar equivalents (with respect to 3.411 mmol of $ZrCl_4$)** | | | | | |
|---|---|---|---|---|---|---|
| | $ZrCl_4$ | DMF | Terephthalic Acid | 1,2,4,5 Benzenetetra-carboxylic Acid | 2,5-Dihydroxyterephthalic acid | Formic Acid |
| **UiO-66** | 1 | 350 | 1 | 0 | 0 | 200 |
| **UiO-66(3A:1B)** | 1 | 350 | 0.75 | 0.25 | 0 | 200 |
| **UiO-66(1A:1B)** | 1 | 350 | 0.5 | 0.5 | 0 | 200 |
| **UiO-66(1A:3B)** | 1 | 350 | 0.25 | 0.75 | 0 | 200 |
| **UiO-66$(COOH)_2$** | 1 | 350 | 0 | 1 | 0 | 200 |

| | | | | | | |
|---|---|---|---|---|---|---|
| **UiO-66(3A:1C)** | 1 | 350 | 0.75 | 0 | 0.25 | 200 |
| **UiO-66(1A:1C)** | 1 | 350 | 0.5 | 0 | 0.5 | 200 |
| **UiO-66(1A:3C)** | 1 | 350 | 0.25 | 0 | 0.75 | 200 |
| **UiO-66(OH)$_2$** | 1 | 350 | 0 | 0 | 1 | 200 |

## C. MOFS CHARACTERIZATION

All MOFs synthesized are fully characterized using specific techniques to allow for a detailed description of their structure and properties, and to better assess the reason behind their catalytic performance. The characterization techniques used and the settings chosen are explained below in detail.

### *1. Powder X-Ray Diffraction (PXRD)*

Structural characteristics of the synthesized MOFs were determined using PXRD diffraction. PXRD is a non-destructive analytical tool used to identify the crystalline structure of a sample, which is usually done by comparing the measured diffractogram of the tested sample with a simulated pattern from the crystal structure reported in the literature.

Powder X-ray diffraction (PXRD) patterns were obtained using a Bruker D8 advance X-ray diffractometer (Bruker AXS GmbH, Karlsruhe, Germany) at 40 kV, 40 mA (1600 W) using Cu Kα radiation (k=1.5418 Å).

### *2. Thermogravimetric Analysis (TGA)*

TGA is used to determine the thermal stability of the MOF. This technique records the change of mass of a substance with respect to temperature while being

heated using a controlled heating rate, gas atmosphere, and flow rate. Thermogravimetric Analysis (TGA) was performed with a Netzsch TG 209 F1 Libra apparatus. The analyses were recorded in airflow from 30 to 1000°C at a heating rate of 3 K. $min^{-1}$. In addition, TGA was used to determine the number of missing linkers in the synthesized MOFs.

As mentioned in the literature review, the presence of defects on the MOF metal cluster due to missing linkers creates active sites that could affect the catalytic activity of the MOFs. For this reason, the number of defects per cluster for every MOF structure was assessed using the results obtained from TGA. Previous studies have reported the calculation of the number of missing linkers per MOF cluster[79], however, the method used in this study will be briefly described again for clarification.

It is assumed in this method that 6($ZrO_2$) is the only solid product obtained from the combustion of the standard and functionalized UiO-66 samples. The combustion of the standard UiO-66 samples is given in the following equation:

$$Zr_6O_4(OH)_4(BDC)_6(s) + 45\ O_2(g) \rightarrow 6\ ZrO_2(s) + 48\ CO_2(g) + 12\ H_2O\ (g)$$

Theoretically, and taking the standard UiO-66 as an example, the weight-loss plateau is the ratio of the molar mass of the hydroxylated UiO-66 to that of the 6 $ZrO_2$. Normalizing the TGA curve so that the final weight percent obtained at the end is equal to 100%, the theoretical weight-loss could then be calculated given the following formula:

$$WLP_{th} = \frac{MW_{MOF}}{MW_{6\ ZrO_2}} * WL_{final}$$

Where

$WLP_{th}$: is the theoretical weight-loss plateau of the studied hydroxylated MOF structure (%)

$MW_{6\ ZrO_2}$: is the molecular weight of 6 $ZrO_2$ (g/mol)

$WL_{final}$: is the final value of the weight-loss which is set to be 100% in the normalized curve (%)

However, the experimental weight-loss plateau $WLP_{exp}$ is the horizontal line that passes through the intercept between the TGA curve and the vertical line at the temperature indicated $T_{link}$. $T_{link}$ is the temperature after which the weight-loss is attributed to the combustion of the linker. The value for $WLP_{exp}$ is thus obtained experimentally from the TGA results.

The theoretical weight-loss attributed to one linker $WL_{link}$ is the difference between the theoretical weight-loss plateau and the final weight-loss obtained divided by the theoretical number of linkers in the cluster. $WL_{link}$is thus calculated given the following formula:

$$WL_{link} = \frac{WLP_{th} - WL_{final}}{NL_{th}}$$

Where $NL_{th}$ is the theoretical number of linkers per hydroxylated $Zr_6$ unit.

Knowing the theoretical weight-loss attributed to each linker, the actual number of linkers $NL_{exp}$ could be expressed as the ratio between the experimental and theoretical weight-losses attributed to the linker, which is expressed as follows:

$$NL_{exp} = \frac{WLP_{exp} - WL_{final}}{WL_{link}}$$

The number of missing linkers, $NL_{mis.}$ is then expressed as the difference between the theoretical number of linkers $NL_{th}$, and the experimental number of linkers $NL_{exp}$.

$$NL_{mis.} = NL_{th} - NL_{exp}$$

### *3. Scanning Electron Microscopy (SEM)*

SEM images were taken to assess the morphology, particle size, and shape of the MOFs. SEM was performed using a MIRA3 Tescan electron microscope after the samples were coated with a thin layer (20 nm) of Gold.

### *4. $N_2$ sorption for Brunauer-Emmett-Teller (BET) Calculation*

The surface area of the samples synthesized was determined by an autosorb iQ-Microscope-XR (Quantachrome Instruments, Boynton Beach, FL, USA) gas analyzer using Nitrogen gas. The Brunauer-Emmett-Teller (BET) and Langmuir methods were used to determine the surface area with respect to P/P0. The measurement of the surface area was done after degassing and thus activation of the samples at 170°C overnight.

## D. ESTERIFICATION REACTION FOR BUTYL BUTYRATE PRODUCTION

Prior to their testing, catalysts were put in the vacuum oven overnight at 140°C for dehydration. The esterification reaction was carried out in a 50 mL round-bottom flask to which 10 mL of butanol, 5 mL of butyric acid. The appropriate catalyst type and loading were added to the reaction medium at the beginning of the reaction. In the following sections, the catalyst loading unit will be abbreviated as wt% representing the

weight percentage of catalyst added with respect to the initial weight of the butyric acid. The round bottom flask was connected to a water condenser and heated to 110°C using an oil bath placed on a magnetic stirrer/ heater, and the solution was mixed with a magnetic bar. These experimental conditions were chosen based on related reports in the literature [14]. The reaction was allowed to occur for 24 hours and samples of 60µL were collected from the reaction medium at 0, 2, 4, 6, 8, and 24 hours, using an electronic pipette. The time t=0 hours was the time at which the temperature of the reaction medium reached 110 °C. The samples were added to a 4 mL vial containing 2 mL of an n-heptane/octanol solution where the concentration of the octanol was known. The diluted solution was then placed in a 5 mL syringe fitted with a filter (0.2 µm PTFE filter) to remove catalyst particles. The filtered samples were placed in GC vials for analysis which was done using gas chromatography (Thermo Scientific, Trace GC Ultra, Gas Chromatograph), equipped with an FID detector. The components of the samples were separated on a Teknokroma capillary wax column (30 m × 0.32 mm × 0.25 µm). After the end of the reaction, the catalyst was separated from the reaction medium by centrifugation, it was then washed again with DMF and with DCM and dried under vacuum at 140°C overnight as described earlier. XRD patterns were recorded for the recycled catalysts and compared with fresh ones to ensure their crystallinity is retained. Samples were taken normally for the reactions where recycled MOFs were used. Every experiment was repeated at least three times to ensure results are reproducible.

# CHAPTER IV

# RESULTS AND DISCUSSION

## A. THE EFFECT OF THE ORGANIC LINKER FUNCTIONALIZATION

### *1. Catalyst characterization*

The PXRD patterns of the synthesized UiO-66, UiO-66($COOH)_2$, and UiO-66($NH_2$) are shown in **Figure S1** in the Annex and reveal sharp narrow peaks that are in complete accordance with the calculated pattern of UiO-66. This reflects the high crystallinity and phase purity of all prepared catalysts. The textural properties of the synthesized MOFs were determined by surface area analysis. The $N_2$ isotherms (**Figure S2**) and the obtained results are summarized in **Table 4.** The calculated BET surface areas and pore volume of the three MOFs are in good agreement with the reported values in the literature [79, 93, 103, 123]. SEM images of different synthesized MOFs are shown in **Figure S3** in the Annex and **Figure 16**. The images show that the samples are pure and display homogeneous octahedral shaped crystals, with UiO-66($COOH)_2$ having a smaller particle size leading to a less clear shape of the crystal as expected by the broader peaks obtained in the PXRD pattern. The average particle size was calculated based on SEM images and the values are reported in **Table 4**. The results obtained in this section will be thoroughly discussed in the following sections.

**Table 4:** Textural properties of the synthesized MOFs

| | Number of missing linkers (Average ± SD) | Surface area ($m^2/g$) | Particle size (Average ± SD, nm) | Pore volume (cc/g) |
|---|---|---|---|---|
| **UiO-66** | 1.39 ± 0.05 | 1052 | 303 ± 75 | 0.327 |
| **UiO-66(COOH)$_2$** | 1.32 ± 0.01 | 284 | 28 ± 7 | 0.115 |
| **UiO-66(NH$_2$)** | 1.72 ± 0.04 | 801 | 93 ± 20 | 0.25 |

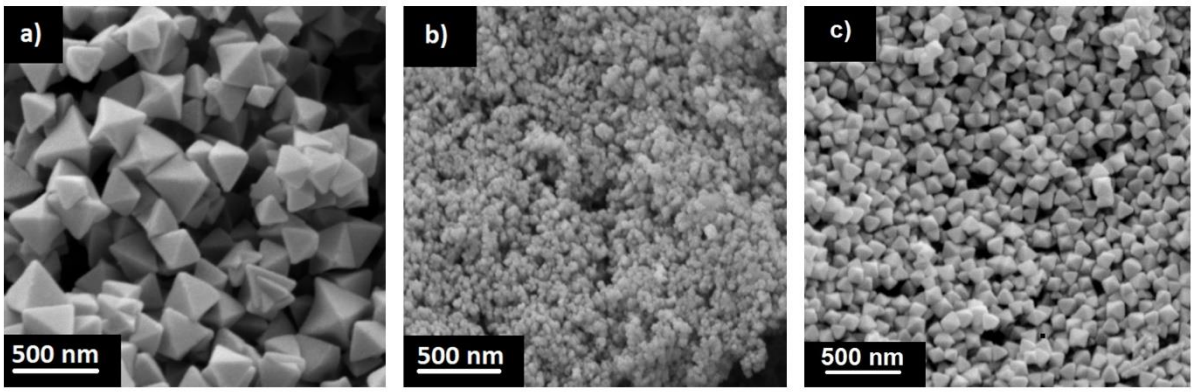


**Figure 16:** SEM images of the studied MOFs (a) UiO-66 (b) UiO-66(COOH)$_2$ (c) UiO-66(NH$_2$)

### *2. Esterification for butyl butyrate production*

The esterification reaction of butyric acid in presence of butanol for butyl butyrate production was allowed to occur in a batch reactor for 24 hours using different catalysts loadings. The tested catalysts were all selective and thus no product other than butyl butyrate was detected. The MOFs were also all active given the high conversion rates to butyl butyrate when they were used as catalysts. The evolution of the conversion to butyl butyrate with respect to time was monitored and the results are shown in **Figure 17**. The time t = 0 hour was the time at which the reaction temperature

reached 110°C. During the first 8 hours of the reaction, the conversion to butyl butyrate was relatively fast and reached almost 65%, 60%, and 45% using 5 wt% loading of UiO-66$(COOH)_2$, UiO-66, and UiO-66$(NH_2)$ respectively. As the reaction progressed in time, the rate of conversion to butyl butyrate decreased regardless of the loading used, and the reaction was allowed to continue until it almost reached equilibrium conversion after 24 hours. This decrease in conversion rate with time could be due to the fact that most of the reactants have been consumed during the first few hours of the experiment, leading to lower concentrations of reactants in the reaction medium and thus to slower conversion rates. Another possible scenario for the decrease in the reaction rate with time is the blockage of catalysts' active sites by the increasing quantity of reaction products, making adsorption sites less accessible for the reactants. Moreover, the trend was the same for the lower loadings of 1 wt% and 2 wt% where UiO-66$(COOH)_2$ yields the highest conversion followed by UiO-66 and then UiO-66$(NH_2)$. These results showing the higher catalytic activity of UiO-66$(COOH)_2$ could indicate that the dangling carboxylic acid functional groups of this MOF's linker might have contributed to its superior performance. However, further analysis in the following sections was done to investigate the actual reason behind this trend.

The effect of changing the catalyst loading of the three different MOFs between 1, 2, and 5 wt% of the butyric acid initial weight was also studied and the results are shown in **Figure 17**. For all three MOFs, an increase in the catalyst loading from 1 wt% to 5 wt% caused an increase in the conversion to butyl butyrate from 70 to 83%, 75 to 90%, and 60 to 74% for UiO-66, UiO-66$(COOH)_2$, and UiO-66$(NH_2)$ respectively. This could be explained by the fact that increasing the catalyst loading will increase the number of active acid sites in the reaction medium. This would make access to those

sites easier for the reacting components and would thus promote a faster reaction between the butyric acid and butanol to form butyl butyrate. Since higher conversion was obtained using 5 wt% loading for all studied MOFs, this catalyst loading will be used throughout the rest of the study.

Additionally, the heterogeneous nature of the catalysts and their reusability were assessed. First, a heterogeneity test was performed for all the used MOFs. The test consists of removing the catalyst from the reaction medium at $t$ = 6 hrs by centrifugation and allowing the reaction to proceed with no catalyst under the same reaction conditions. Samples were normally taken from the reaction medium before and after catalyst removal and the results are depicted in **Figure 18**. It is clearly shown that no significant conversion was obtained after removing the catalyst for all three cases reflecting a heterogeneous nature of the catalysts. The slight increase in the conversion after the removal of the catalyst could be attributed to the autocatalysis of the reaction by the butyric acid as is the case in the blank experiment [14, 52, 53]. Second, in order to test the possibility of the regeneration of the catalysts, MOFs crystals were easily separated from the reaction medium by centrifugation, washed again as explained previously, and reused for three more runs in the esterification reaction that was allowed to occur for 24 hours in every run. Although the obtained conversion using the recycled MOFs showed that they retained their catalytic activity, however, a slight decrease in the conversion could still be noticed. This decrease in conversion from cycle to cycle could be due to partial blockage of MOF pores by the esterification reaction products (**Figure 19**).

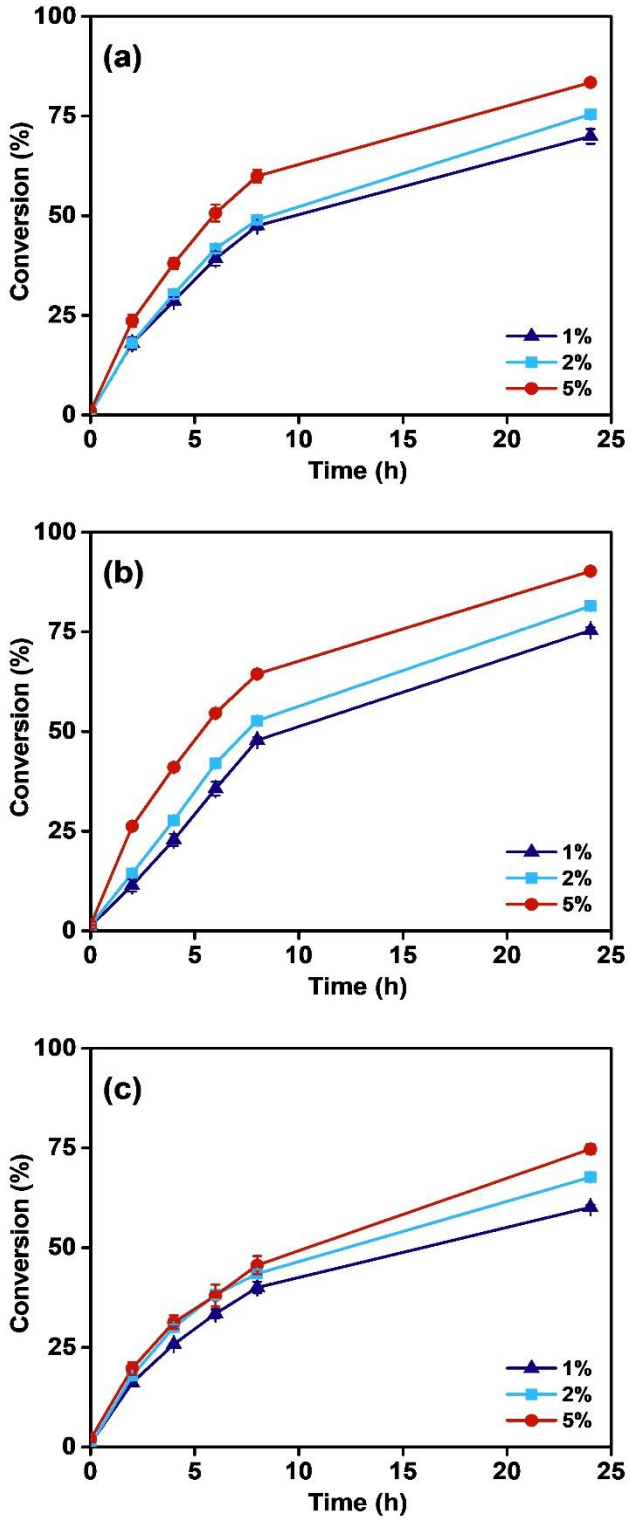


**Figure 17:** Conversion to butyl butyrate over 24 hours in esterification reaction of butyric acid in presence of butanol using different catalysts. (a) UiO-66 (b) UiO-66$(COOH)_2$ (c) UiO-66$(NH_2)$

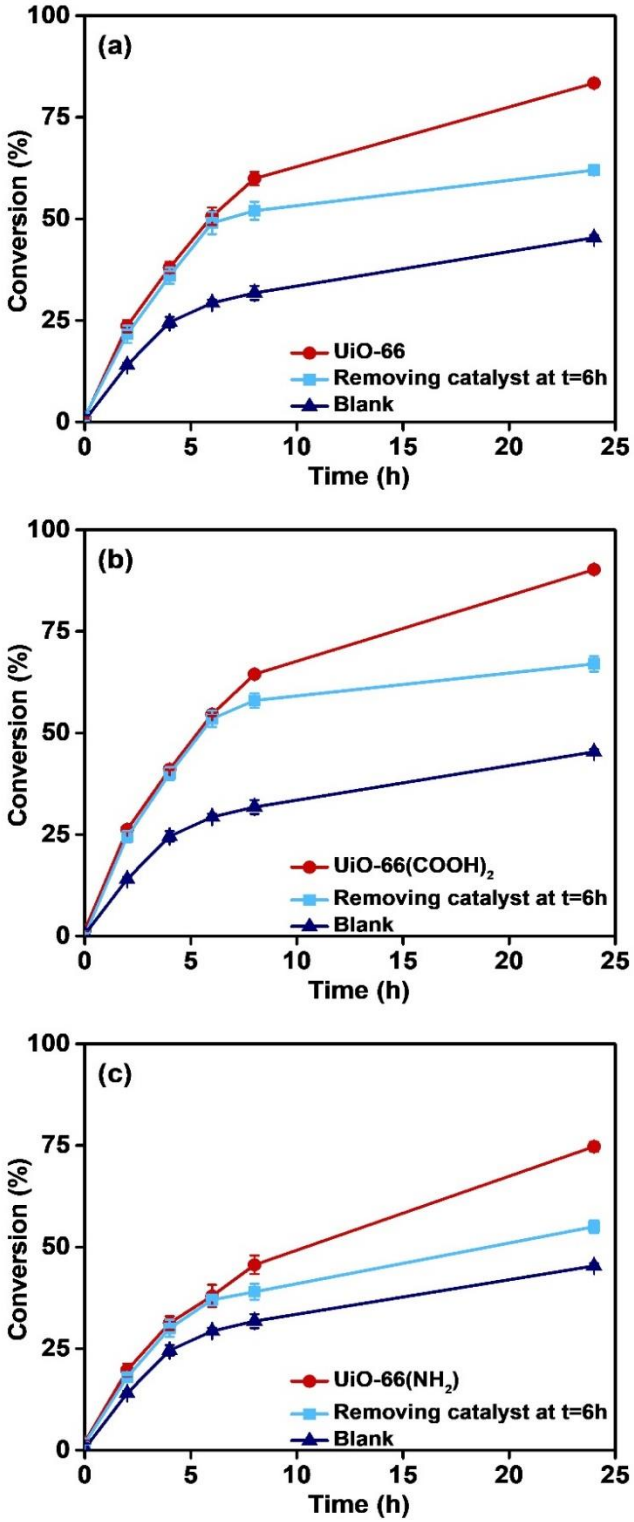


**Figure 18:** Effect of catalyst removal on the esterification reaction of butyric acid in presence of butanol under 5 wt% loading of (a) UiO-66 (b) UiO-66$(COOH)_2$ (c) UiO-66$(NH_2)$

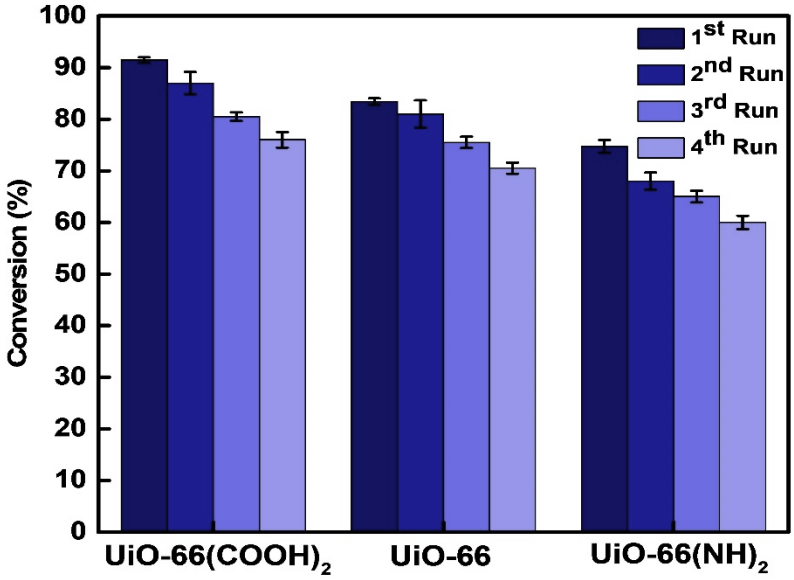


**Figure 19:** Reusability of synthesized catalysts under 5 wt% loading of the relevant catalyst over 4 cycles and after 24 hours of the esterification reaction

Furthermore, the same reaction was performed under the same experimental conditions using different catalysts and no catalyst at all (**Figure 20**). In the case where the reaction was allowed to run without catalyst, the conversion obtained could be attributed to the butyric acid that can auto-catalyze the reaction up to a certain level [14, 52, 53]. Additionally, the reaction was allowed to occur using 5 wt% of the liquid acid catalyst $H_2SO_4$. As expected, $H_2SO_4$ performed considerably better than the MOFs especially at the beginning of the reaction, while stabilizing the conversion to butyl butyrate at a value of 95%, a value comparable to the 90% obtained using 5 wt% of the UiO-66(COOH)$_2$ after 24 hours of reaction. The superior catalytic activity of the strong liquid acid catalyst is typical when compared with heterogeneous acid catalysts, however, given the negative impact of using liquid acids in the reaction medium, it is mostly of interest to compare the performance of the MOFs with other heterogeneous acid catalysts used in the same experimental conditions. For this reason, two types of

zeolites were tested for the esterification reaction of butyric acid, and results are displayed in **Figure 20**. The zeolite catalysts used were 5 wt% loading of the acidic H-USY and H-Beta. Interestingly, UiO-66($COOH)_2$ performed better than the other heterogeneous catalysts used. Moreover, H-USY yielded a conversion to butyl butyrate similar to that of UiO-66, while the use of H-Beta leads to a result slightly better than that obtained when using UiO-66($NH_2$). Additionally, a recent study reported better activity of sulfonated char-based solid acid catalysts with the best catalyst material leading to a conversion of 94.5% under the same reaction conditions reported in this study [14], but this result was counteracted by the disadvantage of excessive leaching of sulfonic acid groups in the reaction and upon recycling, which considerably reduced the activity of the catalysts in the second cycle [14]. Another study by the same research group reported the use of sulfonated char-based heterogeneous acid catalysts for the production of butyl butyrate, the best catalyst used showed less acid leaching in the reaction medium and was thus used for several cycles without significant losses in the reaction yield [10]. Only a few other studies on this reaction exist, but the results were not reported as they were done under different experimental conditions [124, 125].

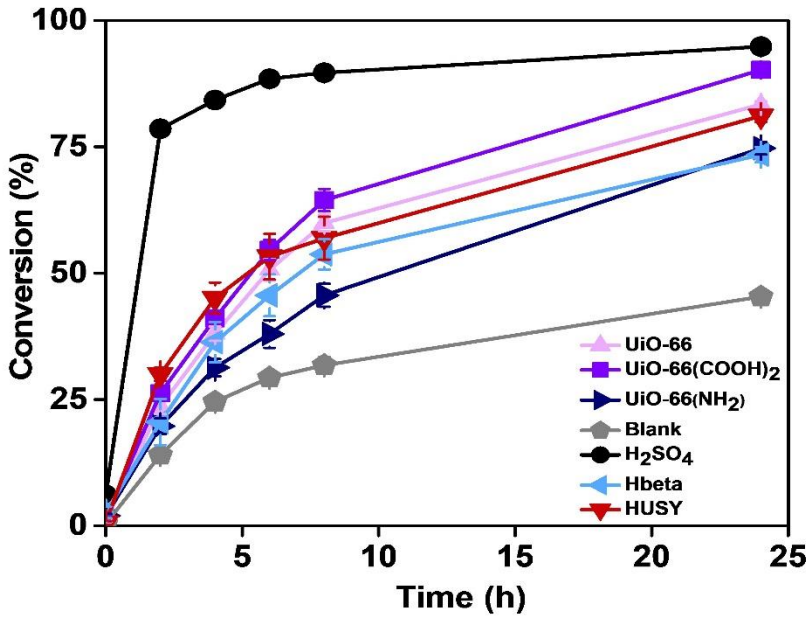


**Figure 20:** Evolution of conversion to butyl butyrate over 24 hours in the esterification reaction of butyric acid in presence of butanol using 5 wt% loading of different acid catalysts

### *3. Effect of MOFs characteristics on catalytic activity*

Following the previously obtained results, and to test the role of the functional groups attached to the linker of the framework in the previously tested MOFs, many characterization techniques have been used. The aim was to investigate the parameters that mostly governed the conversion rates and to understand where the linker choice stands within these parameters when designing a MOF for a given application. In recent years, the confusion behind the catalytic activity of UiO-66 was addressed, and it was mostly attributed to defects in the framework, or in other words coordination vacancies in the cluster as discussed previously [89, 102, 106]. Therefore, it was of significant interest to study the effect of those defects on the catalytic activity of each studied Zr-MOF and to check if there is a direct dependence between the two. For this reason, thermogravimetric analysis (TGA) of activated MOFs was used to estimate the number

of missing linkers in each studied structure. The method used for the calculation of the number of missing linkers was reported in detail in a previous valuable study [79], and it is briefly described in the Annex. The TGA curves presented in **Figure 21** are normalized in order to calculate the number of missing linkers, and the minimum weight attained by the sample, $WL_{final,}$ is taken to be 100%. $WLP_{th}$ represents the theoretical weight-loss plateau, $T_{link}$ is the temperature after which the weight-loss is attributed to the linker combustion, and $WLP_{exp}$ represents the experimental weight-loss plateau. Details about how these plateaus were calculated are represented in the Annex.

Closely observing the three TGA curves, three weight-loss phases could be distinguished in each one of them with the help of the first derivative of TGA curves, the DTG curves. The first weight-loss observed is in the range of 35-100$^{o}$C and it is attributed to the volatilization of the adsorbed $H_2O$. This weight-loss is common between all three MOFs in terms of the temperature range. The second weight-loss is attributed to the dehydroxylation of the Zr cluster and the removal of the monocarboxylate ligands [89, 126, 127], and it is accompanied by a peak of the DTG curve [79]. The temperature range for this phase is relatively clear in the case of the UiO-66 TGA curve and it extends from 100-350$^{o}$C [79]. As for the functionalized UiO-66 samples, the determination of the maximum temperature of this phase was harder as the peak attributed to it was slightly merged with the one after it [103]. The third phase is the destruction of the framework by the combustion of the linker in the structure. This phase is expressed by a very clear peak in the case of UiO-66. However, an extra peak is observed in this phase in the case of functionalized linkers and it could be attributed to the departure of the functional groups from the framework. This makes the temperature range for this last phase different for each MOF. For UiO-66, the weight-

loss attributed to the linker is the one that occurs above the temperature $T_{link}$, of 390° C, where the peak before the combustion of the linker ends. Whereas for the functionalized linkers, the weight-loss attributed to the linker should include the temperature range of the combustion of the functional groups. Therefore, considering the DTG curves in **Figure 21,** $T_{link}$ in UiO-66$(COOH)_2$ and UiO-66$(NH_2)$ was approximately taken to be 300°C and 305°C respectively [128, 129].

Many of the recent studies on defective MOFs have used TGA as a useful tool to account for defects in the structure quantitatively [79, 128]. The basic theory behind this was the knowledge that the weight-loss plateau attributed to the combustion of the linker is inversely proportional to the number of missing linkers in the structure [111, 130]. In other words, the more missing linkers in the framework, the less the percentage of the linker mass relative to the total mass of the framework, and the smaller the relevant weight-loss plateau. It should be noted here that both types of defects, missing-linker and missing-cluster, cause linker deficiencies in the framework, which means that defects are accounted for in both cases [79, 106]. However, it is not possible to distinguish between the two types of defects using only TGA [79], but this is not required for this discussion.

**Figure 21** shows the results of the TGA analysis. The gap between WLPth and WLfinal and that between WLPexp and WLfinal indicate respectively the theoretical and experimental weight-losses attributed to the combustion of the linker. It could be clearly seen that for all samples, the experimentally measured weight-loss is lower than the theoretical one for the three different linkers. This means that all of the studied frameworks are linker deficient and that these defective sites could have had an important role in the high conversion rates of the catalysts. This is particularly true since

the Lewis acid sites created by the defects on the cluster could have been modified into Brønsted acid sites by the adsorption of the alcohol, butanol in this case, or water molecules produced as explained in the introduction [100]. Additionally, in previous studies, it had been shown that defect-free structures have significantly lower catalytic activity than defective ones, especially in the case of chemical reactions activated by acid sites [79, 102]. This indicates that for a given linker and thus for a given MOF structure, the catalytic activity was shown to have a direct relationship with the number of defects [79]. However, in our systems, we can clearly see that the number of defects was not the main parameter governing the conversion rate and catalytic activity. As shown in **Table 5**, UiO-66 had almost 1.39 missing linkers out of 6, this value is slightly higher than values noted in other reports with similar modulation synthesis procedure [79]. Although the same amount of modulators was used in the synthesis procedure, functionalized UiO-66 had a different number of missing linkers per cluster. UiO-66($NH_2$) showed 1.72 missing linkers per cluster, while UiO-66$(COOH)_2$ had 1.32.

To explain the obtained results, the catalytic reaction steps should be taken into account, mainly the internal and external diffusion, and the adsorption of reactants onto active sites. In a liquid-phase esterification reaction, the acid would usually adsorb onto the active sites of the surface of a solid catalyst, then react with the alcohol to yield the relevant ester [131, 132]. In order for this process to occur efficiently, the reactants must first diffuse through the liquid film of the reaction solution surrounding the catalyst particles to reach the catalyst external solid surface [133]. When the external mass transfer resistance is high, the reaction rate might be decreased [133]. To make sure this was not the case in our reaction, three different stirring speeds were tested (200, 500, and 800 RPM) and 500 RPM was found to be adequate to overcome the external mass

transfer resistance **(Figure S5)**. As can be seen in **Figure S5**, the conversion to butyl butyrate for the stirring speeds of 500 and 800 RPM is almost identical while the conversion with a lower stirring speed of 200 RPM is significantly lower. These results demonstrate that a stirring speed of 500 RPM was enough to eliminate external mass transfer resistance and to allow the reactants to reach the external surface of the solid catalyst.

Although the reaction does not show external mass transfer resistance, the obtained results might indicate that the internal active sites within the porous network of the MOFs were not equally accessible as the external ones for the proper adsorption of butyric acid. In fact, the pore openings of UiO-66 are expected to allow for proper diffusion of the butyric acid in the framework's cavities as explained in previous reports [52, 134], this is not necessarily the case for the functionalized frameworks, and this drop in conversion when substituting UiO-66 with UiO-66($NH_2$) could be due to the inaccessibility of the internal active sites. Moreover, despite UiO-66($NH_2$) had the highest number of defects, it showed lower catalytic activities than both counterparts.

In a previous study on the relative catalytic activity of UiO-66 and UiO-66($NH_2$) with linker deficiencies of 13.2% and 8% respectively [52], slightly better performance of the amino-functionalized catalyst was observed. The reason behind this higher activity of UiO-66($NH_2$) samples was attributed to a dual basic-acidic activation mechanism. In such a mechanism, the carboxylic acid would adsorb to the acid active sites of the MOF cluster, while the basicity of the amino groups favors the increase in the nucleophilic character of the oxygen atom in the alcohol by hydrogen bonding, which promotes its condensation with the carboxylic acid [52, 53]. However, it is worth noting here that the amino group in the UiO-66($NH_2$) have been proved incapable of

catalyzing the esterification reaction by alcohol activation due to its low level of basicity [52]. Despite the previously suggested mechanism, and based on the reported dependency between the pseudo-order kinetic rate constant and the linker deficiency, it was predicted that after a certain number of missing linkers, the density of Lewis acid sites caused by the defects will increase to a point where the dual activation mechanism will no longer have a significant effect, and the catalytic activity of UiO-66 will overcome that of UiO-66($NH_2$) [52]. In our study, this result was confirmed given that deficiencies reached higher levels of around 23.2% and 28.7% for UiO-66 and UiO-66($NH_2$) respectively. It would be expected that with an increase in the number of Lewis acid sites, the adsorption of the carboxylic acid could become harder in the case of UiO-66($NH_2$) because of a crowding effect caused by the amino groups which make the active sites partially inaccessible [52].

As for the UiO-66$(COOH)_2$, the calculated missing linker ratio was 1.32 missing linkers out of 6. This value is comparable to that of UiO-66 but below that for UiO-66($NH_2$). Despite the bulky structure of the UiO-66$(COOH)_2$ with two dangling carboxylic acid functional groups, which might also block the way to active sites inside the pores, this MOF showed the highest catalytic activity among the other two. This interesting result shows that unlike the trend in recent reports in the literature [79, 89, 104, 108], the catalytic activity of the MOFs was not directly dependent on the number of defects when different organic linkers were used. This had shifted our attention to other characteristics that might have had a higher influence on the relative catalytic activities of the studied MOFs.

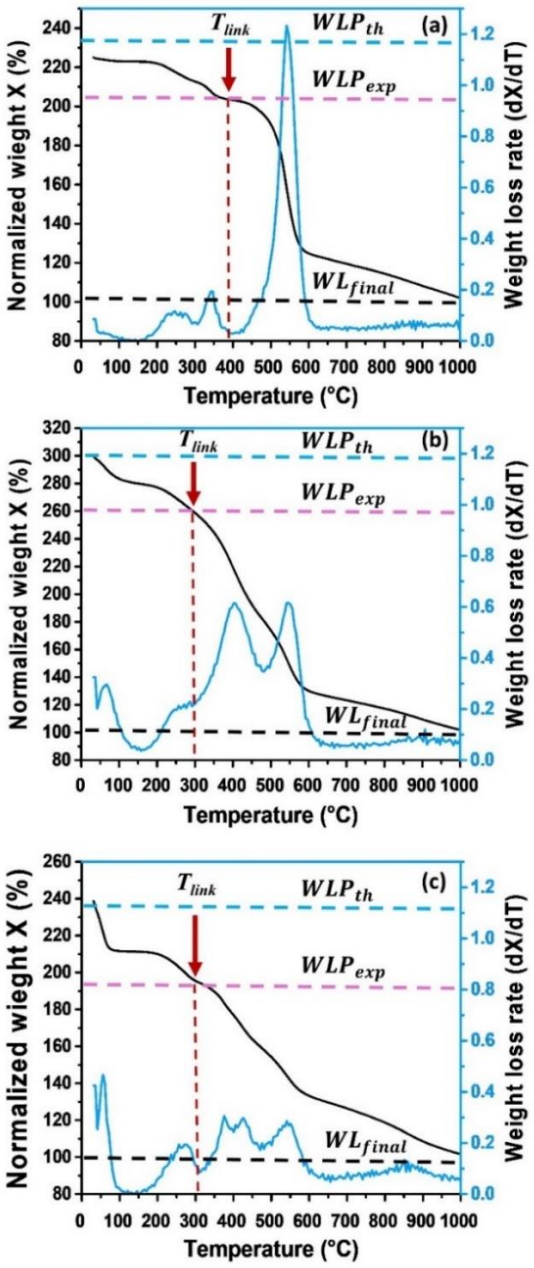


**Figure 21:** TGA and DTG curves of the studied MOFs structure. Black solid line, left axis – TGA curve, Blue solid line, right axis – DTG curve. (a) UiO-66 (b) UiO-66(COOH)$_2$ (c) UiO-66(NH$_2$). (- -) Lower black horizontal line represents the lower end of the theoretical TGA weight-loss plateau, WL$_{final}$ (- -) upper blue horizontal line represents the upper end of the theoretical TGA weight-loss plateau, WLP$_{th}$ (- -) middle pink horizontal line represents the upper end of the experimental TGA weight-loss plateau, WLP$_{th}$ (¦) vertical line represents the temperature of the combustion of the linker, T$_{link}$

Other important factors to consider for the explanation of the obtained results are the surface area and the particle size of the catalysts. When looking at surface area values depicted in **Table 5**, the first thing to notice is that although UiO-66($COOH)_2$ has the lowest surface area, when compared to UiO-66 and UiO-66($NH_2$), it still exhibited superior catalytic performance compared with the aforementioned two MOFs, which means that the catalytic activity was not a function of surface area for MOFs with different organic linkers. Theoretically, the higher the surface area of a catalyst, the closer its performance is to that of homogeneous catalysts, and thus the higher its efficiency is for a given number of active sites per g of catalyst. This should be correct in case the same catalyst with the same density of active sites and with the same particle size is being tested. However, the MOFs used in this study present different functional groups attached to their ligands along with different particle size, and this could explain the obtained results to some extent.

Regarding the effect of the particle size, the SEM images of the three MOFs (**Figure 16** and **Figure S3**) clearly reveal the octahedral shaped crystals for both the UiO-66 and UiO-66($NH_2$). However, this shape was not clear for UiO-66($COOH)_2$ because of their significantly smaller particle size, which was confirmed by the broader peaks obtained in their PXRD (**Figure S1**). This result comes in accordance with the higher activity of UiO-66($COOH)_2$ since the smaller the particle size, the higher the fraction of the external surface area of the catalyst, which thus increases the number of active sites readily accessible for the activation of the butyric acid reducing the negative impact of internal diffusion resistance [52, 134] and thus allowing for better mass transfer [52, 134]. Furthermore, having a catalyst with lower surface area, lower pore volume, and smaller particle size but with higher catalytic activity, such as the case of

UiO-66(COOH)$_2$, suggests that the reaction could be mostly taking place at the outer surface of the catalyst and not inside the porous network. This is especially true for the functionalized structures, UiO-66(COOH)$_2$ and UiO-66(NH$_2$) that offer lower pore volumes and bulkier functional groups that could be increasing internal mass transfer resistance by blocking the way to the porous network as explained previously.

The higher activity of UiO-66(COOH)$_2$, when compared to UiO-66, could be explained by the fact that even in the absence of linker deficiencies, the UiO-66(COOH)$_2$ catalyst offers two uncoordinated active acid sites per linker [103]. With 12 linkers being connected to the Zr cluster, this makes UiO-66(COOH)$_2$ catalyst abundant in active acid sites even in the absence of missing linkers and cluster-coordination vacancies. This is an advantage that UiO-66(COOH)$_2$ has got over UiO-66 that does not offer uncoordinated active sites in its defect-free form [102, 108]. This means that the activity of UiO-66 is highly dependent on the structural defects [79, 104]. As for UiO-66(NH$_2$), the amino groups seem to be promoting internal mass transfer resistance by blocking the way to the internal acid sites without being active themselves, which hinders the esterification by decreasing the rate of activation of butyric acid.

It is worth noting here that synthesizing UiO-66 samples with a smaller modulator concentration would decrease the particle size of the sample, which has a positive impact on the diffusion, but it would also decrease its defect density [79, 89, 106]. Furthermore, studies have shown that UiO-66 samples with a lower number of structural defects show lower catalytic activity even for significantly smaller particle sizes [52, 89]. Additionally, the use of MOFs with dangling acid sites, such as the case is with UiO-66(COOH)$_2$, but with lower steric bulk could increase the surface area and the accessibility of active sites in the porous framework, which could have a positive

impact on its catalytic activity. A good example could be the use of UiO-66(COOH) or UiO-66(OH) [135, 136].

## *4. Conclusions*

In this research work, the activity of a new class of heterogeneous, chemically and thermally stable catalysts was investigated. Zr-based MOFs, UiO-66, UiO-66$(COOH)_2$, and UiO-66$(NH_2)$, were shown to be active, selective, and reusable as catalysts of the esterification reaction of butyric acid to produce a gasoline and Diesel emerging bio-alternative/additive, butyl butyrate. For all catalysts used, an increase in the catalyst loading leads to a better Butyl Butyrate yield. A 5 wt% loading of UiO-66$(COOH)_2$ leads to 90% conversion to butyl butyrate, a value close to the conversion reached using the conventional homogeneous acid catalyst $H_2SO_4$ (95 %). Additionally, all catalysts were easily separable from the reaction medium and they were recovered and successfully used for other esterification reactions over three recovery cycles without a significant loss in the catalytic activity. The abundance and accessibility of active sites in the catalysts were critically related to the organic ligand used in the structure of the framework. Catalysts with uncoordinated active acid sites showed better catalytic activity even for lower surface area and defect number. Additionally, although external mass transfer resistance was shown to be overcome by efficient mixing of the reaction solution, internal mass transfer limitations in the functionalized UiO-66 samples seemed to block the way to internal active sites inside the porous network of those structures. However, the smaller particle size of UiO-66$(COOH)_2$ helped boost the conversion by increasing the external surface of the catalyst with readily accessible active sites. Finally, we believe that further optimization of MOFs structures by the

selective choice of the organic linker to increase the surface area and pore size, decrease the particle size, and generate more defects on the cluster could be a very interesting approach to develop the next generation of industrial catalysts for biofuels production.

## B. THE EFFECT OF DEFECTS ENGINEERING

### *1. Structural Characterization*

The PXRD patterns of all 15 MOFs synthesized were recorded and the results are shown in **Figure 22**. As can be seen, **Figure 22** reveals well defined narrow peaks that are in excellent agreement with patterns reported in the literature, except for the one obtained for the UiO-66$(COOH)_2$ synthesized without a modulator (CB) sample. In fact, the CB sample seems to have yielded an amorphous product. The obtained product could be a type of amorphous MOFs, indicated aMOFs, which are known for their short-range periodic repetition of their building blocks[137]. This results in having broad humps rather than narrow peaks in the PXRD pattern of aMOFs.[138]. However, having amorphous MOFs cannot be confirmed from the PXRD pattern, but the results obtained in other characterization techniques for the CB sample will be reported for further investigation. Additionally, the peaks obtained for all UiO-66$(COOH)_2$ samples, shown in **Figure 22**, seem to be broader with lower relative intensities, which reveal a smaller crystal size of the relevant samples as will be further confirmed in the following section when discussing SEM results.

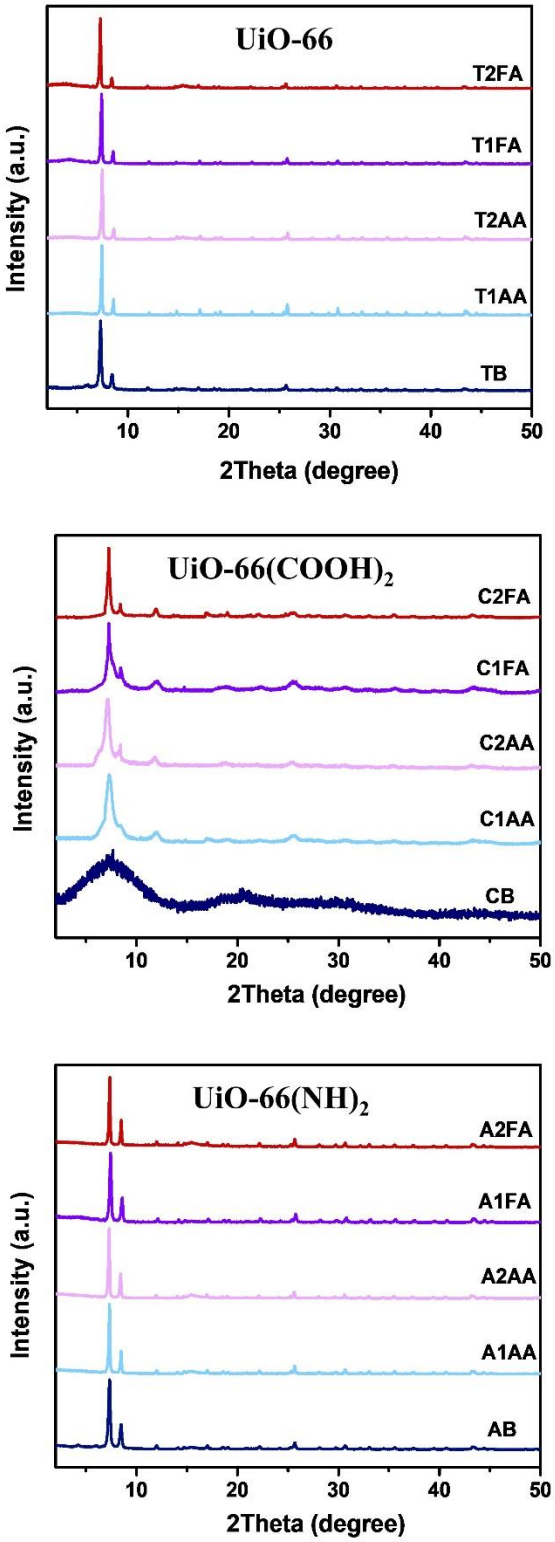


**Figure 22:** PXRD patterns of the fresh activated 15 MOFs catalysts synthesized

In order to analyze the effect of changing the modulation synthesis conditions and the linker type on the morphology and crystal size of the samples, SEM images for the 15 MOFs samples synthesized were taken and the obtained images are shown in **Figure 23** and **Figure S6**. A qualitative assessment of the obtained images reveals a clear trend for both UiO-66 and UiO-66($NH_2$) in terms of both morphology and crystal size. Quantitative data on the crystal size of the different samples are given in **Table 5**.

The synthesis of both MOFs without the use of a modulator resulted in the formation of very small inter-grown cubes (ca. 108 nm for TB and 205 nm for AB)[139] while adding a modulator in the synthesis mixtures yielded much larger well-defined octahedrals [79]. The crystals obtained when FA was used instead of AA have smaller sizes, while the increase in the modulator concentration lead to an increase in the crystal size whether FA or AA was used. Additionally, increasing the modulator concentration to 200 equivalents resulted in more heterogeneous and poly-dispersed octahedral crystal sizes as shown from the standard deviation reported in **Table 5**. This trend is previously reported for UiO-66 samples in recent studies [79], and although the functionalized structures have been reported to have defects in previous studies [140] [141] but we report for the first time this trend for the functionalized structures in this systematic manner.

The reason behind the increase in the crystal size of the MOF with the addition of the modulator could be attributed to the "competition" between the modulator and the organic ligand to bind to the SBUs, which slows down nucleation while promoting the growth of the crystal [79, 139]. However, the crystals obtained for the UiO-66$(COOH)_2$ samples reveal much smaller crystals that seem to remain as inter-grown cubes for all modulation synthesis conditions, while their particle size trend follows the ones noted

for UiO-66 and UiO-66($NH_2$). This could be attributed to the relatively higher acidity of the linker used for the UiO-66$(COOH)_2$ synthesis, which boosts its competitiveness with respect to modulators in the synthesis mixture thus allowing for faster nucleation [108]. Since their small particles made it hard to estimate their particle size using SEM, the Scherrer equation was used to calculate an estimate of the average particle size of C1AA, C2AA, C1FA, and C2FA [142]. Other MOFs' particle sizes were also calculated using the Scherrer equation to allow for a better comparison of the results. As for the CB sample, the determination of the particle size was not possible from the Scherrer equation since its PXRD pattern reveals an amorphous material. Additionally, its SEM shows big aggregations rather than separate particles which made it impossible to estimate a particle size from SEM, and so the particle size for CB was not reported, but it is expected to be smaller than its counterparts of the UiO-66$(COOH)_2$ samples.

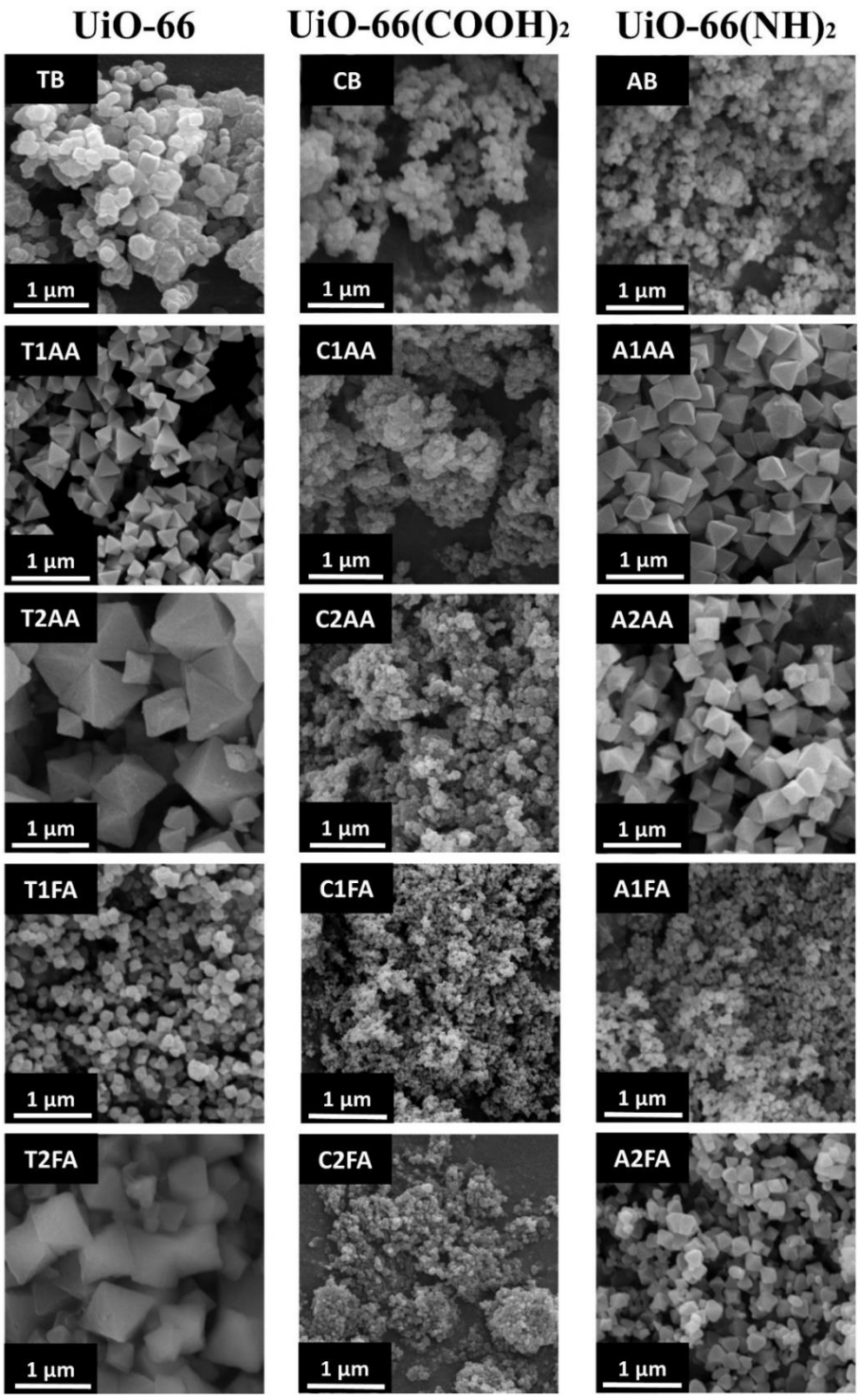


**Figure 23:** SEM images at a 1 µm scale for all the fresh activated 15 MOFs catalysts synthesized

The nitrogen sorption isotherms of all 15 samples were performed at 77K and are shown in **Figure 24**. The first thing to notice in the isotherms is that all of them exhibit type I isotherms which is consistent with the microporous nature of the MOFs. In addition, for any linker used, the nitrogen uptake varies significantly when changing the modulator and its concentration during the MOF synthesis. For all the MOFs being tested, the nitrogen uptake increased when the modulator concentration was increased. Moreover, the nitrogen uptake was higher when the FA was used instead of AA for a given modulator concentration. This observation had been made before for UiO-66 where the nitrogen uptake was reported to increase with the concentration and strength of acid being used as a modulator[79]. With this trend being also valid for functionalized UiO-66 samples, the use of modulators in the synthesis mixture of these samples shows the extent to which the porosity of these samples could be tuned with the systematic manipulation of the concentration and type of the modulator. This is especially true when observing the significantly lower nitrogen uptake and porosity of samples synthesized without the use of a modulator (TB and AB in **Figure 24**). However, the CB sample exhibits negligible porosities relative to its counterparts, which further demonstrates its amorphous nature [137, 138].

The Brunauer–Emmett–Teller (BET) surface areas and the pore volumes of the samples were quantitatively extracted from the nitrogen isotherms and the results are given in **Table 5**. It could be easily noticed how the introduction of modulators have significantly increased the BET surface areas from 1049 $m^2/g$ for TB to 1813 $m^2/g$ for T2FA, which is one of the highest surface areas obtained for a UiO-66 sample, and from 51 $m^2/g$ for CB to 522 $m^2/g$ for C2FA, and from 1016 $m^2/g$ for AB to 1723 $m^2/g$ for A2FA. Additionally, the pore volumes calculated from the $N_2$ sorption-desorption

isotherms show the same trend. However, it could be noticed that the surface area for the MOFs synthesized with 200 equivalents of AA (pKa=4.76) for all three functional groups (T2AA, C2AA, and A2AA) are lower than those synthesized with only 100 equivalents of FA of pKa=3.77 (T1FA, C1FA, and A1FA) as elaborated in **Figure 24**. This stresses on the importance of the pKa of the modulators used relative to their concentration, as using half the quantity of FA relative to AA yielded comparable effects on the surface area[79]. Moreover, the surface area reached using 200 equivalents of FA in T2FA is similar to that obtained using only 40 equivalents of trifluoroacetic acid (TFA) of pKa of 0.23 as reported in a previous study [79]. This confirms that the lower the pKa of the modulator used, the less the amount required to increase its porosity and surface area to a given level.

Another important result here is the change in the surface area of the functionalized UiO-66 samples after the introduction of the active sites onto their organic linkers. **Figure 25** shows the relatively lower surface area of UiO-66($NH_2$) when compared to UiO-66 for all the modulation conditions used. Additionally, UiO-66$(COOH)_2$ is characterized by significantly lower surface areas and pore sizes compared to the other two counterparts. This shows that part of the porous network of the UiO-66 samples is blocked by the bulky functional groups that are covalently bound to the linker, which causes this noticeable decrease in the surface area.

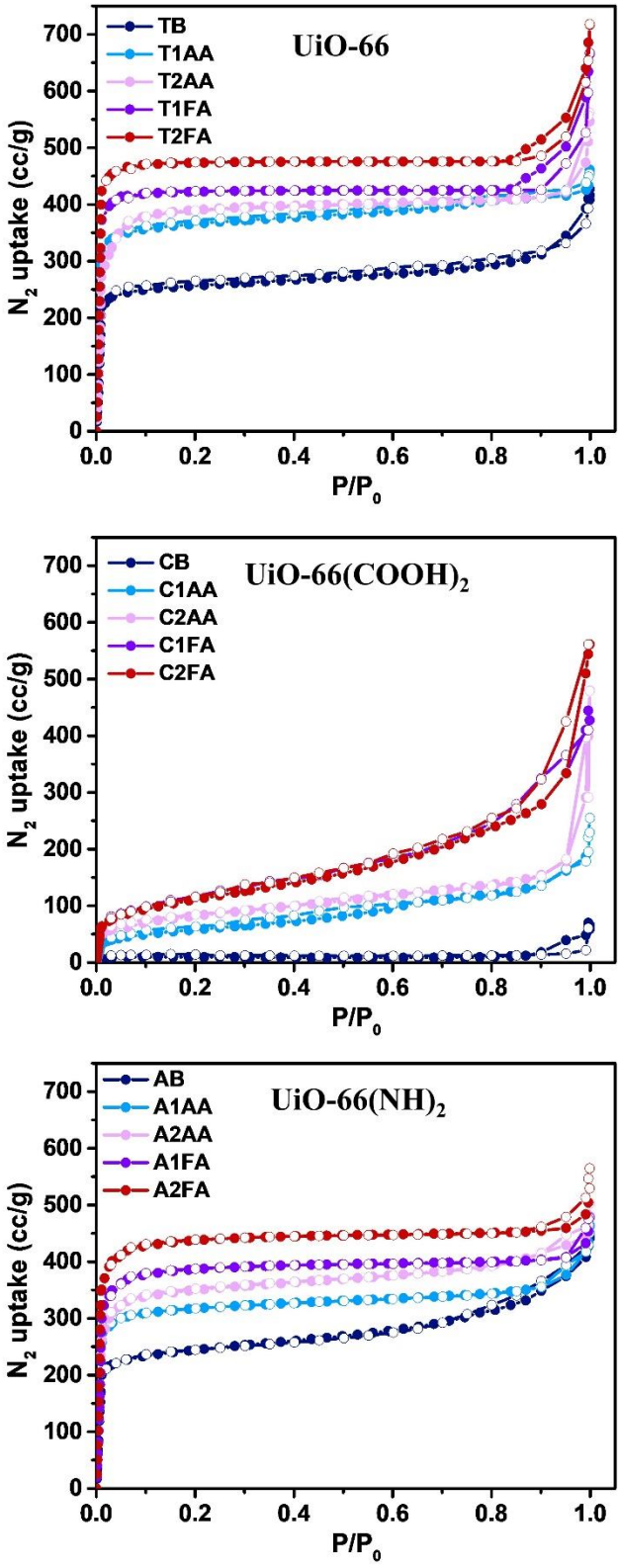


**Figure 24:** Nitrogen adsorption-desorption isotherms recorded at 77K for all 15 MOFs catalysts synthesized,• Adsorption ◦ Desorption.

**Table 5:** Quantitative results of the characterization and testing of the 15 MOFs catalysts synthesized. Particle size [a] is estimated using SEM and Particle size [b] is calculated using the Scherrer equation.

| MOF | BET surface area ($m^2/g$) | Pore volume ($cm^3/g$) | Defects number | Particle size [a] (nm) | Particle size [b] (nm) | Conversion to butyl butyrate |
|---|---|---|---|---|---|---|
| **TB** | 1049 | 0.348 | 1.36 | 108 ± 19 | 87 | 57.2 |
| **T1AA** | 1490 | 0.515 | 1.50 | 273 ± 53 | 224 | 70.4 |
| **T2AA** | 1593 | 0.548 | 1.53 | 623 ± 206 | 410 | 78.1 |
| **T1FA** | 1695 | 0.645 | 1.72 | 143 ± 23 | 125 | 83.6 |
| **T2FA** | 1813 | 0.728 | 1.86 | 477 ± 151 | 331 | 89.1 |
| **CB** | 51 | 0.014 | 0.88 | - | - | 63.3 |
| **C1AA** | 268 | 0.047 | 1.38 | - | 9 | 77.4 |
| **C2AA** | 376 | 0.052 | 1.44 | - | 24 | 81.5 |
| **C1FA** | 517 | 0.105 | 1.9 | - | 7 | 88.2 |
| **C2FA** | 522 | 0.121 | 1.93 | - | 17 | 91.5 |
| **AB** | 1016 | 0.301 | 1.50 | 55 ± 7 | 48 | 64.2 |
| **A1AA** | 1294 | 0.453 | 1.67 | 318 ± 38 | 285 | 69.6 |
| **A2AA** | 1434 | 0.468 | 1.73 | 340 ± 47 | 311 | 77.2 |
| **A1FA** | 1570 | 0.591 | 1.87 | 54 ± 8 | 51 | 80.3 |
| **A2FA** | 1723 | 0.634 | 2.02 | 202 ± 37 | 172 | 84.7 |

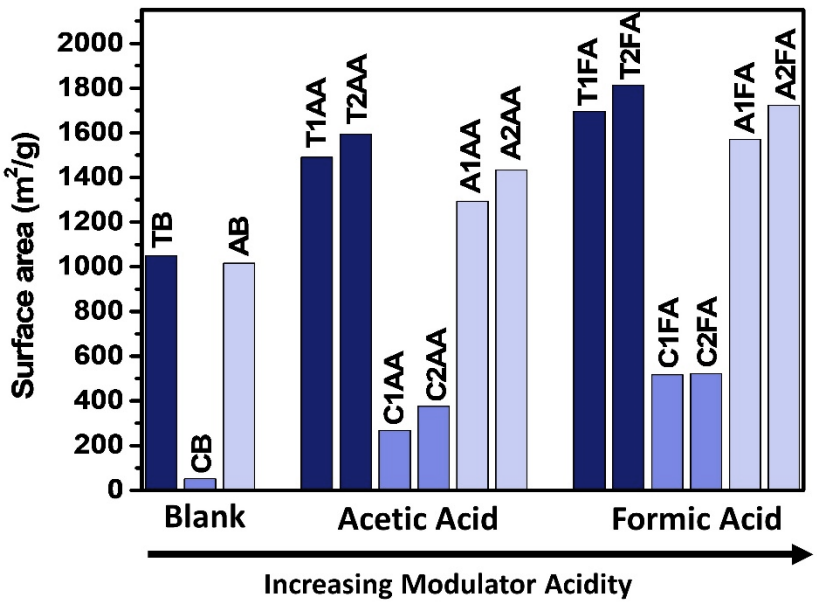


**Figure 25:** The change in the surface area of the 15 MOFs catalysts synthesized with the modulation conditions used during synthesis

In order to study the thermal stability of the MOFs and to determine the number of missing linkers in the defected MOF structures, TGA analysis on the MOF samples was performed and the results are shown in **Figure 26**. The obtained TGA curves display the change of the mass of the 15 samples with temperature starting from 30°C and up to 1000°C. The TGA curves are normalized so that the final weight-loss is set to be 100%, which is represented by the horizontal black pointed curve, $WL_{final}$. Moreover, $WLP_{th}$ is the high end of the theoretical weight-loss expected from each structure as calculated in the Annex and based on previous reports[79]. The lower end of this weight-loss is the black horizontal pointed line indicated as $WL_{final}$. The dashed colored curves represent the DTG curves (right axis), or the first derivatives of the TGA curves, which are very helpful in determining the phases where major weight-losses have occurred.

Throughout the temperature range of the analysis, there are three main weight-losses that could be observed regardless of the structure of the MOF or the modulation synthesis conditions. The first weight-loss occurs between 35$^{o}$C and 100$^{o}$C, where the water adsorbed onto the structure of the MOF is volatilized. The second weight-loss is usually attributed to the removal of the monocarboxylate ligands, or to what is known as the dehydroxylation of the zirconium clusters, and it extends from 100$^{o}$C till $T_{link}$ indicated in **Figure 26.** $T_{link}$ is the temperature after which the weight-loss is attributed to the combustion of the linker [89, 126, 127]. The third major weight-loss in the TGA curve is thus attributed to the destruction of the framework by the combustion of the organic linker. This weight-loss is expressed by a clear sharp peak in the case of UiO-66, but with an extra merged peak in the case of functionalized frameworks. This merged peak was attributed to the combustion of the functional groups being covalently bound to the organic linker of the framework. The temperature after which the weight-loss in the framework is attributed to the combustion of the linker, $T_{link,}$ is approximated as the temperature reached at the end of the DTG peak attributed to the combustion of the linker [79]. $T_{link}$ is taken to be 390$^{o}$C, 300$^{o}$C, and 305$^{o}$C for UiO-66, UiO-66(COOH)$_2$, and UiO-66($NH_2$) respectively. [128, 129, 143] It should be noted here that the TGA curve for the CB sample follows the same trend of other UiO-66(COOH)$_2$ samples, which is that of the combustion of a framework composed of the same cluster/linker combination, suggesting that it is an amorphous MOF [137].

Almost all of the studies that have focused on the presence of defects in the MOFs' structures have used TGA to quantitatively account for these defects [79, 128]. The theory behind this is as follows; if the theoretical weight-loss plateau attributed to the linker based on the molecular weight of the structure is higher than the experimental

one calculated based on TGA, then this difference in weight-loss is attributed to missing linkers in the framework that could quantitatively describe the number of defects in the structure[79]. The higher end of the experimental weight-loss plateau attributed to the linker combustion for each MOF is the horizontal line passing through the intersection between the TGA curve and the vertical line $T_{link}$, but these lines are not represented in **Figure 26** to keep it clear.

Observing the TGA curves of all 15 MOFs, It is noticed that the experimental weight-loss attributed to the linker combustion is clearly lower than the theoretical one. This means that all of the 15 structures are linker-deficient and have structural defects. However, the interesting trend is that the weight-loss due to the linker combustion is lower when the concentration of the same modulator is increased. Furthermore, this same weight-loss is lower when 100 equivalents of FA are used in the synthesis instead of 200 equivalents of AA. The structures are thus more defective when using FA even for lower concentrations as reported in previous studies for UiO-66 [79].

Following a method provided in the literature[79], the number of missing linkers for each of the 15 studied MOFs had been calculated, and the results are given in **Table 5**. It could be clearly seen that the number of linker deficiency significantly increases from 1.36 in TB to 1.86 in T2FA, and from 0.88 in CB to 1.93 in C2FA, and from 1.50 in AB to 2.02 in A2FA for UiO-66, UiO-66$(COOH)_2$, and UiO-66$(NH_2)$ respectively. This trend of the increasing number of missing linkers with the increase in modulator concentration/acidity comes in line with reports on the competitive role of the modulator which acts as a reacting agent and replaces the linker in the MOF structure [106, 144].

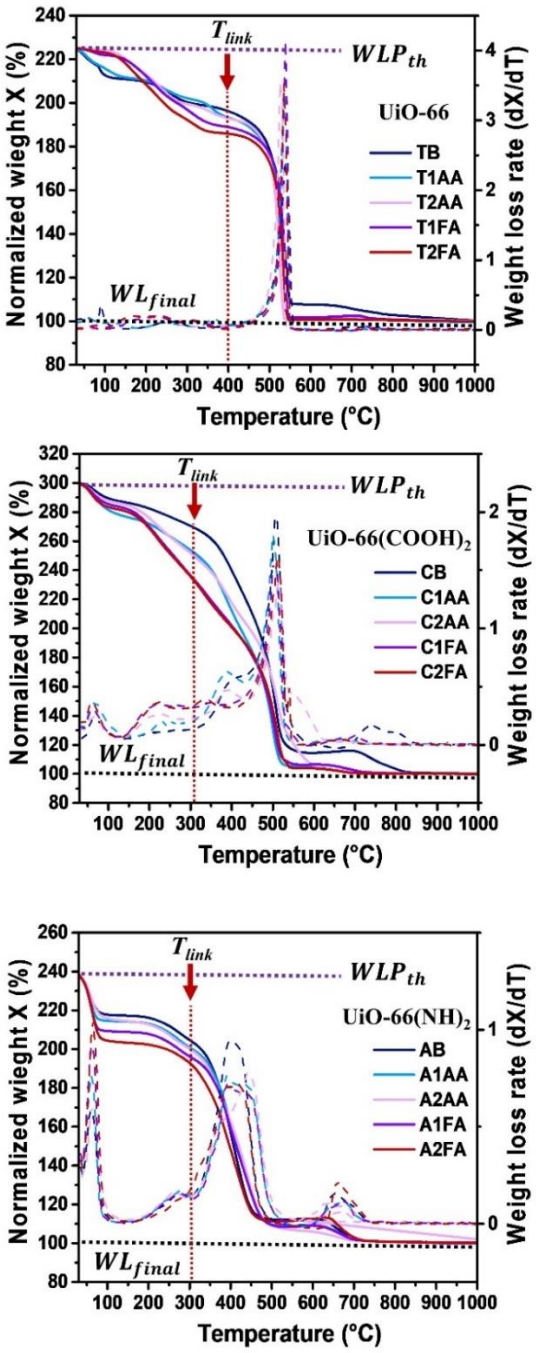


**Figure 26:** TGA and DTG curves of the 15 studied MOFs catalysts. solid lines, left axis – TGA curve, Dashed lines, right axis – DTG curve. (a) UiO-66 (b) UiO-66(COOH)$_2$ (c) UiO-66(NH$_2$). (…) Lower black pointed horizontal line represents the lower end of the theoretical TGA weight-loss plateau, $WL_{final}$ (…) upper violet pointed horizontal line represents the upper end of the theoretical TGA weight-loss plateau, $WLP_{th}$ (⋮) vertical pointed red line represents the temperature of the combustion of the linker, $T_{link}$

### *2. MOFs testing in esterification reaction for butyl butyrate production*

a. Conversion to butyl butyrate

Following their synthesis and full characterization, all MOFs had been used as heterogeneous catalysts in the liquid phase esterification reaction of butyric acid in presence of butanol for butyl butyrate production. The reaction was allowed to occur for 24 hours using 2 wt% of MOF catalysts, while one reaction was performed using the same loading of the homogeneous $H_2SO_4$ acid catalyst. Samples were regularly taken from the reaction medium and analyzed using GC. The results showing the evolution of the conversion to butyl butyrate over time are given in **Figure 27**, while **Figure 28** compares the conversion obtained after 24 hours of reaction using all different 15 MOF samples. It should first be noted that the reaction of butyric acid and butanol yielded only butyl butyrate and water at the end of the 24 hours, and thus the selectivity to butyl butyrate was 100%.

**Figure 27** indicates a clearly noticeable trend in the conversion to butyl butyrate using all three different linkers in MOFs. The lowest conversion is obtained using the catalysts synthesized without the use of a modulator (TB, CB, and AB), then the conversion increases using the catalysts synthesized in the presence of 100 equivalents of AA (T1AA, C1AA, A1AA), 200 equivalents of AA (T2AA, C2AA, A2AA), 100 equivalents of FA (T1FA, C1FA, A1FA), and 200 equivalents of FA respectively (T2FA, C2FA, A2FA). Moreover, the simple manipulation of adding 200 equivalents of FA into the synthesis mixture of the used MOF leads to an increase in conversion of about 32%, 28%, and 20% for UiO-66, UiO-66$(COOH)_2$ and UiO-66$(NH_2)$ respectively after 24 hours of reaction (**Figure 27**). Furthermore, the conversion obtained using 2 wt% loading of the MOFs synthesized using 200 equivalents of FA is considerably

higher than that obtained using 5 wt% loading (250 mg) of the same MOFs using only 80 equivalents of AA, as reported in our previous study using the same reaction conditions[143]. This demonstrates how by only optimizing the synthesis conditions of the same MOF structure, the catalytic activity could be significantly enhanced, and thus less MOFs' loading would be needed to obtain higher conversions for the same reaction conditions. This trend of increased catalytic activity for higher modulator concentration and lower modulator pH is becoming more and more famous for the standard UiO-66, but it is reported for the first time in this study for the functionalized structures that have been noted for their defects in previous studies [140] [141].

As expected, $H_2SO_4$ still performed better especially at the beginning of the reaction. This suggests that the reaction is not limiting the conversion and that the mass transfer limitations could be affecting the performance of MOFs as will be explained further later on. Furthermore, at the end of the reaction after 24 hours, a similar conversion to butyl butyrate of 95% and 91% was achieved using $H_2SO_4$ and C2FA respectively.

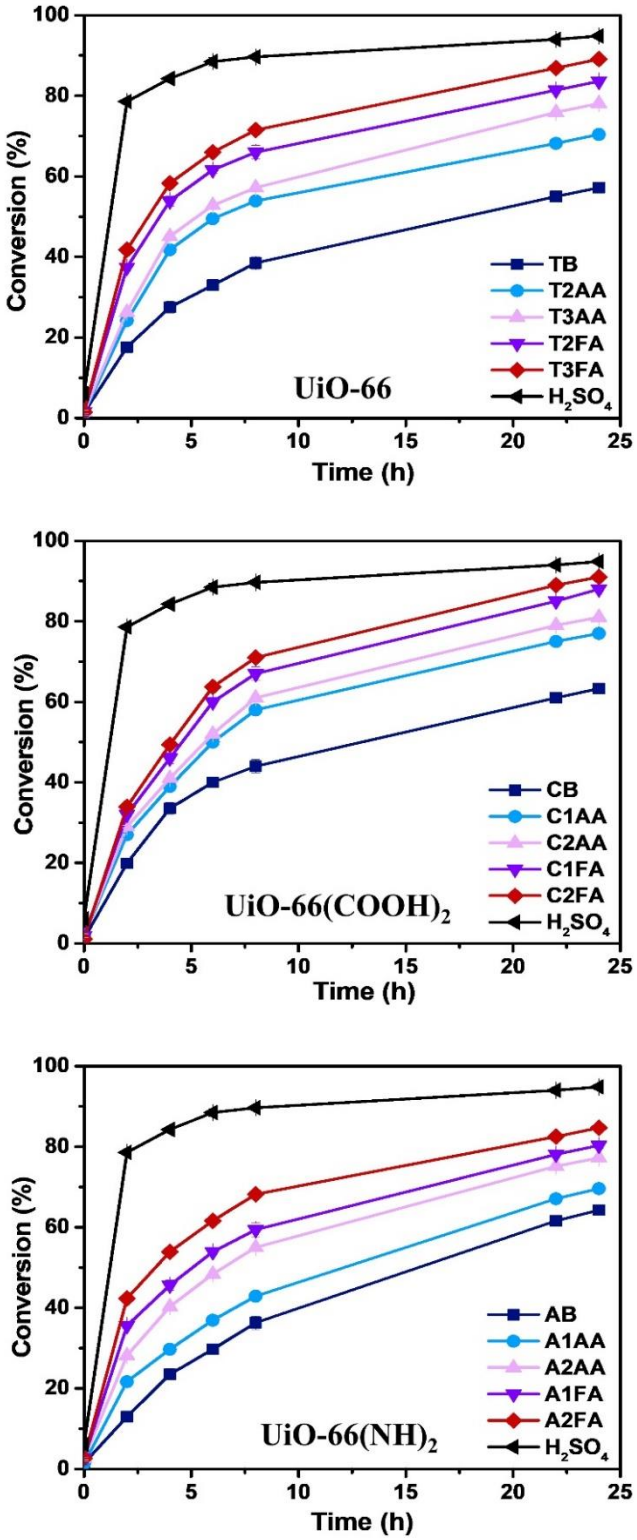


**Figure 27:** The evolution of conversion to butyl butyrate under 2 wt% of each MOF catalyst

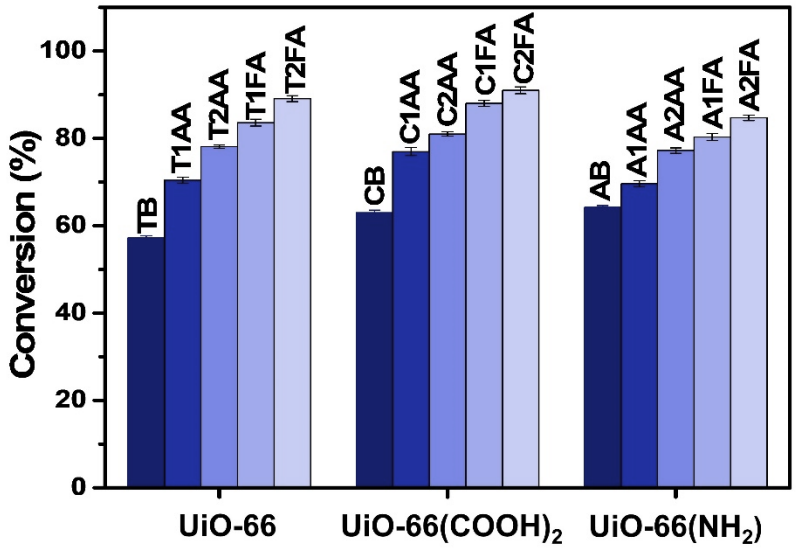


**Figure 28:** Conversion to butyl butyrate obtained after 24 hours of reaction under 2 wt% of the 15MOFs catalysts

In order to make sure that the stirring speed used of 500 RPM was enough to overcome external mass transfer limitations, T2FA, C2FA, and A2FA were used as catalysts in the esterification reaction at different stirring speeds of 200 RPM and 800 RPM. The results obtained were compared in **Figure S10** that shows no noticeable increase in the conversion obtained at a stirring speed higher than 500 RPM. In fact, the conversion seems to be lower at 200 RPM for all three MOFs, which reveals an external mass transfer limitation at this stirring speed. However, as the stirring speed increases to 500 RPM, the effect of the external mass transfer starts to fade away as the conversion does not continue to increase at a stirring speed of 800 RPM. This suggests that a stirring speed of 500 RPM is sufficient for this application to overcome external diffusion limitations.

Following their testing in the esterification reaction, the 15 MOF catalysts were washed with DMF and DCM as detailed in the Annex, and their PXRD patterns were

recorded. The results shown in **Figure S7** show that the PXRD patterns of synthesized samples remain the same after their use as catalysts, which reveals their stability in the application they are used for. Additionally, to ensure that MOFs catalytic activity and stability are retained over several usages, T2FA, C2FA, and A2FA were recycled and reused in the esterification reaction for 4 consecutive cycles. The conversion to butyl butyrate obtained in each of the 4 cycles is indicated in **Figure 29**. As can be seen, only negligible changes in the conversion to butyl butyrate could be noticed which shows that the synthesized MOFs retain their catalytic activity. Furthermore, the PXRD patterns and SEM images of the recycled MOFs after their use in 4 consecutive reactions are shown in **Figure S8** and **Figure S9.** The sharp narrow peaks obtained in the PXRD patterns in **Figure S8** along with the SEM images in **Figure S9** show the retained morphology of the recycled MOFs and thus reveal their stability in the relevant application of this study.

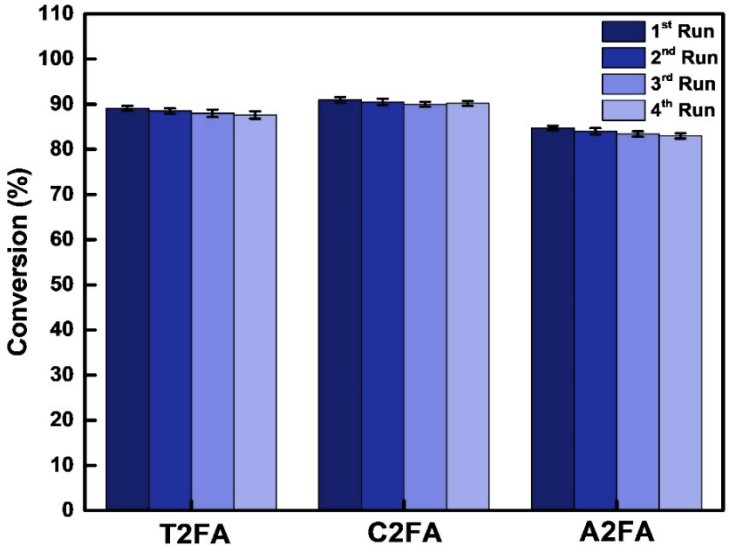


**Figure 29:** Conversion to butyl butyrate obtained using T2FA, C2FA, and A2FA recycled over 4 consecutive esterification reactions

b. The effect of linker deficiency, surface area, and particle size on conversion

Many parameters of the MOF structure change when the modulator used and its concentration change, which is clearly reported in the results of the previously discussed MOFs characterization (**Table 5**). Thus, the effect of the change of the modulation synthesis conditions on the conversion to butyl butyrate should be discussed in light of the subsequent change in MOFs' characteristics and their effect on the reaction mechanism. To this end, the change in the main parameters that could have had an effect on the catalytic activity of the MOFs, are compared to the subsequent change in the conversion to butyl butyrate in **Figure 30** to **Figure 32**, to evaluate the correlation between the obtained conversions and the structural properties.

**Figure 30** shows the change in conversion to butyl butyrate compared to the change in the number of missing linkers in the MOF catalysts. The reason behind the interest in defects density in the framework is that the non-functionalized and defect-free UiO-66 has theoretically no open active sites, and UiO-66 samples synthesized with very low defects number exhibits small catalytic activity[102]. When successfully used for catalytic purposes, its catalytic activity was thus attributed to the effect of missing-linker or missing-cluster defects, which both yield a linker-deficient framework, that could unintentionally occur during synthesis[108]. Moreover, having a defective UiO-66 cluster means that a number of the BDC linkers are removed from the $[Zr_6O_4(OH)_4]^{12+}$ cluster, leaving behind open Lewis acid sites on two adjacent Zr atoms for every missing linker[20]. One of the ways this charge imbalance could be compensated, in presence of water, is by the coordination of a hydroxyl group to the Zr cluster [52, 107]. The activity of the three MOFs in the esterification reaction suggests that the active Lewis sites could have been converted into Brønsted acid sites, which is

possible through reaction with water [20, 107]. This means that an increase in the number of defective sites offers additional catalytic centers [102, 106, 108], which comes in accordance with the results obtained in **Figure 28**. Additionally, **Figure 30** and **Figure 28** show that the conversion changes in the same fashion for all three organic linkers used as it increases when the number of missing linkers increases.

Furthermore, regardless of the functional group attached to the linker, all three MOF structures have the same Zr-cluster, and having a higher number of missing linkers will lead to more open active sites on the SBU[20]. The obtained results show a consistent correlation between the catalytic activity of the MOF catalyst and the number of defects per cluster in this MOF structure. This had set the foundation to propose a mechanism in which the presence and increase in the number of these defects plays a predominant role as catalytic centers for reactants' adsorption and activation in MOFs with different functional groups on their organic ligands. In a recent study[105], a detailed reaction mechanism was proposed based on this principle for a hydrated UiO-66 cluster, where two water molecules would compensate for a missing linker. One of these two water molecules was suggested to be chemisorbed to form a Zr-OH group with hydrogen on the $\mu_3$-oxygen, and the other would be physisorbed on the adjacent Zr. In this case, the carboxylic acid would bind to a Zr atom by displacing the physisorbed water molecule and subsequently react with the alcohol chemisorbed on the neighboring Zr atom. The presence of water was thus shown to help the formation of stable complexes between the two reactants, namely carboxylic acid and alcohol, with the MOF cluster as the catalyst[105]. The previously proposed mechanism seems to be backed-up by the experimental data obtained as one of the ways the reaction is taking

place, and it could be concluded that this reaction mechanism extends to include functionalized UiO-66 structures.

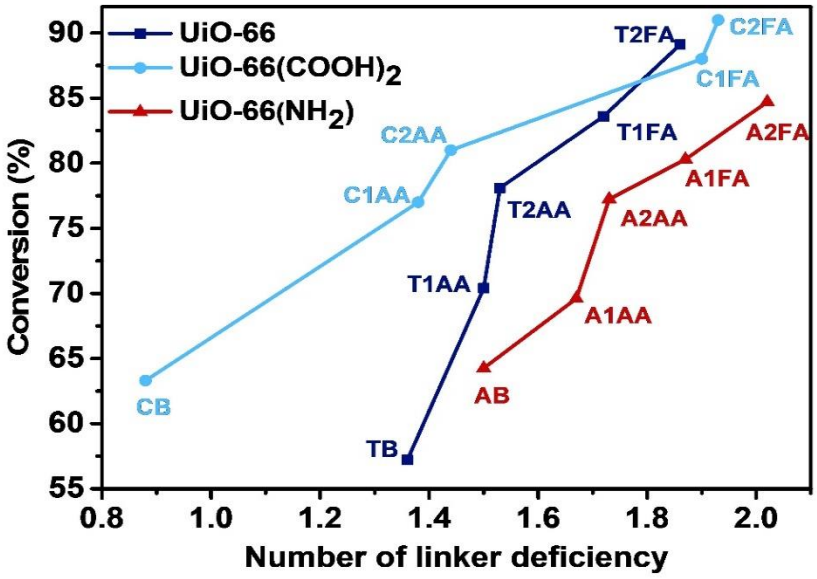


**Figure 30:** Trends obtained by plotting the change in conversion to butyl butyrate against the number of missing linkers in the corresponding MOF catalyst used

In addition, other parameters could have played a role in the increase of the catalytic activities with the increase in modulator concentration and decrease in modulator pKa. Moreover, **Figure 31** shows the change in the conversion to butyl butyrate compared to that of the BET surface area for UiO-66, UiO-66($COOH)_2$, and UiO-66($NH_2$) synthesized in different modulation conditions. One of the most interesting traits in MOFs in general, and specifically in catalysis, is their significantly large surface areas. In heterogeneous catalysis, the activation of the reactants and the subsequent reactions in terms of bonds making and breaking take place at the surface of the catalyst[20]. Thus, in theory, having a catalyst with the same characteristics but with a larger surface area should increase its catalytic activity as it would have more catalytic centers exposed to the reactants. The previously mentioned could have also contributed

to the trend obtained in **Figure 31,** where the higher the surface area for a given MOF structure, the higher is the conversion to butyl butyrate.

In addition, **Figure 32** shows the change in the conversion along with that of the catalysts' particle size. At a first glance, no clear pattern could be noticed in the figure, but taking into account the modulation synthesis condition, a few observations could be made. For all organic linkers, the MOFs synthesized in the presence of modulators have a bigger particle size than those synthesized without one, but they also have higher catalytic activity. Moreover, the increase in modulator concentration increases the particle size along with the catalytic conversion. However, using FA yields smaller particles that have higher catalytic activity than their bigger counterparts synthesized using AA as a modulator. This makes the evaluation of the intra-molecular transport limitations challenging at this point, especially that the synthesis of two MOFs with similar properties but different particle sizes had been reported to be very difficult [20]. However, this stresses on the predominant role of active sites created by defects which increase the catalytic activity of MOFs even for significantly bigger particle sizes.

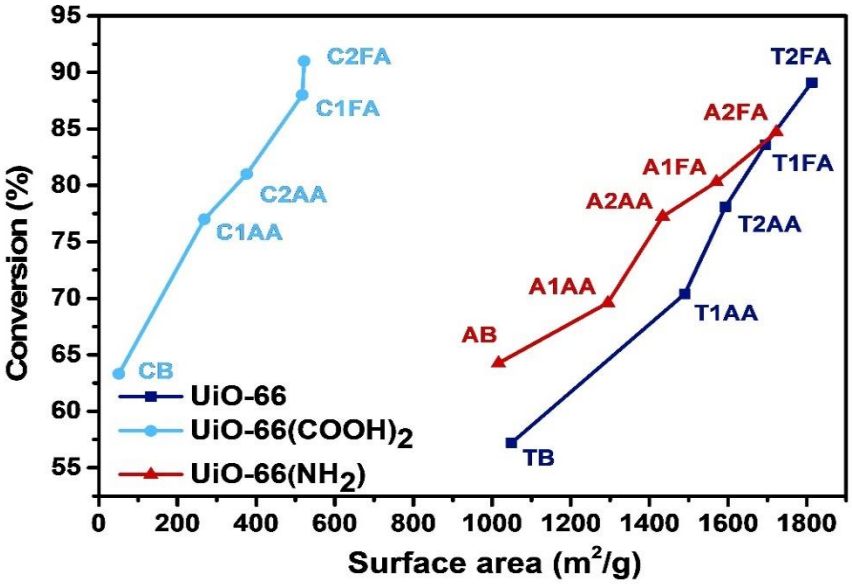


**Figure 31:** Trends obtained by plotting the change in conversion to butyl butyrate against the surface area of the corresponding MOF catalyst used

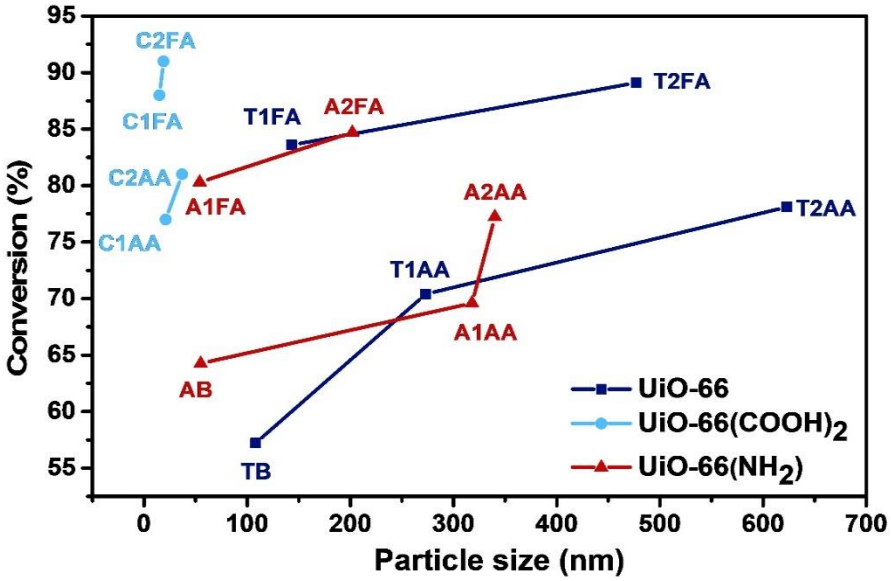


**Figure 32:** Trends obtained by plotting the change in conversion to butyl butyrate against the particle size of the corresponding MOF catalyst used

To conclude this section, it is important to categorize the discussed variables in terms of their influence on the catalytic activity of the MOFs. To start with, the particle size did not have a direct and clear correlation with the conversion to butyl butyrate, which means that its effect comes last compared to the other changes taking place in the MOF structure. However, although both the number of defects and the surface area of each MOF had an almost linear correlation with the conversion, the number of defects is still considered to be the primary factor affecting the conversion for each MOF structure. In fact, the increase in the linker deficiency not only means an increase in the abundance of active sites, but it also means making these sites more accessible by offering a more open MOF structure. In other words, the increase in the number of defects causes this noted increase in the surface area, which makes the effect of the defects on the conversion primary compared to that of the surface area since it directly influences the structure of the MOF, causing the other changes to occur.

c. The effect of organic linker on conversion

The previous conclusions hold true if the results for each MOF are observed separately. However, comparing the results for UiO-66, UiO-66($COOH)_2$, and UiO-66($NH_2$), new assumptions could be made explaining why the previous conclusions on the predominant role of the defects do not seem to extend when the organic ligand used changes. In fact, the functional groups covalently bind on the MOF structure offer incredible opportunities for enhancing the catalytic properties of MOFs as supported by the obtained results [20, 52].

Following the same structure as before, **Figure 30** will be discussed first. Comparing the three curves in **Figure 30** together, the three MOFs structures yield

similar conversions for significantly different number of defects, such is the case when comparing points C1AA, T2AA, and A2AA. Additionally, comparing points of a similar number of defects such as C2AA, T1AA, and AB, the conversion obtained using the three different structures is considerably different. Based on the above discussion, this means that the dependence of the conversion on the number of defects cannot be generalized when structures with different organic linkers are being compared. The choice of the organic ligand thus seems to have a pronounced effect on the catalytic activity of the MOFs when compared to the effect of the defect density. Additionally, the trend in relative catalytic activity for structures with different organic linkers seems to be changing with the number of defects per cluster. Moreover, the UiO-66$(COOH)_2$ samples yield higher conversion than both counterparts for a number of missing linkers lower than that of around 1.78 per cluster, despite its lower defect density. This higher catalytic activity was attributed to the uncoordinated COOH groups bind to its linker, which could act as important catalytic centers being strong Brønsted acid sites. These uncoordinated acid functional groups thus seem to act as adsorption and activation centers for the butyric acid, which adds up to the active sites caused by the missing linkers.

Although the catalytic activity of UiO-66 depends solely on the presence of the defects on the cluster, this does not seem to be the case in UiO-66$(COOH)_2$. In such a case, another reaction mechanism including the COOH group is assumed to be responsible for this increase in conversion for the same number of defects. The esterification reaction, in this case, could have been initiated by the COOH group donating a proton to the butyric acid. This would then be followed by an attack of the nucleophilic hydroxyl group of the butanol yielding butyl butyrate with the subsequent

release of a water molecule as shown in **Figure 33**. Additionally, although **Figure 31** shows that UiO-66(COOH)$_2$ has a considerably lower surface area and porosity, **Figure 32** indicates that it also benefits from smaller particle size. In fact, smaller catalyst particles have a higher outer surface area with active sites easier to access than those inside the porous network of the MOFs. This highlights the importance of the careful selection of the modulator since using the FA resulted in smaller crystal size, higher defect density, and higher surface area, which is very beneficial to the catalytic activity of the MOFs being used.

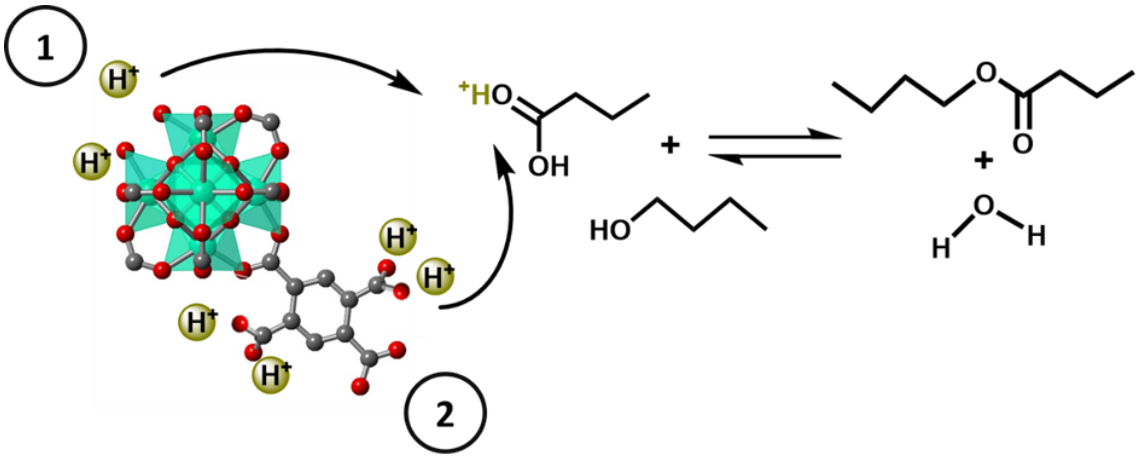


**Figure 33:** Mechanism of the esterification reaction under UiO-66(COOH)$_2$ catalyst showing two sources of active sites (1) the defective sites on the cluster and (2) the functional groups on the linker

However, this higher catalytic activity compared to UiO-66 changes as the two curves cross around a defect density of 1.78 where the catalytic activity of T2FA seems to be higher than that of C1FA even for lower defects number. This change in trend could be explained by taking into account the negative impact of having bulky functional groups, indicated by the pore volume and surface area data in **Table 5**, which

could be blocking the way of reactants to active sites inside the porous network of the framework. The structure of UiO-66 allows for easier diffusion of the reactants to reach the additional active sites inside the pores, which significantly boosts its catalytic activity when the defect density increases [52]. On the other hand, the COOH groups attached to the linker of the cluster seem to be hindering the internal diffusion which makes part of the additional active sites inaccessible to reactants. Although the COOH groups could offer substituent catalytic centers, the increase of the defects density above 1.78 linkers per cluster seems to have made UiO-66 more abundant in accessible active sites. The synthesis of UiO-66 samples with a higher number of defects is required to know whether this trend changes again as the porosity of UiO-66$(COOH)_2$ further increases with the increased number of defects allowing for more accessibility of internal active sites.

Considering the amino-functionalized UiO-66, a different kind of change in trend could be noticed. Using the catalyst AB with defects number slightly higher than TB yields considerably better conversion to butyl butyrate. This suggests that having another AB sample with the same defects number as that of TB could probably still yield higher conversion. The reason behind this higher catalytic activity of UiO-66$(NH_2)$ for a lower number of defects was previously attributed to a dual acidic-basic activation mechanism[52]. Moreover, the free $NH_2$ groups could increase the nucleophilic character of the butanol oxygen, which drives its condensation with the butyric acid for butyl butyrate production[52]. This highlights the role of having functional groups grafted to the organic linker with the ability to enhance the conversion by dual activation mechanism [20]. However, as the number of defects increases, this trend seems to be changing since the conversion using the standard UiO-66 becomes

significantly higher than that of UiO-66($NH_2$) even for higher defects number of the latter. In fact, the increase in the conversion to butyl butyrate as the number of defects increases in UiO-66 seems to be much more pronounced than its functionalized counterparts. This could again be due to having some of the active sites inside the porous network inaccessible for the reactants to bind to due to the presence of the $NH_2$ group which could be causing intramolecular transport limitations. Such a claim is supported by the results shown in **Figure 27** and **Figure S10** where it is concluded that it is not the slow reaction, nor the external mass transfer that is limiting the conversion to butyl butyrate. In this case, the benefit of having an acidic functional group attached to the linker is that it becomes itself an active catalytic center that could compensate for the inaccessible active sites.

### *3. Conclusion*

This study investigates the catalytic activity of UiO-66-based samples using the coupled effect of functionalizing the organic linker and systematically introducing defects onto the metal cluster. Catalyst' synthesis was optimized to enhance the production of butyl butyrate, a novel biofuel additive. Five different samples of each of UiO-66, UiO-66($COOH)_2$, and UiO-66($NH_2$) were synthesized using different modulation conditions, and a systematic increase in the number of defects was observed with increased acidity and concentration of modulators. A direct correlation between the number of defects and the surface area and pore size was observed, whereas the particle size trend seemed to be different. The increase in the number of defects significantly increased the conversion of the esterification reaction of butyric acid and butanol to butyl butyrate. A conversion improvement from 57.2% to 89.1%, from 63.3% to 91.5%,

and from 64.2% to 84.7% is observed when adding 200 molar equivalents of formic acid to the synthesis mixtures of UiO-66, UiO-66($COOH)_2$ and UiO-66($NH_2$) respectively. Nonetheless, UiO-66($COOH)_2$ yielded the best conversion even for a lower number of defects, which suggests that the uncoordinated COOH groups introduced to the linker were involved as active catalytic centers along with the defective sites on the cluster. The trends in conversion evolution with respect to the number of defects suggests though that UiO-66 could overcome the catalytic activity of both counterparts if its defect number increased. This was attributed to the higher surface area due to its open structure that allows for better internal diffusion of the butyric acid than the functionalized structures. MOFs engineering that was demonstrated in this study could thus be generalized to include other organic linkers suitable for different applications. This approach could be coupled with the systematic introduction of defects as a tool to fine-tune properties such as surface area, pore size, and particle size and as means to control the effect of diffusion limitations.

## C. MULTIVARIATE (MTV-MOFS) OR MIXED-LINKER APPROACH

### *1. Structural Characterization*

a. Powder X-ray diffraction (PXRD)

Before the PXRD patterns recording, the MOF samples were placed in a vacuum oven at 120°C for 72 hours to ensure most of the solvent molecules trapped inside the pores are removed. This is important in order to dilute the effect of the solvation that is known to cause cell expansion while avoiding dehydroxylation of the structures which causes cell contraction. [118, 145] The recorded PXRD patterns of the 9 synthesized

MOF samples are shown in **Figure 34** and reveal well-defined peaks that are in complete agreement with the simulated patterns for UiO-66, which indicates the high crystallinity and the phase purity of all the samples. In the case of a physical mixture with two phases present, it is expected that the peaks would be split or show shoulder peaks [145], which is obviously not the case as is clear in **Figure 34**. Moreover, **Figure S11** in the SI file displays a narrow 2theta range of the pattern that highlights a slight shift to a lower angle of the characteristic peaks of the MOF structure upon the increased incorporation of the functionalized linkers for both series of MTV-MOFs. This reflects a cell expansion caused by the gradual introduction of functionalized ligands in the structure which is reported previously for other MTV-MOFs but highlighted herein for the first time for these structures. The synthesized structures thus seem to follow Vegard's law confirming further the overall homogeneous incorporation of the functionalized linkers in the MOFs and that any potential short-range heterogeneity does not seem to have an important effect. [118, 145] Peaks that figure in the pattern recorded for UiO-66 are the narrowest, and those of UiO-66$(COOH)_2$ are the broadest. This reveals a smaller particle size of the functionalized structures as will be further discussed with SEM results.

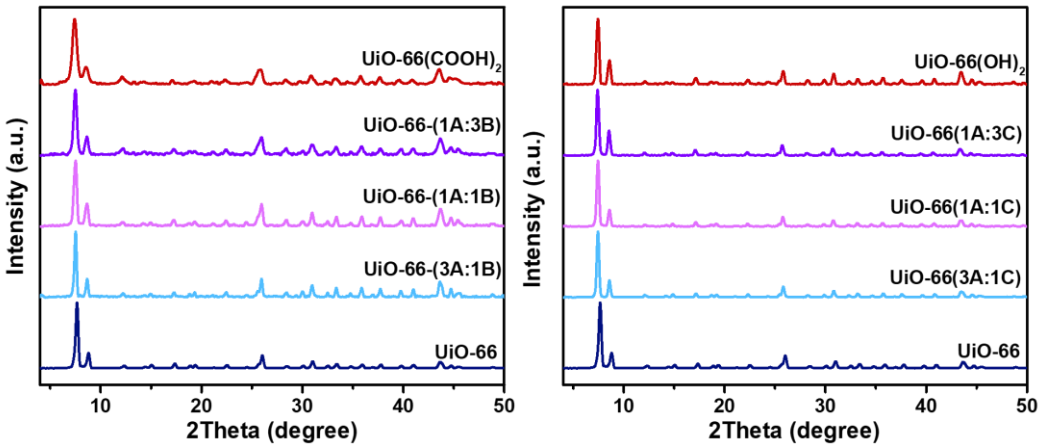


**Figure 34:** PXRD patterns of the activated single component and MTV-UiO-66 catalysts synthesized

b. Proton Nuclear Magnetic Resonance ($^1$H-NMR)

$^1$H-NMR spectra were recorded to monitor the level of incorporation of each linker in all synthesized samples and results are shown in **Figures S12** to **S17** in the supporting information file. A singlet at a chemical shift $\delta$ of around 8.43 ppm is present in all spectra and it was attributed to the residual DMF inside the pores of the MOFs. The aromatic zone of the $^1$H-NMR spectrum reveals a singlet at around $\delta$=7.85 ppm in all spectra as well and it is attributed to the four equivalent aromatic protons of the terephthalic acid. For MTV-MOFs, a singlet appears at $\delta$=7.49 ppm in the spectra of the structures synthesized with the addition of 1,2,4,5-benzenetetracaboxylic acid, for which this singlet had been attributed. Similarly, a singlet is present at $\delta$=7.29 ppm for structures synthesized with the addition of 2,5-dihydroxyterephthalic acid for which this singlet was attributed. The percentage of actual incorporation of each of the linkers in every structure was calculated based on the results of the $^1$H-NMR spectra obtained and

the results are shown in **Figure 35**. As can be seen, the gradual increase in the amount of the functionalized linker in the synthesis mixture led to an increase in the percent ratio of their actual incorporation in the framework as reflected by the increasing intensity of the $^{1}$H-NMR signals associated with these linkers (**Figure 35**). This clearly demonstrates the incorporation of both organic linkers in the MOF crystals. However, it seems that the level of incorporation was preferential with respect to terephthalic acid for both MTV-MOF systems as it is always higher than the starting molar ratios used.

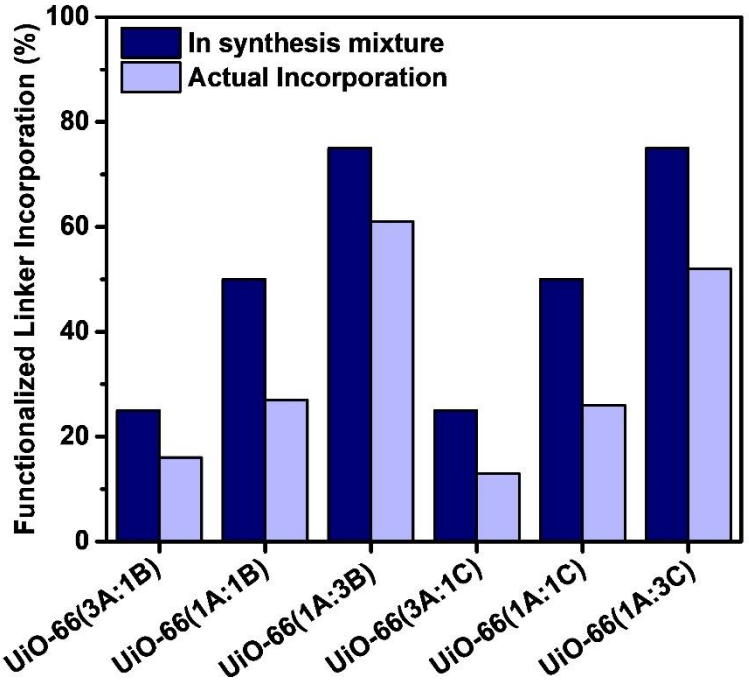


**Figure 35:** A comparison between the starting percentages of functionalized linker versus its actual incorporation in the framework of the different MTV-MOFs as determined from $^{1}$H-NMR. The functionalized linker being 1,2,4,5-benzenetetracarboxylic acid in UiO-66(3A:1B), UiO-66(1A:1B) and UiO-66(1A:3B), and 2,5-dihyroxyterephthalic acid in UiO-66(3A:1C), UiO-66(1A:1C) and UiO-66(1A:3C).

c. Scanning Electron Microscopy (SEM)

**Figure 36** shows the SEM images taken for all the 9 MOF structures synthesized. Particle sizes for all synthesized MOFs are also calculated based on PXRD patterns using the Scherrer equation and are reported in **Table 6**. UiO-66 crystals have a clear octahedral shape with the highest particle size among other samples (331 nm). MTV-MOFs constructed with the addition of the 1,2,4,5-benzenetetracarboxylic acid, namely UiO-66(3A:1B), UiO-66(1A:1B), and UiO-66(1A:3B), seem to have crystals with particle sizes decreasing with the decreased level of incorporation of terephthalic acid. Their particle sizes seem to decrease from levels similar to UiO-66 (331 nm) until they become similar to that of UiO-66$(COOH)_2$ crystals (28 nm) which reveal small inter-grown spheres. This trend is not maintained for the MTV-MOFs incorporating 2,5-dihyroxyterephthalic acid, namely UiO-66(3A:1C), UiO-66(1A:1C), and UiO-66(1A:3C), as they all seem to have similar small particle sizes around 50 nm with sphere-like morphology, while UiO-66$(OH)_2$ reveal bigger clear truncated octahedral crystals (252 nm).

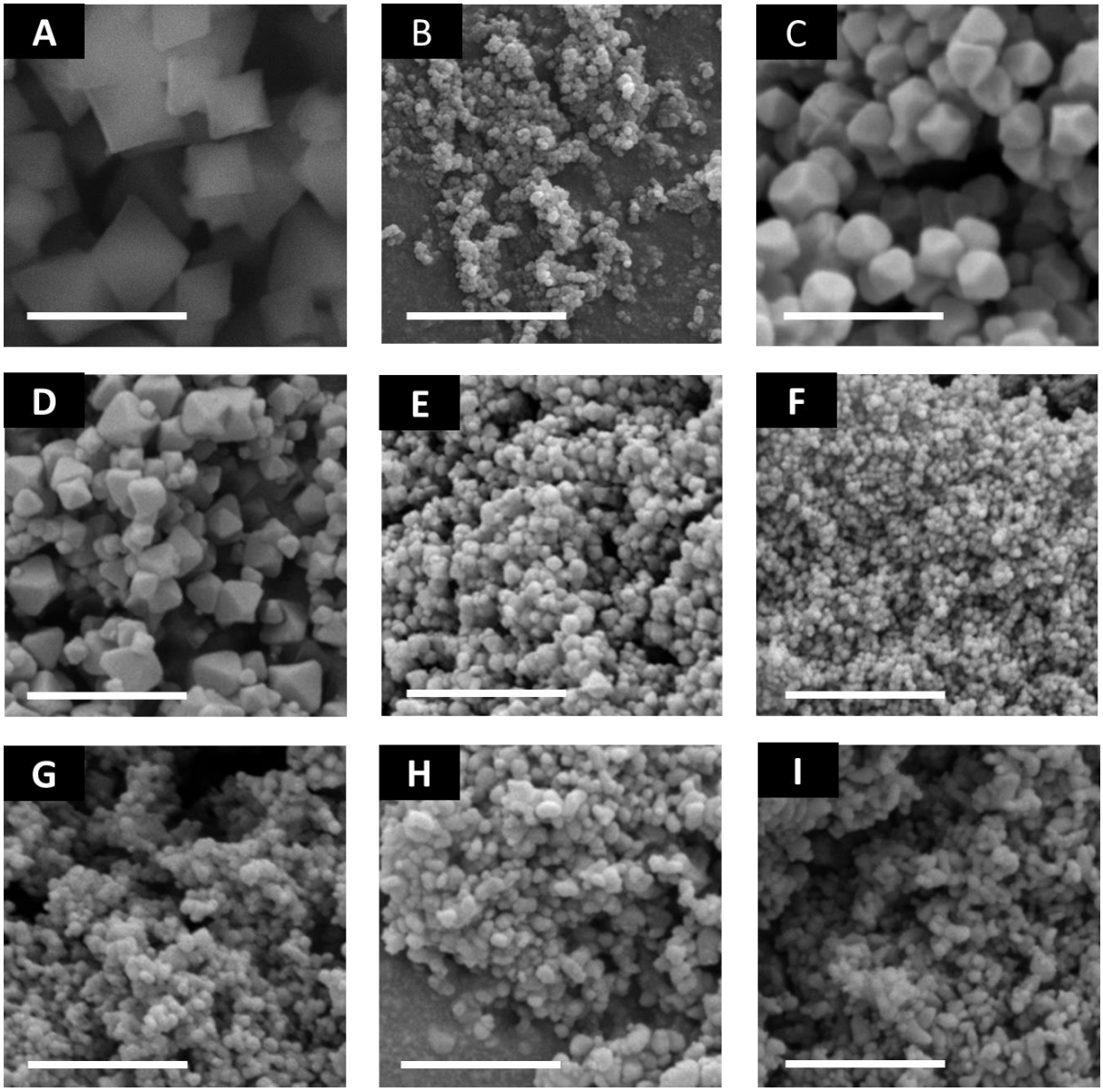


**Figure 36:** SEM images at a 1 μm scale bar for single component and MTV-UiO-66 catalysts synthesized. A: UiO-66 - B: UiO-66$(COOH)_2$ - C: UiO-66$(OH)_2$ - D: UiO-66(3A:1B) E: UiO-66(1A:1B) - F: UiO-66(1A:3B) - G: UiO-66(3A:1C) - H: UiO-66(1A:1C) - I: UiO-66(1A:3C).

d. Surface area analysis

**Figure 37** shows the nitrogen sorption isotherms of all synthesized MOFs which are recorded at 77K. As expected, type I isotherms are obtained for all MOF crystals

which are in accordance with the microporous nature of MOFs. As can be seen, the different levels of incorporation of the functionalized organic linkers within the MOF structures caused a significant change in their nitrogen uptake. For all structures tested, the increase in the level of incorporation of functionalized linkers in the structure had caused a subsequent decrease in the nitrogen uptake. Additionally, MTV-UiO-66$(OH)_2$ comprising terephthalic acid and 2,5-dihydroxyterephthalic acid, UiO-66(3A:1C), UiO-66(1A:1C), and UiO-66(1A:3C), had higher levels of surface areas than MTV-UiO-66$(COOH)_2$ having terephthalic acid and 1,2,4,5-benzenetetracarboxylic acid, UiO-66(3A:1B), UiO-66(1A:1B), and UiO-66(1A:3B). This could because the carboxylic functional groups are bulkier than the hydroxyl groups. In general, the increased incorporation of functionalized linkers seemed to decrease the accessibility of the porous network of MOF samples which is reported previously for other MTV-MOF systems. [146]

**Table 6** reports the calculated Brunauer–Emmett–Teller (BET) surface areas and the pore volumes of the activated MOF samples. In accordance with the nitrogen uptake observations, the level of the surface area is noticeably decreasing with the increased levels of functionalized BDC inside the framework. This decrease in surface area is more significant in MTV-MOF-$(COOH)_2$ where the surface area drops from 1290 $m^2/g$ for UiO-66(1A:3C) to 760 $m^2/g$ for UiO-66(3A:1C). Moreover, the calculated pore volumes follow the same trend. **Figure 38** shows the change in the surface areas of synthesized MOFs with respect to the level of incorporation of functionalized linkers within the framework. It could be seen that the decrease in surface area is significant upon the introduction of even a low percentage of functionalized linkers to the structure.

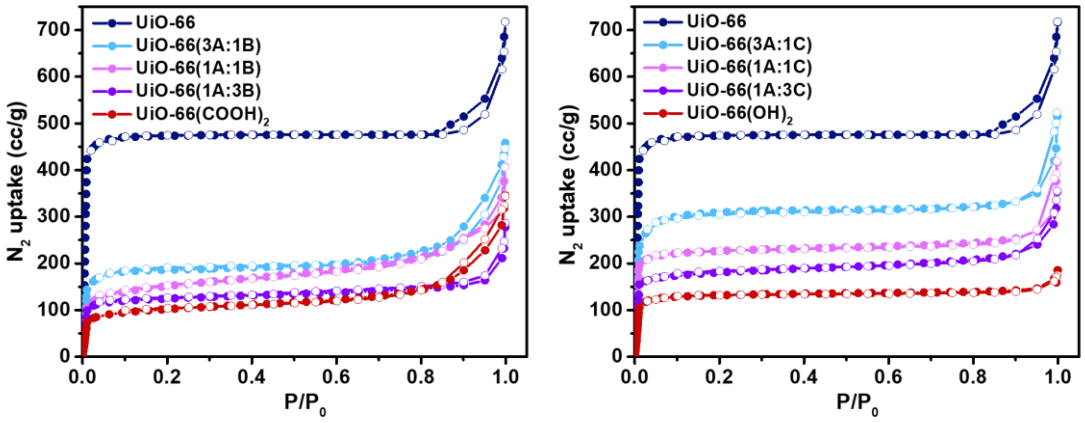


**Figure 37:** Nitrogen adsorption-desorption isotherms recorded at 77K for all synthesized MOF catalysts synthesized. • Adsorption ◦ Desorption. The functionalized linker being 1,2,4,5-benzenetetracarboxylic acid in UiO-66(3A:1B), UiO-66(1A:1B) and UiO-66(1A:3B), and 2,5-dihyroxyterephthalic acid in UiO-66(3A:1C), UiO-66(1A:1C) and UiO-66(1A:3C).

**Table 6:** Quantitative results extracted from the characterization and testing of all the MOF catalysts.

| MOF | BET surface area ($m^2/g$) | Pore volume ($cm^3/g$) | Defects number | Particle size (nm) | Conversion to butyl butyrate |
|---|---|---|---|---|---|
| **UiO-66** | 1812 | 0.73 | 1.87 | 331 | 75.1 |
| **UiO-66(COOH)2** | 522 | 0.11 | 1.93 | 28 | 76.6 |
| **UiO-66(OH)2** | 602 | 0.19 | 1.51 | 252 | 80.5 |
| **UiO-66(3A:1B)** | 773 | 0.26 | 1.83 | 302 | 70.3 |
| **UiO-66(1A:1B)** | 657 | 0.16 | 2.14 | 83 | 85.3 |
| **UiO-66(1A:3B)** | 609 | 0.16 | 1.98 | 38 | 88.8 |
| **UiO-66(3A:1C)** | 1290 | 0.46 | 1.33 | 45 | 72.5 |
| **UiO-66(1A:1C)** | 947 | 0.33 | 1.73 | 55 | 86.5 |
| **UiO-66(1A:3C)** | 761 | 0.24 | 1.90 | 51 | 92.2 |

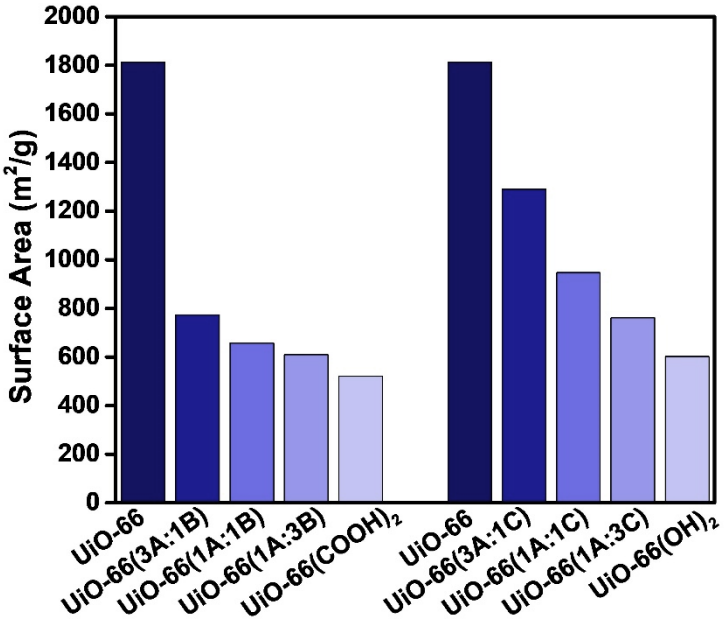


**Figure 38:** Decreasing levels of BET surface area with the increased percentage of incorporation of the functionalized organic linkers in the MOF structure

e. Thermogravimetric Analysis (TGA)

The Thermal stability and structural defects of the synthesized samples were assessed using TGA which shows the change of the mass percentage of the samples while increasing the temperature between 30 °C and 1100 °C, and the results are shown in **Figure 39**. Following a well-established method in the literature for defects number calculation, [79] the TGA curves were normalized so that the final weight-loss is 100% as illustrated in **Figure 39**. As can be seen in the figure, the thermal stability of the pure UiO-66 was higher than that of both pure functionalized structures, namely UiO-66$(COOH)_2$ and UiO-66$(OH)_2$. The decreased stability of the functionalized structures was attributed in previous studies to the lower metal-linker interaction in the functionalized structures when compared to pure UiO-66 [118]. The thermal stability of

MTV-MOF structures had fluctuated in between those of both single component structures as could be seen in the TGA curves in **Figure 39**. The shift in thermal stability in MTV-MOFs is more pronounced in the MTV-MOF$(OH)_2$ systems, (UiO-66(3A:1C), UiO-66(1A:1C), and UiO-66(1A:3C)), given the wider gap between the thermal stability of UiO-66 and UiO-66$(OH)_2$.

The number of defects for the single component structures is calculated following a method previously reported in the literature [79], which was also used for the MTV-MOF systems with minor changes in the calculation of the molecular weight of the cluster-linker unit. The molecular weight is calculated based on the level of introduction of each organic linker in the structure making it an average for the whole relevant structure. The defects number for UiO-66(3A:1B), UiO-66(1A:1B), and UiO-66(1A:3B) is estimated to be around 1.83, 2.14, and 1.98 out of 6 linkers per cluster respectively. An ascending defects trend with increased incorporation of the functionalized structure was noted for the second MTV-MOF system with 1.33, 1.73, and 1.90 missing linkers for UiO-66(3A:1C), UiO-66(1A:1C), and UiO-66(1A:3C) respectively. However, the number of defects for MTV-MOF structures are not bounded by that of single linker structures. Moreover, the number of missing linkers for UiO-66, UiO-66$(COOH)_2$, and UiO-66$(OH)_2$ is estimated to be around 1.87, 1.93, and 1.51 respectively. Having no direct correlation between the change in the number of defects and the decrease in the thermal stability of the MTV-MOF structures reflects a minimal effect of defects on the thermal stability of these structures. This further highlights that the decrease in the thermal stability was caused by the increased incorporation of the functionalized linkers that have weaker interaction with the cluster, which is previously

reported for similar structures, but for the first time in this study for the studied systems [118, 145].

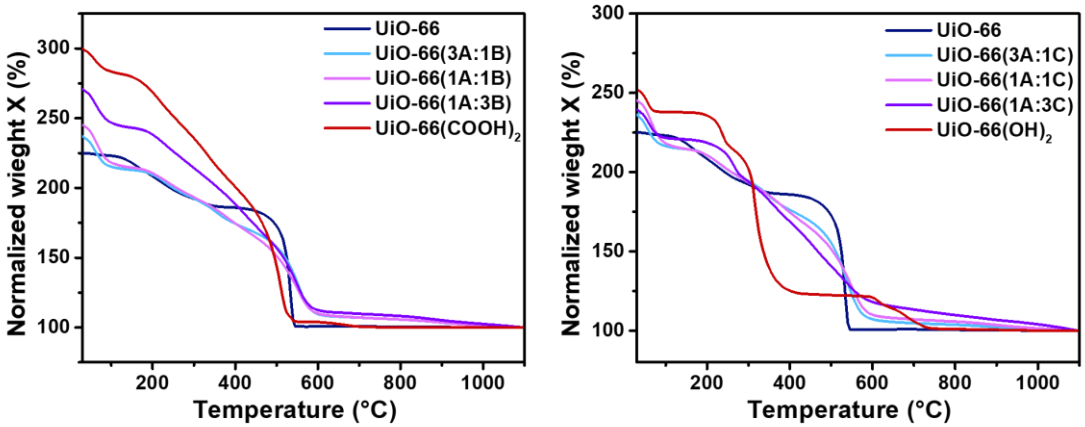


**Figure 39:** TGA curves of all synthesized MTV-MOF catalysts. The functionalized linker being 1,2,4,5-benzenetetracarboxylic acid in UiO-66(3A:1B), UiO-66(1A:1B) and UiO-66(1A:3B), and 2,5-dihyroxyterephthalic acid in UiO-66(3A:1C), UiO-66(1A:1C) and UiO-66(1A:3C).

### *2. Esterification Reaction for Butyl Butyrate Production*

a. Effect of the level of incorporation of the functionalized linkers

Activated MOFs are used as catalysts in the esterification reaction of butyric acid and butanol for butyl butyrate production. The reaction time was set to be 24 hours and only 1 wt% catalyst is used in this study, which is equivalent to around 50 mg of MOF powder. As a reference for MOFs catalytic activity, one reaction is allowed to occur without the use of a catalyst, noted Blank, and another reaction is performed under 1 wt% $H_2SO_4$. Samples were regularly taken from the reaction medium once every two hours for the first 8 hours, and at 22 hours and 24 hours, then these samples were analyzed using GC.

The results of the evolution of the conversion to butyl butyrate with respect to time are shown in **Figure 40**, while **Figure 41** compares the conversion obtained using each MOF catalyst after 24 hours of reaction. No reactants other than butyl butyrate were detected in GC analysis which means that the selectivity to the desired product is 100%. Observing the performance of MOF catalysts with respect to time as illustrated in **Figure 40**, an interesting trend could be noted.

Starting with the MTV-MOF series, it is noticeable that for both systems, structures with 50% and 75% functionalized linker starting molar ratio had the highest catalytic activity. In fact, the increased conversion to butyl butyrate when using these MTV-MOF systems is more pronounced at the beginning of the reaction. Moreover, compared to UiO-66 which yields around 53% conversion to butyl butyrate after 8 hours of reaction, around 72% and 74% are obtained when using UiO-66(1A:3B) and UiO-66(1A:3C) respectively. In fact, the best performance is obtained when UiO-66(1A:3B) and UiO-66(1A:3C) catalysts are employed.

In order to put these results into context, the structural characterization results obtained and reported in **Table 6** are discussed. Comparing UiO-66 and UiO-66(1A:3B), the first thing to notice is the higher active site density of the latter given the higher defects number and the 61% level of incorporation of 1,2,4,5-benzenetetracarboxylic acid linkers with its COOH groups. Additionally, the particle size of UiO-66(1A:3B) is considerably smaller which increases the external surface area and thus the accessibility of active sites. This explains the higher performance of UiO-66(1A:3B) when compared to the open structure of pure UiO-66. On the other hand, when compared to UiO-66$(COOH)_2$, UiO-66(1A:3B) is characterized by a much higher

level of defectiveness and higher surface area, which could explain its better performance.

Almost the same goes for the comparison between UiO-66 and UiO-66(1A:3C) where the latter, although having lower surface area, benefits from a higher level of active site density, given the incorporation of 2,5-dihydroxyterephthalic acid up to 52% along with higher level of defects. However, in the case of MTV-UiO-66$(OH)_2$, the role of the active sites on the organic linker differs from that of the active sites on the cluster. While the cluster provides active acid sites, the OH groups are possibly favoring a dual acid-base activation mechanism as previously suggested by Cirujano et al. [52, 53]. In such a mechanism, the butyric acid would adsorb onto the acid sites of the cluster, which increases the electrophilic character of the carbon atom in the carboxylic group. At the same time, the OH groups of the linker are thought to form hydrogen-bonded adducts that increase the nucleophilicity of the O atom of the butanol's hydroxyl group, which could favor its reaction with the butyric acid. This reaction mechanism could explain the superior activity of this catalyst over its counterparts that are only acid catalyzed.

Observing other characteristics that might have contributed to the superior performance of UiO-66(1A:3C), it can be noted that it also benefits from smaller particle size relative to UiO-66, and has a higher surface area and defects number compared to UiO-66$(OH)_2$. This thus shows that the mixed-linker approach has a positive effect on increasing the level of active sites compared to the pure UiO-66 structure while maintaining higher surface area values when compared to the pure functionalized structures.

However, this trend could not be generalized, since not all MTV-MOF systems have better catalytic activity than their single-component counterparts. In fact, UiO-66 and UiO-66(COOH)$_2$ both performed better than UiO-66(3A:1B), while UiO-66 and UiO-66(OH)$_2$ both performed better than UiO-66(3A:1C). Although these MTV-MOFs have higher surface areas than their pure functionalized counterparts, namely UiO-66(COOH)$_2$ and UiO-66(OH)$_2$, and despite them having part of their linkers functionalized, these MTV-MOFs still had lower catalytic activity. When comparing the structural characteristics of UiO-66(3A:1B) with those of UiO-66, it could be noticed that the two structures have comparable defects number while UiO-66(3A:1B) has a much lower surface area. Additionally, relative to UiO-66(COOH)$_2$, UiO-66(3A:1B) has lower active site density given both the lower defects' number and the lower partial incorporation (16%) of functionalized linkers in the structure. Again, and as for UiO-66(3A:1C), its lower catalytic activity could be attributed to the noticeably lower defects' number when compared to that of UiO-66 and UiO-66(OH)$_2$.

The best performing MOF, UiO-66(1A:3C), yields 92% conversion to butyl butyrate which is comparable to that obtained using 2 wt% of the best performing UiO-66(COOH)$_2$ structure in our previous study [121]. So in this study, we managed to synthesize materials of significantly higher catalytic activity which yielded similar conversion to butyl butyrate compared to their counterparts even when half the catalytic loading is used. This reveals the successful implementation of the MTV-MOF strategy by benefiting from the advantages of both the open structure of UiO-66, the high active density of functionalized structures of UiO-66(COOH)$_2$ and UiO-66(OH)$_2$, along with the high number of defects from the addition of high concentrations of the formic acid modulator. Although $H_2SO_4$ still performed better than MOF catalysts, the gap between

the performances of the two systems was lowered when using the MTV-MOFs approach. Additionally, the final yield after 24 hours of the reaction using $H_2SO_4$ and the best performing MOF, UiO-66(1A:3C), as catalyst was comparable being 95% and 92% respectively.

b. Effect of the organic linker steric bulk

After comparing the structures in terms of the level of incorporation of the functionalized linker, it is necessary to compare their performance with respect to the type of this linker being incorporated and the functional group it is adding to the structure (**Figure 42**). To begin with, the single component functionalized MOFs which have lower surface area than pure UiO-66, both have relatively higher catalytic activity, which could be the result of the dangling functional groups on their linkers. This trend had been previously reported for UiO-66$(COOH)_2$ with relatively comparable defects number with UiO-66 [121], but this is reported for the first time using UiO-66$(OH)_2$ which has considerably lower defects number than both pure counterparts. In fact, UiO-66$(OH)_2$ had 1.51 missing linkers per cluster compared to 1.86 and 1.93 missing linkers in the case of UiO-66 and UiO-66$(COOH)_2$ respectively, which is a gap in defectiveness that could potentially hinder the catalytic activity of a UiO-66-based MOF structure. However, while UiO-66 depends only on the number of defects to obtain open catalytic centers for the esterification reactions [102, 108], this is not the case for UiO-66$(COOH)_2$ and UiO-66$(OH)_2$ which offer additional active sites that could act as catalytic centers. On the other hand, despite having no other active site than the defects, the catalytic performance of UiO-66 was comparable to its pure functionalized isostructures. The reason behind this is probably due to its open structure which allows

for easier diffusion of the reactants inside the porous network and the subsequent access of the internal active sites [52, 134].

A similar approach could be used when analyzing the results obtained using UiO-66(COOH)$_2$ and UiO-66(OH)$_2$. Although both MOFs contributed to similar conversion to butyl butyrate, UiO-66(OH)$_2$ has considerably lower defects number but slightly better conversion. Many parameters could have contributed to this result but the most obvious could be the functional group attached to the linker which differs in both systems. First, and as previously discussed, the different functional groups on the organic linkers of both systems are thought to cause different reaction mechanisms. While MOFs with COOH groups benefit from higher levels of acid active sites, the structures with OH groups benefit from a dual acid-base mechanism which is reported to increase the catalytic activity, as previously reported for systems with $NH_2$ groups, namely UiO-66($NH_2$) [52, 53]. Additionally, the COOH groups seem to have a more pronounced negative effect on the diffusion of the reactants when compared to the less bulky OH groups. In fact, at this level of defects obtained in UiO-66(COOH)$_2$, its catalytic activity is expected to be higher, but diffusion problems could have made its catalytic centers less accessible [52, 134].

Additionally, the surface area is a critical parameter in heterogeneous catalysis as the activation and subsequent reaction takes place on the outer surface of the catalyst. It is thus expected that having a catalyst with the same properties but with a higher surface area would have better catalytic activity. **Table 6** shows that UiO-66(OH)$_2$ has a higher surface area than that of UiO-66(COOH)$_2$ which could explain why UiO-66(OH)$_2$ performed better regardless of its lower defects density.

Comparing UiO-66(3A:1B) to UiO-66(3A:1C), UiO-66(1A:1B) to UiO-66(1A:1C), and UiO-66(1A:3B) to UiO-66(1A:3C), these structures had a comparable level of incorporation of functionalized linkers in their structure and thus a comparable level of active sites' density provided by the linker. However, the MTV-UiO-66$(OH)_2$ structures have a lower number of defects but consistently better catalytic performance. This could again be attributed to the dual acid-base mechanism and the lower steric bulk of the OH groups which allowed for better accessibility of the active sites. Additionally, MTV-UiO-66$(OH)_2$ structures have higher levels of surface area, which could be attributed to the higher surface area of UiO-66$(OH)_2$ when compared to its functionalized counterpart UiO-66$(COOH)_2$. This higher level of surface area would extend the surface for catalysis and reactants activation especially when the particle size of MTV-UiO-66$(OH)_2$ and MTV-UiO-66$(COOH)_2$ become comparable.

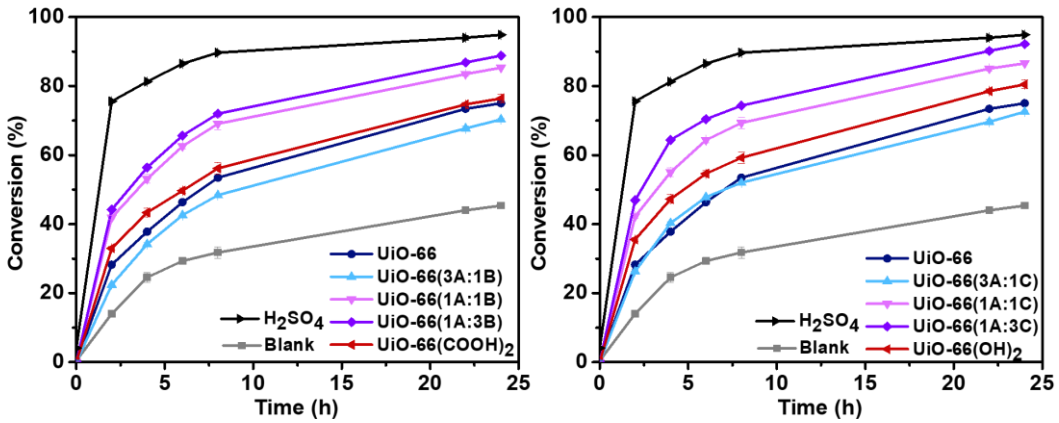


**Figure 40:** The conversion to butyl butyrate with respect to time using 1 wt% of each MOF catalyst. The functionalized linker being 1,2,4,5-benzenetetracarboxylic acid in UiO-66(3A:1B), UiO-66(1A:1B) and UiO-66(1A:3B), and 2,5-dihyroxyterephthalic acid in UiO-66(3A:1C), UiO-66(1A:1C) and UiO-66(1A:3C).

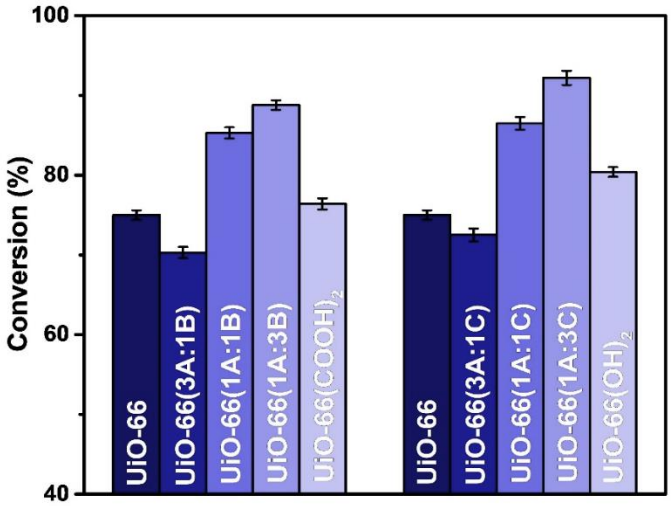


**Figure 41:** Final conversion to butyl butyrate after 24 hours of reaction under 1 wt% of each MOF catalyst

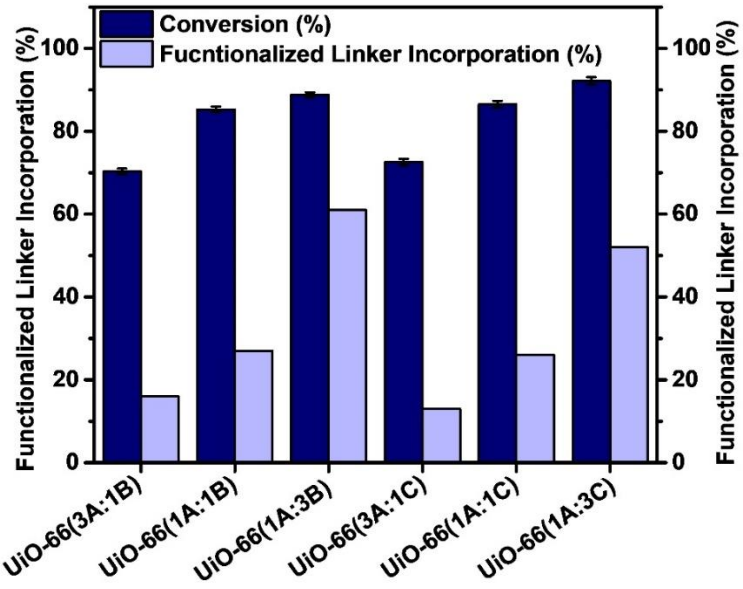


**Figure 42:** Change in conversion compared to change of the functionalized linker incorporation in MTV-MOFs structure. The functionalized linker being 1,2,4,5-benzenetetracarboxylic acid in UiO-66(3A:1B), UiO-66(1A:1B) and UiO-66(1A:3B), and 2,5-dihyroxyterephthalic acid in UiO-66(3A:1C), UiO-66(1A:1C) and UiO-66(1A:3C).

### *3. Conclusion*

This study reports the use of MTV-UiO-66 structures as catalysts for butyl butyrate production. Besides the single component structures, two mixed-linker systems are synthesized: MTV- UiO-66$(COOH)_2$ which incorporates both terephthalic acid (A) and 1, 2, 4, 5-benzenetetracarboxylic acid (B), and MTV-UiO-66$(OH)_2$ which includes both terephthalic acid (A) and 2,5-Dihydroxyterephthalic acid (C), at three different ratios, yielding a total of nine structures. The obtained structures are fully characterized and showed homogeneous incorporation of the functionalized linkers within the MOF crystals, which also benefited from a high level of cluster defects thanks to the modulation synthesis conditions. The values of surface area and pore volume decreased with the increased level of functionalized linkers' incorporation, which is found to be slightly lower than the starting molar ratio as indicated by $^1$H-NMR results. For both systems, MTV-UiO-66 incorporating starting molar percentages of 75% functionalized linkers and 25% BDC yielded the best performance with 89% and 92% of butyl butyrate conversion using UiO-66(1A:3B) and UiO-66(1A:3C) respectively, using only 1 wt% catalyst loading. This performance was attained using double the catalyst loading for highly defective single component functionalized structures in our previous studies, which highlights the success of using the multivariate approach to boost their catalytic activity. This is achieved by increasing the level of active sites' density through partial functionalization while maintaining higher surface areas and pore volumes than the purely functionalized structures which allowed for easier access to these sites. However, not all MTV-MOFs perform better than their single linker counterparts, and this is the result of a sum of factors related to the density of active sites on one hand, and the internal diffusion limitations on the other. This further highlights the MOFs'

characteristics that govern their catalytic activity and the importance of classifying these characteristics in terms of their influence on the conversion to butyl butyrate to guide the engineering of MOF catalysts for this specific application.

## D. REGRESSION MODEL

Following our previous studies on functionalized, defected, and MTV-MOFs-based catalysts for the production of butyl butyrate, [121, 143] a simplified regression model is suggested to predict the final conversions. Moreover, our studies have focused in-depth on the effect of the different characteristics of MOFs on their catalytic activity, and it had been concluded that a few main characteristics mostly govern the conversion and appear to be critical in the engineering of new UiO-66 based catalysts for esterification reactions. Modeling was thus suggested to be used as it helps to (i) extract an empirical relationship between the MOFs characteristics and the conversion to butyl butyrate, (ii) provide a tool for conversion prediction without having to run the esterification reaction, and (iii) screen the characteristics used as input of the model to identify which ones are more important than others in increasing the yield of butyl butyrate [147]. This highlights the parameters that are more critical to engineer in a MOF structure in order to maximize its catalytic activity.

For this reason, a regression model is proposed to predict the catalytic activity of UiO-66-based MOFs taking into account these main characteristics as a general scheme to design and develop a MOF catalyst of better performance. To simplify the interpretation of model predicted conversion and to minimize the computational requirements of the model, a simple multiple weighted linear regression model is

adopted to fit the data of the three studies. The output of the model is the conversion to butyl butyrate and the parameters that were concluded to be governing the catalytic activity of the UiO-66-based catalysts are used as input. These mainly include the surface area, the number of defects, the catalyst loading, and the level of incorporation of the active functionalized organic ligands in the MOF structure. These parameters had been changed throughout 33 different reactions conditions performed in our studies and their actual values are depicted in **Table S3** in the supporting information. **Table S4** represents the normalized values of the relevant parameters between 0 and 1. The normalization of the parameters allows for constructive discussion on the relative effect of each of them on the conversion to butyl butyrate. The suggested linear regression model is presented below:

$$Conv_{mod,i} = a * \%A_i + b * \%B_i + c * \%C_i + d * SA_i + f * CL_i + e * DN_i + Cst$$

Where:

$i$: refers to experiment number $i$ out of the total number of experiments performed in our three studies which is 33

$Conv_{mod,i}$: is the model-predicted conversion to butyl butyrate based on the governing parameters of the MOF structure for experiment $i$

$\%A_i$: is the level of incorporation of the terephthalic acid linker in the MOF structure used in the experiment $i$, which varies between 0 and 100% and is normalized between 0 and 1

$\%B_i$: is the level of incorporation of the 1, 2, 4, 5-benzenetetracarboxylic acid linker in the MOF structure used in the experiment $i$, which varies between 0 and 100% and is normalized between 0 and 1.

$\%C_i$: is the level of incorporation of the 2,5-Dihydroxyterephthalic acid linker in the MOF structure used in the experiment $i$, which varies between 0 and 100% and is normalized between 0 and 1.

$SA_i$: is the surface area of the MOF used in the experiment $i$, which varies between a minimum of 51 $m^2/g$ and a maximum of 1813 $m^2/g$ throughout the studies and is normalized between 0 and 1.

$CL_i$: is the catalyst loading used in the experiment $i$, which varies between 1, 2, and 5 wt% throughout the studies and is normalized between 0 and 1.

$DN_i$: is the defects' number of the MOF used in the experiment $i$, which varies between 0.88 and 2.14 missing linkers out of 6 throughout the studies and is normalized between 0 and 1.

$Cst$: is the y-intercept of the model, when all parameters are equal to zero, or in other words, when no catalyst is being used.

$a, b, c, d, e, and\ f$: are the regression coefficients, or weights, attributed to each of the parameters chosen and are calculated using Microsoft Excel Regression Analysis, provided in the data analysis tool.

After setting the experimental conversion as the output to be predicted and the normalized values of the chosen parameters, as indicated in **Table S4,** as the independent variables to be used for the prediction, Excel Data Analysis was used to determine the suitable regression model as follows:

$$Conv_{mod,i} = 6.87 * \%A_i + 21.93 * \%B_i + 25.25 * \%C_i + 16.19 * SA_i + 15.38 * CL_i + 25.07 * DN_i + 39.94$$

**Figure 43** depicts the correlation between the model-predicted conversion and the experimentally obtained conversion to butyl butyrate.

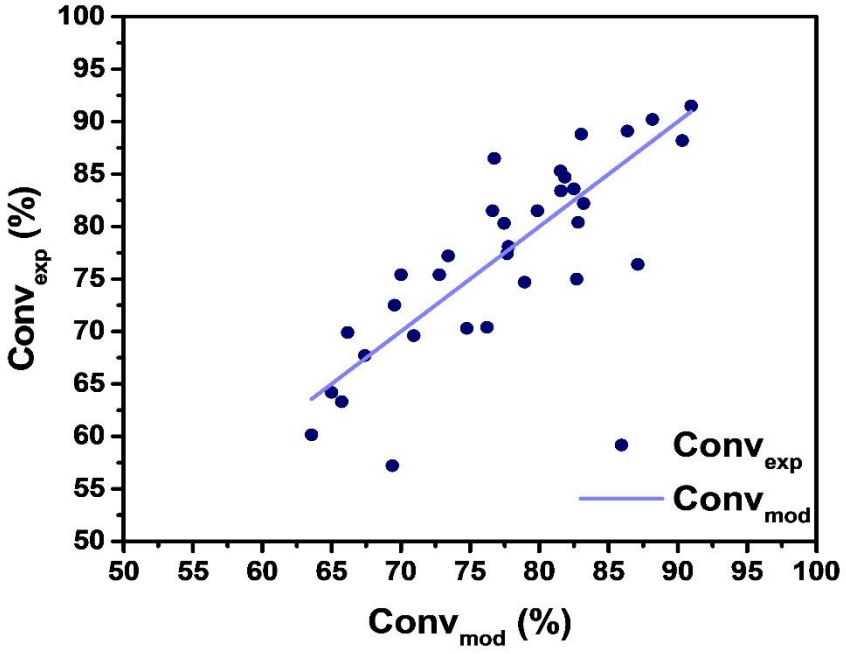


**Figure 43:** The correlation between the experimentally obtained conversion to butyl butyrate and the suggested linear model

**Table S5** shows the calculated weights and intercept along with their P-Values which is an expression of the statistical significance. The P-values that are less than 0.05 indicate strong evidence against the null hypothesis, which is the hypothesis that there is no relationship between the independent variable and the output to be predicted. Since the P-values of the chosen independent variables are all well below 0.05 (**Table S5**), this reflects their suitability for the prediction of the conversion to butyl butyrate [147]. This reveals that our assumption of the relationship between the chosen MOFs characteristics and the conversion to butyl butyrate is statistically valid. The correlation coefficient Multiple R is shown in **Table S6** and it reflects the strength of a linear relationship between a set of variables and the predicted output. The absolute value of this number indicates how related the variables and the output are, and the closer the number is to 1, the stronger the relationship. Having a Multiple R of 0.85 shows a strong linear relationship between the chosen parameters and the conversion to butyl

butyrate [147]. This is further confirmed with an $R^2$ value of 0.723 and an adjusted $R^2$ of 0.659 showing that the majority of the obtained results in the three studies could be explained by the suggested model. The average error of 5.19% and the comparison between the model-predicted results, and the experimentally obtained values of the conversion to butyl butyrate shows that the model well represents the results obtained experimentally (**Table S7**). Additionally, having the significance F value lower than 0.05 means that the model is statistically acceptable in predicting the desired output [147].

Since the values of the input parameters are normalized, the regression coefficients estimated become valuable tools, not only for the prediction of the conversion to butyl butyrate given different parameters of UiO-66-based structures but also in the engineering of these parameters. The regression weights help highlight the relative influence of each of the characteristics in boosting the catalytic activity of the structure. Moreover, comparing the a, b, and c weights of 6.87, 21.93, and 25.25 respectively for %A, %B, and %C, attributed to the level of incorporation of the different linkers, it could be clearly seen that the model assigned higher weight for the functionalized linker in the prediction of the conversion. This means that the addition of linkers with active functional groups had a better impact on the increase of the conversion than the addition of the terephthalic acid linkers as previously concluded. Additionally, the weight of the defects number was estimated to be 25.07, which is similar to that assigned for the incorporation of the linkers functionalized with two hydroxyl groups and reflects comparable importance of the defects number and the additional functional groups on the performance of the UiO-66 structures in this reaction. Moreover, the surface area and the catalyst loading were assigned 16.18 and

15.38 regression weights respectively, which also emphasizes a similar effect on the catalysis of the reaction. It seems though that the latter parameters are less significant when compared to the density of active sites as is previously discussed in our studies [121, 143].

The model also assigned an intercept value $Cst$ of around 40% as the conversion to butyl butyrate if no catalyst is used in the reaction. This prediction is relatively accurate as around 45% conversion is obtained when no catalyst is used which is mainly due to the autocatalytic effect of butyric acid itself as indicated in the linker functionalization study [143]. Besides the conclusions on the relative importance of these parameters in governing the conversion to butyl butyrate, the model predicts this conversion at an error of around 5% which makes it a valuable tool in predicting the conversion for design purposes while changing the MOFs parameters without having to actually synthesize the MOF or run the esterification reaction at all.

## E. KINETIC MODELLING

The esterification reaction of butyric acid (A) in presence of butanol (B) to produce butyl butyrate (E) and water (W) is given in the reaction below

$$A + B \leftrightarrow E + W$$

A pseudo-homogeneous model was chosen to represent the reaction kinetics as previously suggested in the literature [148, 149]. Furthermore, since butanol is always in excess, the reaction was assumed to be zero-order with respect to it. The rate equation for this reaction could be thus expressed as follows

$$-\frac{dC_A}{dt} = \frac{dC_E}{dt} = \frac{dC_W}{dt} = k_1 C_A - k_2 C_E C_w \quad (1)$$

With

$$C_E = C_w = C_{A0} - C_A$$

$$K_{eq} = \frac{k_1}{k_2}$$

Where

$C_A$, $C_E$ , and $C_w$ are the concentrations of butyric acid, butyl butyrate, and water respectively, and $C_{A0}$ is the initial concentration of butyric acid. $k_1$ and $k_2$ are the rate constants for the forward and reverse reactions and $K_{eq}$ is the overall reaction equilibrium constant.

Two models were considered for this reaction. The first model is based on the rate equation previously shown. Solving the differential equation would result in an expression of the concentration of butyric acid with respect to time as follows

$$C_A = \frac{-R_2 S e^{-(R_2 - R_1)tk_1} + R_1}{1 - S e^{-(R_2 - R_1)tk_1}} \qquad (2)$$

Where:

$$R_1 = \frac{-b-\sqrt{\Delta}}{2a};\ R_2 = \frac{-b+\sqrt{\Delta}}{2a};\ S = \frac{C_{A0} - R_1}{C_{A0} - R_2}$$

And

$$a = \frac{k_1}{K_{eq}};\ b = -k_1\left(1 + 2\frac{C_{A_0}}{K_{eq}}\right);\ c = C_{A0}^2 \frac{k_1}{K_{eq}};\ \Delta = b^2 - 4ac$$

$K_{eq}$ at 110°C was estimated using the following equation

$$K_{eq} = e^{-\frac{(\Delta H - T\Delta S)}{RT}} \qquad (3)$$

The kinetic parameters were estimated by minimizing the following objective function

$$F_{obj} = \frac{\sum_{i=1}^{N}(C_{i,mod} - C_{i,\exp})^2}{N} \qquad (4)$$

Where $N$ is the total number of experimental points, $C_{i,mod}$ is the concentration of component $i$ calculated by the model, and $C_{i,\exp}$ is the concentration of component $i$ obtained experimentally.

As for the second model, the reaction was assumed to be non-reversible since the temperature of the reacting solution was kept at 110°C throughout the study. This would reduce the reaction rate to the following form

$$-\frac{d\,C_A}{dt} = kC_A \qquad (5)$$

And so the concentration of the butyric acid as a function of time could be expressed as

$$C_A = C_{A0}e^{-kt} \qquad (6)$$

Where $k$ is the reaction rate constant of the irreversible reaction. For this model, $k$ was also estimated by minimizing the objective function shown in equation 4.

The two kinetic models developed were tested to fit the experimental data obtained and to further investigate the effect of different variables on the reaction. **Figure 44** shows the evolution of the concentration of butyric acid with respect to time which is calculated by the two kinetic models for the esterification reaction using the two top-performing catalysts in the three studies. The estimated rate constant of the forward reaction in the reversible model, k1, and the rate constant in the irreversible

model, k, for all 33 reactions are shown in **Table 7**. Although both models show a good fit of the experimental points, especially for the first few hours of the reaction, the coefficients of determination ($R^2$) shown in **Table 7** reveal that the non-reversible model makes a better fit. The conversion however was mostly somewhere between the two conversion rates suggested by the two models. This was assumed to be due to the vaporization of water at the reaction temperature of 110°C which lowers its concentration in the reacting solution, even if it is constantly being refluxed, which pushes the equilibrium towards the forward reaction by constantly eliminating part of the produced water.

A third model was used to assess the average percentage of produced water that is vaporized at a certain time in the reaction. The reversible model was used for this purpose and a fraction $y_i$ was multiplied by the produced water concentration $C_w$, which is the estimated average percentage of water present in the reaction medium at any time. The forward reaction rate constant was set to be the same for the same reaction conditions, and the value of $y_i$ was estimated by minimizing the objective function in equation 4. The results of the altered reversible model are shown in **Figure 44** in dashed lines, and the calculated $y_i$ values are depicted in the figures. The model suggests that the final yields obtained are possible with around 22% to 45% of the water produced being present in the reaction medium, which suggests that an average of 55% to 78% of the water produced is vaporized due to heat and is circulating in the condenser at the time of the reaction.

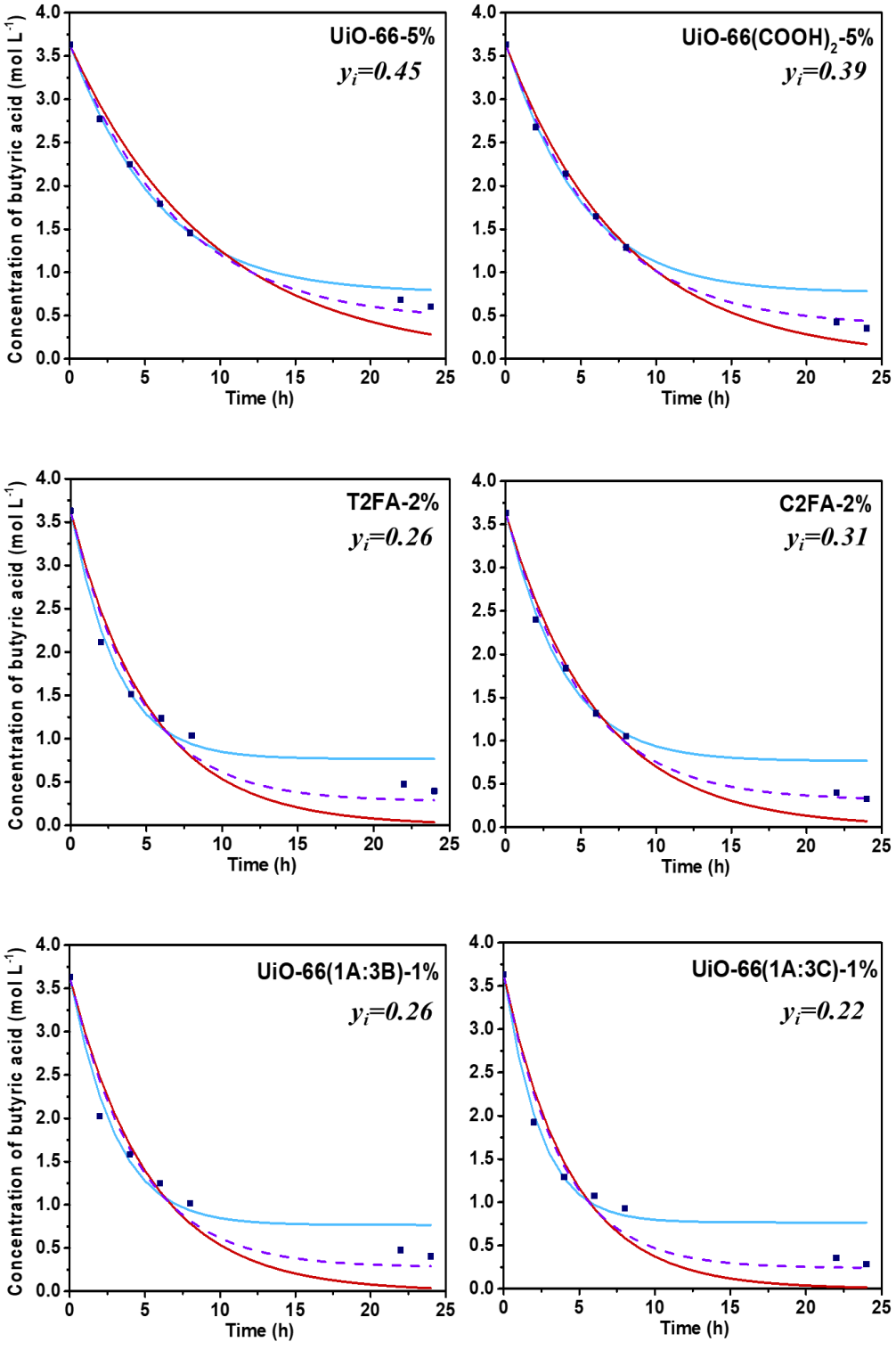


**Figure 44:** The evolution of the concentration of butyric acid with time for different catalysts' types and loadings. (—) Reversible model ( — ) Irreversible model (…) Reversible model taking into account water vaporization ( ▪ ) Experimental points

**Table 7:** Kinetic parameters calculated using the Reversible model ($k_1$) and the Irreversible model (k) for different catalysts' types and loadings

| MOF | Catalyst Loading | $K_1$ ($h^{-1}$) | $R^2_{rev}$ | K ($h^{-1}$) | $R^2_{irr}$ |
|---|---|---|---|---|---|
| **UiO-66** | 5 | 0.0120 | 0.9959 | 0.1064 | 0.9838 |
| **UiO-66(COOH)$_2$** | 5 | 0.0138 | 0.9831 | 0.1275 | 0.9955 |
| **UiO-66(NH)$_2$** | 5 | 0.0081 | 0.9946 | 0.0700 | 0.9826 |
| **UiO-66** | 2 | 0.0085 | 0.9993 | 0.0741 | 0.9797 |
| **UiO-66(COOH)$_2$** | 2 | 0.0090 | 0.9953 | 0.0819 | 0.9911 |
| **UiO-66(NH)$_2$** | 2 | 0.0071 | 0.9892 | 0.0605 | 0.9597 |
| **UiO-66** | 1 | 0.0076 | 0.9943 | 0.0650 | 0.9635 |
| **UiO-66(COOH)$_2$** | 1 | 0.0072 | 0.9954 | 0.0664 | 0.9862 |
| **UiO-66(NH)$_2$** | 1 | 0.0054 | 0.9709 | 0.0483 | 0.9443 |
| **TB** | 2 | 0.0050 | 0.9480 | 0.0453 | 0.9199 |
| **T1AA** | 2 | 0.0111 | 0.9816 | 0.0843 | 0.8969 |
| **T2AA** | 2 | 0.0129 | 0.9918 | 0.1061 | 0.9462 |
| **T1FA** | 2 | 0.0188 | 0.9839 | 0.1577 | 0.9535 |
| **T2FA** | 2 | 0.0229 | 0.9731 | 0.1915 | 0.9707 |
| **CB** | 2 | 0.0071 | 0.9592 | 0.0578 | 0.9071 |
| **C1AA** | 2 | 0.0118 | 0.9954 | 0.0979 | 0.9527 |
| **C2AA** | 2 | 0.0130 | 0.9931 | 0.1116 | 0.9675 |
| **C1FA** | 2 | 0.0162 | 0.9856 | 0.1444 | 0.9835 |
| **C2FA** | 2 | 0.0183 | 0.9785 | 0.1647 | 0.9904 |
| **AB** | 2 | 0.0055 | 0.9965 | 0.0550 | 0.9888 |
| **A1AA** | 2 | 0.0072 | 0.9870 | 0.0621 | 0.9669 |
| **A2AA** | 2 | 0.0115 | 0.9890 | 0.0951 | 0.9538 |
| **A1FA** | 2 | 0.0144 | 0.9753 | 0.1196 | 0.9430 |
| **A2FA** | 2 | 0.0202 | 0.9725 | 0.1678 | 0.9495 |
| **T2FA (1%)** | 1 | 0.0107 | 0.9865 | 0.0874 | 0.9482 |
| **C2FA (1%)** | 1 | 0.0126 | 0.9758 | 0.1015 | 0.9304 |
| **UiO-66(OH)$_2$** | 1 | 0.0148 | 0.9746 | 0.1226 | 0.9419 |
| **UiO-66(3A:1B)** | 1 | 0.0088 | 0.9884 | 0.0704 | 0.9434 |
| **UiO-66(1A:1B)** | 1 | 0.0202 | 0.9748 | 0.1699 | 0.9568 |
| **UiO-66(1A:3B)** | 1 | 0.0230 | 0.9677 | 0.1914 | 0.9663 |
| **UiO-66(3A:1C)** | 1 | 0.0107 | 0.9830 | 0.0837 | 0.9221 |
| **UiO-66(1A:1C)** | 1 | 0.0213 | 0.9734 | 0.1782 | 0.9613 |
| **UiO-66(1A:3C)** | 1 | 0.0287 | 0.9610 | 0.2276 | 0.9691 |
| **Max** | 5 | 0.0287 | 0.9993 | 0.2276 | 0.9955 |
| **Min** | 1 | 0.0050 | 0.9480 | 0.0453 | 0.8969 |
| **Average** | 2 | 0.0129 | 0.9822 | 0.1089 | 0.9581 |

# CHAPTER V

# CONCLUSIONS AND RECOMMENDATIONS

The biofuel industry is in great need of efficient, green, and recyclable catalysts that will help make a breakthrough in the production rate and cost of biofuels. Metal-Organic Frameworks (MOFs) have emerged as a novel class of porous crystalline materials with many interesting features such as high surface area, permanent porosities, and relative ease of design. MOFs had been particularly interesting in catalysis applications as their structures could be tuned to obtain the required characteristics and functional groups required for the specific chemical reaction. In this study, extensive experimental work was done to investigate the potential of Zr-based MOFs, UiO-66, as catalysts for the production of butyl butyrate, a novel biofuel. The research was based on three materials engineering strategies, (i) Linker functionalization, (ii) defect engineering, (iii) MTV-MOFs, or mixed linker MOFs. Every strategy helped in optimizing the process both in terms of reaction conditions and catalyst characteristics needed to maximize the yield to butyl butyrate. After investigating 33 reaction conditions, it was possible to obtain a final conversion of 92% to butyl butyrate, which is comparable to the performance of $H_2SO_4$ with 95% final conversion after 24 hours of reaction. This result was obtained after applying all three materials engineering techniques listed previously and using only 1wt% of catalyst loading, compared to 5 wt% catalyst loading when applying only the linker functionalization technique. This means that simple manipulation of the synthesis conditions of the catalyst helped decrease the need for the catalyst by almost 5 times while keeping the final conversion

at a level close to that of the liquid catalyst. Following a comprehensive discussion on the role of every characteristic in the MOF structure and its effect on the final conversion to butyl butyrate, the development of a weighted linear regression model based on all the data obtained was suggested. This was used as a quantitative evaluation of the relative importance of these characteristics on the catalytic activity of the different structures. The characteristics that were used as input to the model were the ones concluded to mostly govern the catalytic activity of the MOFs based on the experimental observations and these are the surface area, the defects density on the cluster, the level of incorporation of the functional groups on the organic linker, and the catalyst loading. Every characteristic was assigned a weight and the output, which is the estimated conversion to butyl butyrate, was calculated by minimizing the error between the model-predicted conversion and the experimental results. The results showed that the density of active sites through the number of defects or the functional groups on the linker had relatively a higher impact than the levels of surface area and catalyst loading, where both of which had in turn comparable impact on the conversion prediction based on the model results. These interesting findings pave the way for the development of highly efficient UiO-66-based catalysts for biofuel production. Additionally, two kinetic models were developed to simulate the change of the concentration of reactants/products with respect to reaction time and to calculate the corresponding kinetic parameters. The results showed that the experimental data was better represented by the reversible model, which is predictable as the reaction is reversible. However, as the final conversion was higher in the experimental results, it was suggested that the water produced in the reaction is being partially vaporized since the reaction is taking occurring at 110 °C. A modification to the kinetic model was thus suggested where a

vaporization percentage was assigned to the water concentration and the results obtained suggested that around 55 to 78% of the water produced is vaporized and recycled in the condenser at the reaction time. The results obtained by this study help serve as a practical and detailed guide to materials engineers and crystal engineers aiming at developing MOFs-based catalysts, not only for biofuel production but for any chemical reaction, and for this reason, many approaches are proposed to continue this work in the MOFs engineering, reaction type, and modeling.

Regarding the MOFs engineering, work should be done to maximize the accessibility of the active sites of the MOF structures especially in functionalized structures. The reason behind this suggestion is that we believe that the reactants adsorption and activation is mostly taking place on the external surface area, especially in functionalized structures, which hinders the catalytic activity of the MOFs as a big percentage of their active sites is inaccessible. Future researchers in the field can try different synthesis procedures which allow the formation of even smaller crystals in order to increase the external surface area of the catalyst. Another way to enhance the internal way to do it is through choosing organic linkers functionalized with only one COOH group rather than two for example. Another way is to choose a linker with greater length to provide bigger pore sizes and more open porous networks for easier diffusion of the reactants inside the porous network. Besides the active sites on the linker, future researchers could assess the activity of other structures, incorporating cheaper metals in their clusters, in order to boost the economic competiveness of MOFs as catalysts. As we believe that a big part of the active sites of the MOF structures are still not accessible for the reactants, we expect that working on the diffusion inside the porous network could boost the catalytic activity of the MOFs in a way that it behaves

similar to the liquid acid catalyst at the beginning of the reaction and not only after 24 hours, and thus be the next generation of catalysts capable of bridging the gap between homogeneous and heterogeneous catalysis.

The work could also be expanded considering a different type of reaction to produce butyl butyrate such as the One-Step Hydrogenation Esterification reaction instead of the common esterification reaction. In this reaction, the butyric acid is hydrogenated into butanol over a noble metal catalyst, and the butanol reacts with the excess butyric acid to form butyl butyrate under an acidic catalyst Having very large surface area, a sophisticated porous network, and several types of sites where metal nanoparticles can be loaded, MOFs make great support for active metal sites and thus an interesting candidate for OHE reactions for butyl butyrate production, although this had never been investigated before. OHE reactions have the potential of replacing conventional esterification reactions having the advantage of starting with one reactant, the carboxylic acid, rather than two.

Another significantly useful tool to complement this work with is using various modeling tools such as molecular dynamic simulations. Computer simulations will be helpful in understanding the properties of molecules, their structures, and the microscopic interactions between them, which complements experimental work and also guides it by enabling us to understand the phenomenon taking place at a microscopic level. Computer simulations thus act as a link between the microscopic length and time scales, and the macroscopic scale in the laboratory, enabling us to study the interactions between molecules and to predict values of bulk properties. This means that the hidden reasons behind bulk measurements can be understood using computer simulations which act as the bridge between theory and experiment. Developed models

can be tested using the extensive experimental work done as a part of this dissertation, afterwards, theories can be tested using the same model without having to run experimental runs for each one of them.

## A. SUPPLEMENTARY INFORMATION

### *1. The effect of organic linker functionalization*

a. XRD of fresh samples

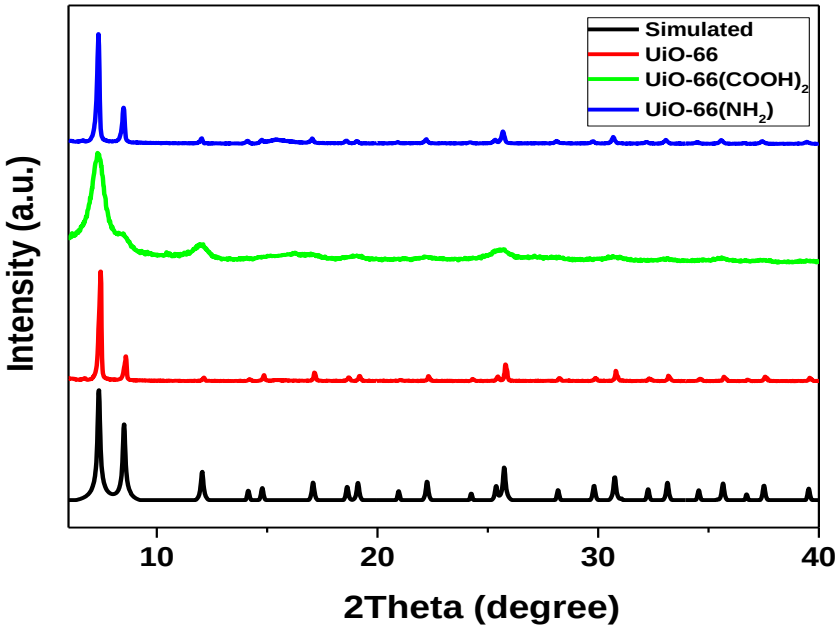


**Figure S1:** PXRD patterns of prepared MOFs compared to the simulated pattern from UiO-66 structure

b. Nitrogen adsorption-desorption isotherms

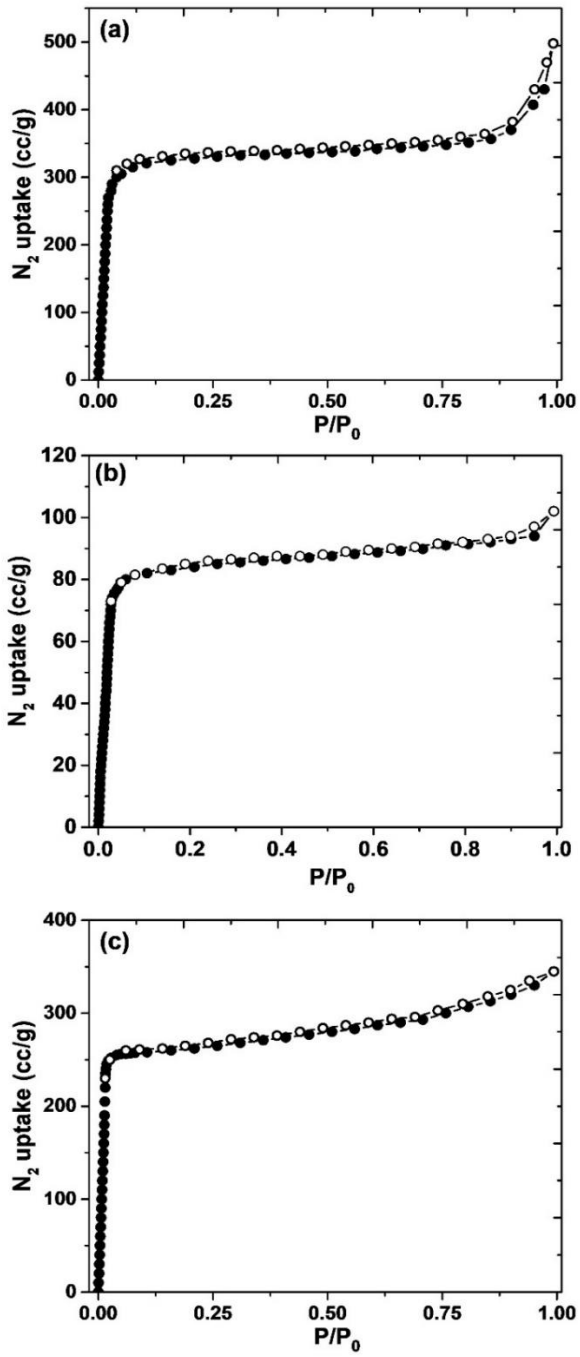


**Figure S2:** Nitrogen adsorption-desorption isotherms of the prepared catalysts at 77 K (a) UiO-66 (b) UiO-66$(COOH)_2$ (c) UiO-66$(NH_2)$. ° Adsorption • Desorption

c. SEM images

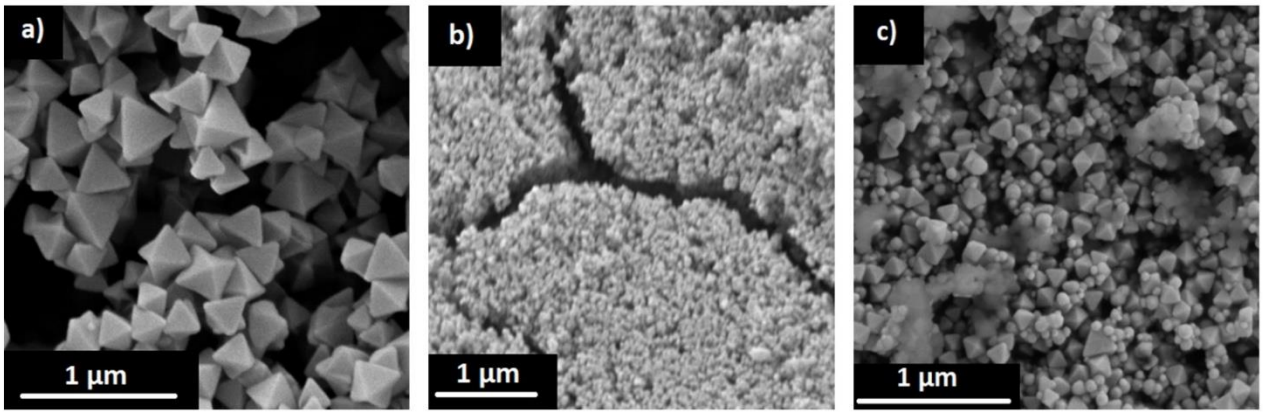


**Figure S3:** SEM images of the studied MOFs (a) UiO-66 (b) UiO-66$(COOH)_2$ (c) UiO-66$(NH_2)$

d. Calculation of missing linkers based on TGA data

The calculation of the number of missing linkers per cluster have been discussed in detail in a previous study [79], but it will be repeated briefly for clarification.

The calculation is based on the assumption that the only solid product remaining after the combustion of the UiO-66 samples is 6 $ZrO_2$. Taking UiO-66 as an example, the reaction for the combustion is given below:

$$Zr_6O_4(OH)_4(BDC)_6\ (s) + 45\ O_2\ (g) \rightarrow 6\ ZrO_2\ (s) + 48\ CO_2\ (g) + 12\ H_2O\ (g)$$

The theoretical weight-loss plateau should be the ratio of the molecular weight of the hydroxylated UiO-66 sample to that of the 6 $ZrO_2$. If the TGA curve was

normalized to have the final weight-loss equal to 100%, then the theoretical weight-loss plateau could be calculated as follows:

$$WLP_{th} = \frac{MW_{MOF}}{MW_{6\ ZrO_2}} * WL_{final}$$

Where $WLP_{th}$ is the theoretical weight-loss plateau of the studied hydroxylated MOF structure, $MW_{6\ ZrO_2}$ is the molecular weight of 6 $ZrO_2$, and $WL_{final}$ is the final value of the weight-loss which is set to be 100% in the normalized curve (**Fig. 7**).

The experimental weight-loss plateau $WLP_{exp}$could be defined as the vertical line passing through the intercept between the TGA curve and the temperature after which the weight-loss is attributed to the combustion of the linker, $T_{link}$. Considering **Fig. 7**, it is clear that there is a gap between the theoretical weight plateau $WLP_{th}$ and the experimental weight plateau $WLP_{exp}$ in all three MOFs used. This shows that all structures are missing linkers and have thus a defective framework.

To account for the theoretical weight-loss attributed to each linker, $WL_{link}$, the following formula is used:

$$WL_{link} = \frac{WLP_{th} - WL_{final}}{NL_{th}}$$

Where $NL_{th}$ is the theoretical number of linkers per hydroxylated $Zr_6$ unit.

The experimental number of linkers per $Zr_6$ unit, $NL_{exp}$, could thus be calculated as follows:

$$NL_{exp} = \frac{WLP_{exp} - WL_{final}}{WL_{link}}$$

And finally, the number of missing linkers, $NL_{mis.}$ is the difference between the theoretical number of linkers $NL_{th}$, and the calculated experimental number of linkers $NL_{exp}$.

$$NL_{mis.} = NL_{th} - NL_{exp}$$

The following table shows the values used for calculation for each MOF structure along with the results.

**Table S1:** Results of TGA cruves analysis

| Zr-MOF | $MW_{MOF}$ (g/mol) | $WLP_{th}$ (%) | $WLP_{exp}$ (%) | $WL_{link}$ (%) | $NL_{exp}$ | $NL_{mis.}$ |
|---|---|---|---|---|---|---|
| **UiO-66** | 1664 | 225.05 | 195.98 | 20.84 | 4.60 | 1.39 |
| **UiO-66(COOH)$_2$** | 2216 | 299.77 | 255.80 | 33.29 | 4.68 | 1.32 |
| **UiO-66(NH$_2$)** | 1765 | 238.77 | 198.91 | 23.12 | 4.27 | 1.72 |

e. Esterification reaction results under different heterogeneous acid catalysts

**Table S2:** Conversion to butyl butyrate over 24 hours in the esterification reaction of butyric acid in presence of butanol using 5% loading of different acid catalysts.

| **Conversion to butyl butyrate (%)** | | | | | |
|---|---|---|---|---|---|
| **Catalyst** | | | | | |
| | 2 hours | 4 hours | 6 hours | 8 hours | 24 hours |
| **UiO-66** | 23.6 | 38.0 | 50.7 | 59.9 | 83.4 |
| **UiO-66(COOH)$_2$** | 26.2 | 41.1 | 54.6 | 64.5 | 90.2 |
| **UiO-66(NH$_2$)** | 19.7 | 31.3 | 38.0 | 45.6 | 74.7 |
| **Blank** | 14.0 | 24.6 | 29.3 | 31.8 | 45.4 |
| **H$_2$SO$_4$** | 78.6 | 84.3 | 88.5 | 89.7 | 94.9 |
| **H-Beta** | 20.5 | 36.3 | 45.6 | 53.7 | 73.5 |
| **H-USY** | 30.0 | 45.1 | 53.3 | 56.9 | 81.1 |

f. XRD patterns of fresh and recycled synthesized MOFs

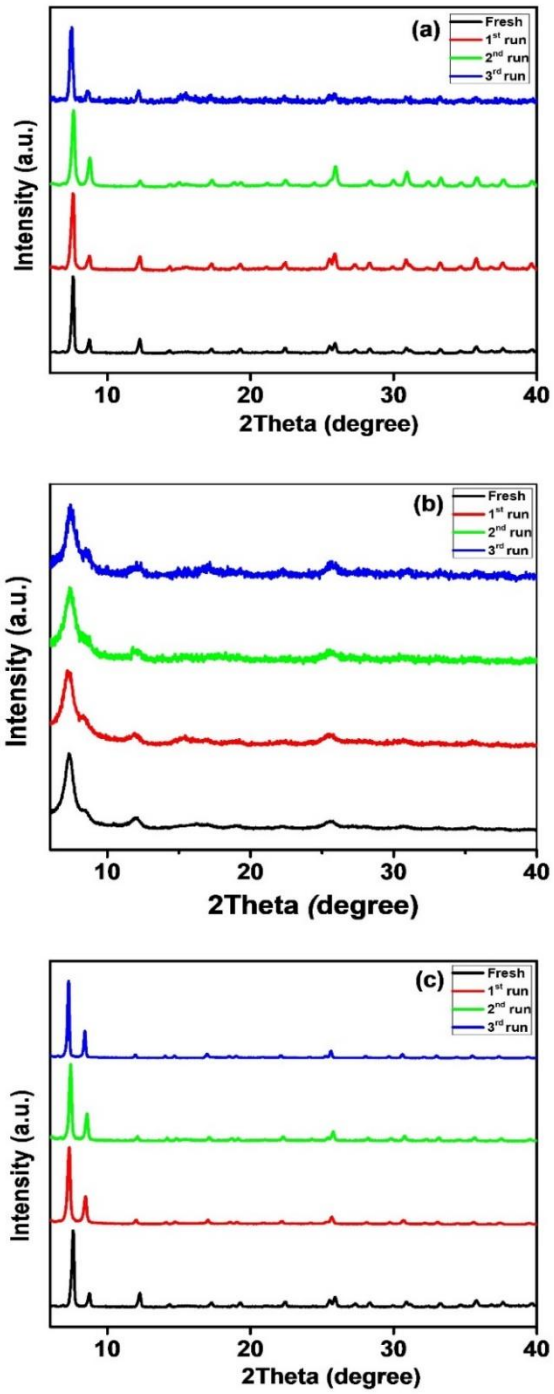


**Figure S4:** XRD patterns of fresh and recycled synthesized MOFs (A) UiO-66 (B) UiO-66($COOH_)2$ (C) UiO-66($NH_2$)

g. Effect of stirring speed on conversion to butyl butyrate

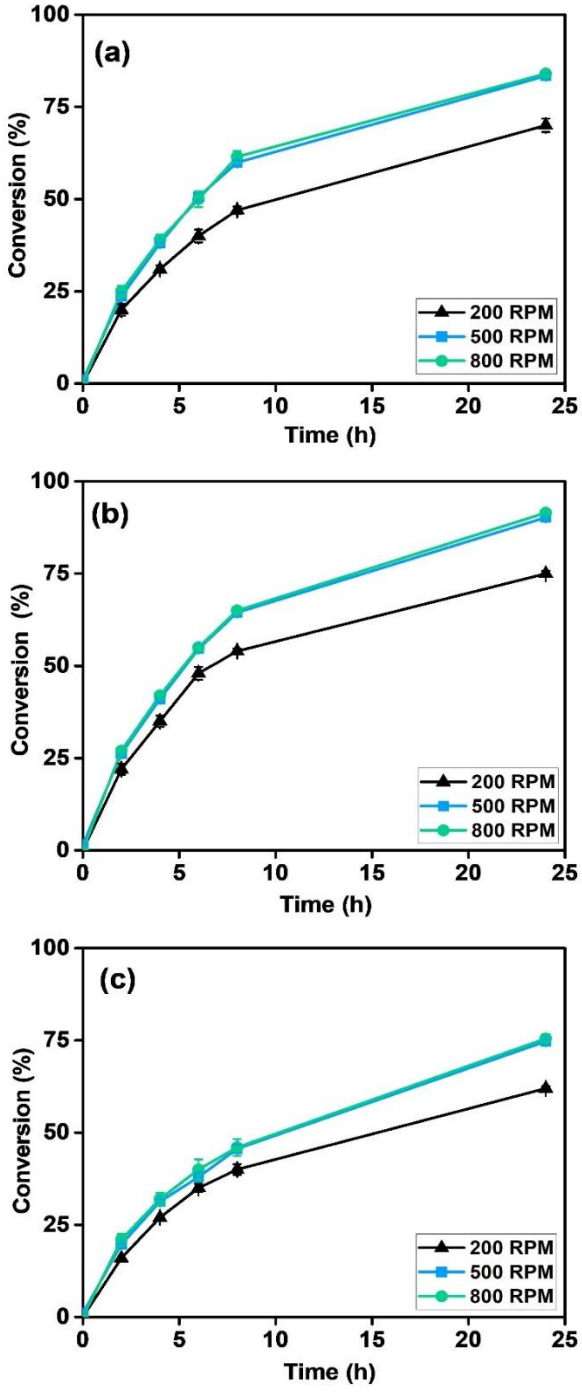


**Figure S5:** Effect of the stirring speed on the esterification reaction of butyric acid in presence of butanol under 5% loading of (a) UiO-66 (b) UiO-66$(COOH)_2$ (c) UiO-66$(NH_2)$

### *2. The effect of defect engineering*

a. Materials

The chemical reagents used for the synthesis of the MOFs and the esterification reaction were commercially available and were used directly without further purification. The organic linkers used for the synthesis of MOFs studied, terephthalic acid ($C_6H_4(CO_2H)_2$, 99%), *1,2,4,5*-benzenetetracarboxylic acid ($C_{10}H_6O_8$, 96%), and *2*-aminoterephthalic acid ($C_8H_7NO_4$, 99%), and the modulators used, acetic acid ($C_2H_4O_2$, 99%), and formic acid ($CH_2O_2$, 98-100%) were obtained from Sigma Aldrich. The Metal used for the synthesis of MOFs, zirconium chloride ($ZnCl_4$, 98%), and the chemicals required for the esterification reaction, GC calibration, and GC running, *1*-butanol ($C_4H_{10}O$, 99%, extra pure), *n*-butyric acid ($C_4H_{18}O_2$, 99%, extra pure), butyl butyrate (98%, Acros Organics), heptane ($C_7H_{16}$, HPLC grade) and *1*-octanol ($C_8H_{18}O$, 99%, pure), were obtained from Acros Organics. *N*,*N*-dimethylformamide (DMF, Analytical reagent grade), and dichloromethane (DCM, Analytical reagent grade) were purchased from Fisher Scientific.

b. Supplementary results

i. Scanning electron microscopy (SEM)

Additional SEM images of the samples were taken at a scale of 2 μm as indicated in **Figure S6**.

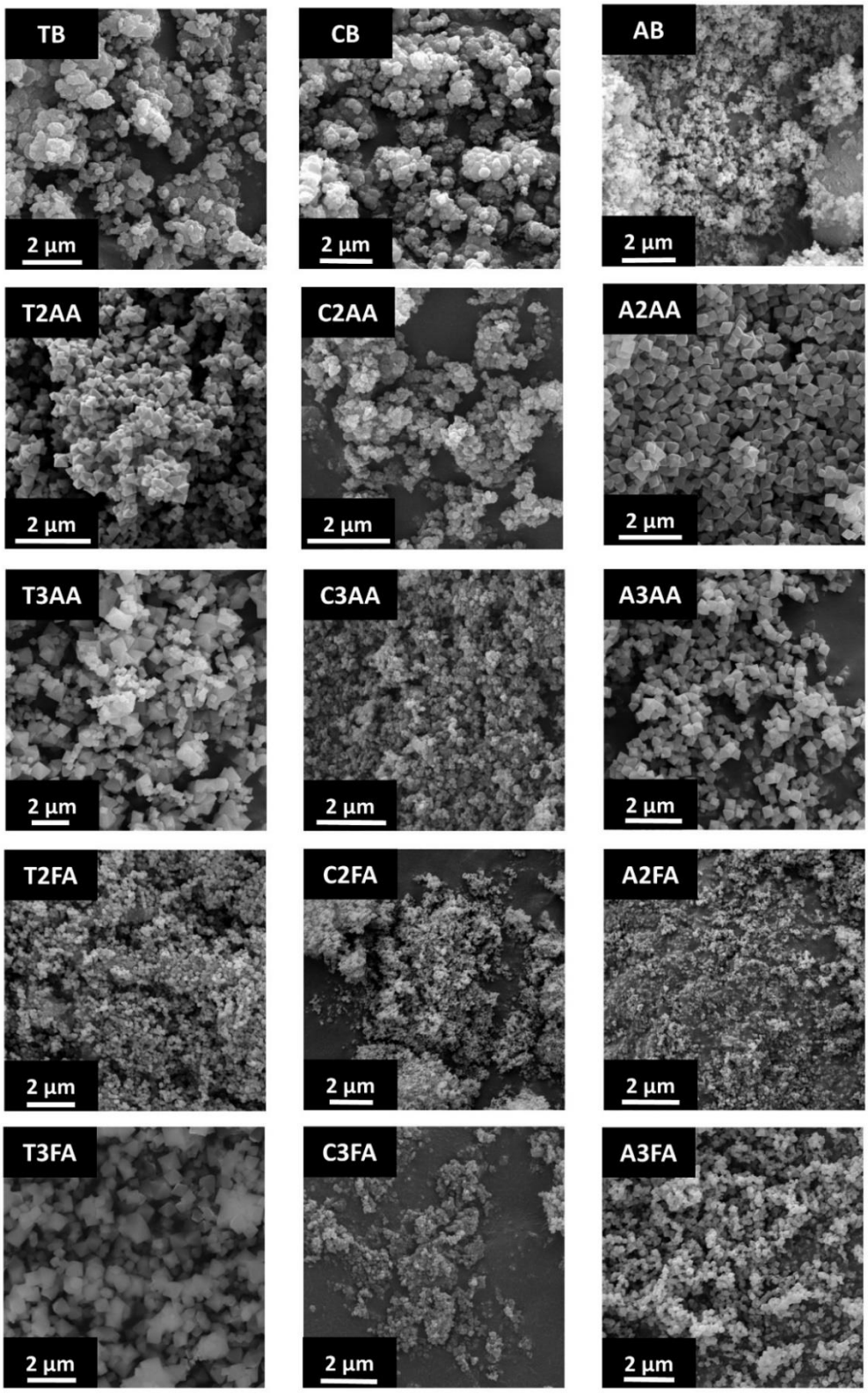


**Figure S6:** SEM images at a 2 µm scale for all the 15 MOF catalysts synthesized

ii. Powder X-Ray Diffraction (PXRD)

**Figure S7** shows the PXRD patterns of MOF catalysts after being used in the esterification reaction and washed for a second time. The obtained patterns match the ones of the fresh samples indicating that the samples remain stable after the esterification reaction of butyric acid in presence of butanol.

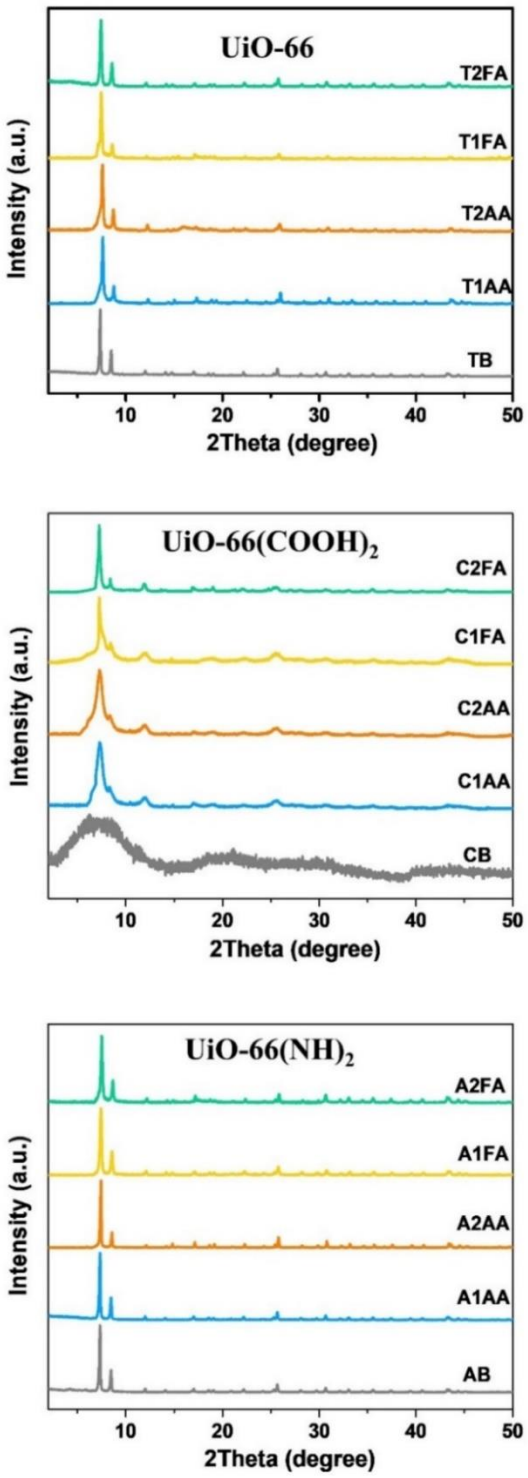


**Figure S7:** PXRD patterns of the recycled 15 MOFs catalysts synthesized after washing and activation

iii. Catalysts recyclability and stability

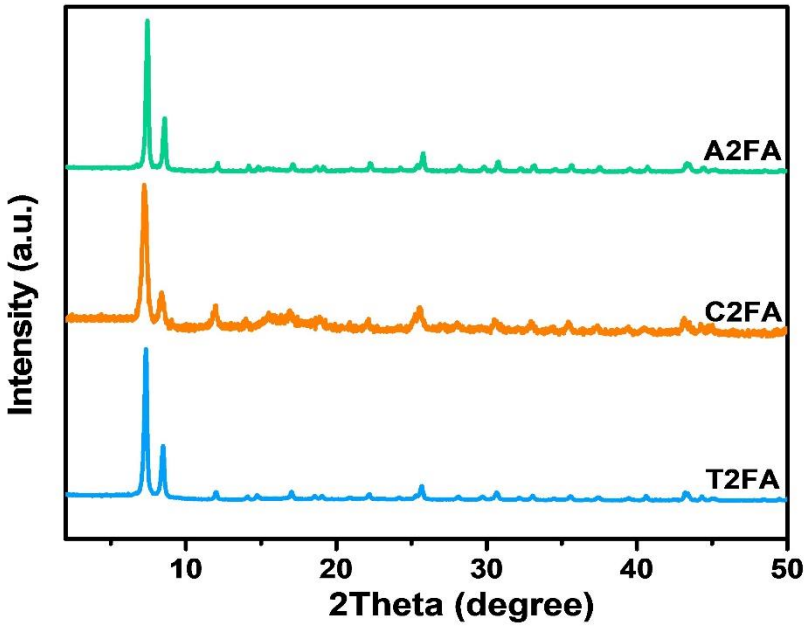


**Figure S8:** PXRD patterns of the recycled T2FA, C2FA, and A2FA catalysts after washing and activation following the 4$^{th}$ use in the esterification reaction

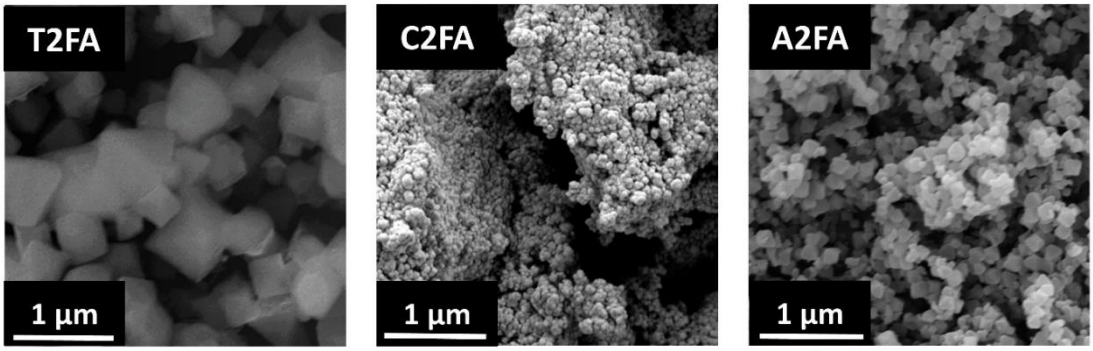


**Figure S9:** SEM images of the recycled T2FA, C2FA, and A2FA catalysts after washing and activation following the 4$^{th}$ use in the esterification reaction

iv. Effect of stirring speed

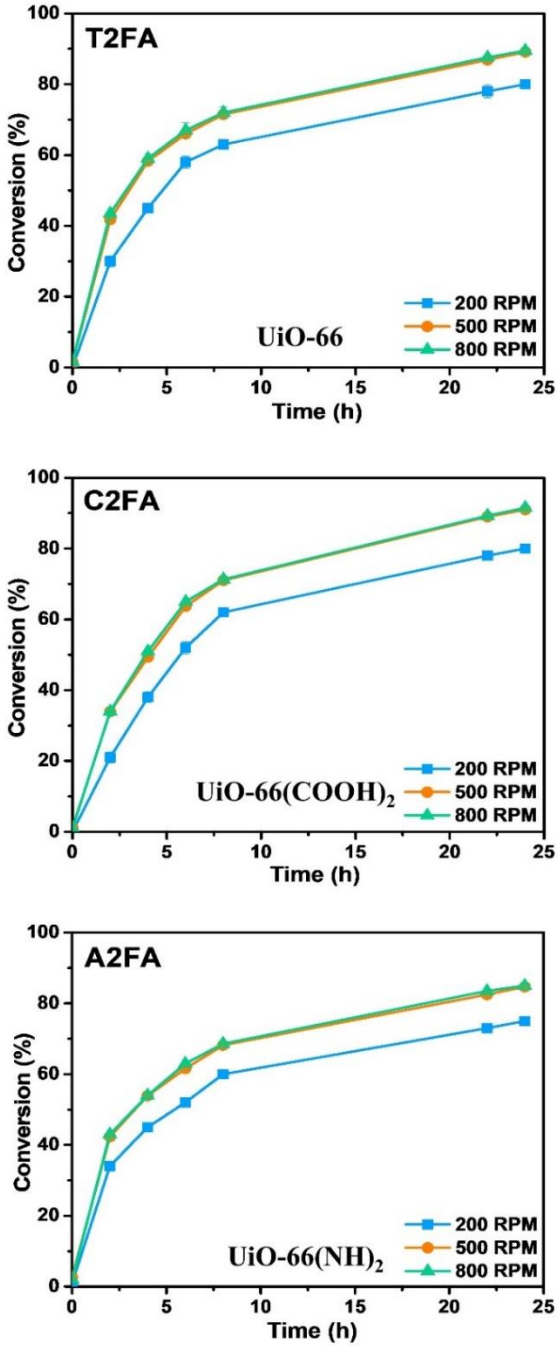


**Figure S10:** The effect of the stirring speed in the esterification reaction on the conversion to butyl butyrate using T2FA, C2FA, and A2FA

### *3. Multivariate (MTV-MOFs) or Mixed-Linker approach*

a. Materials

The chemicals used in this study were commercially provided and used directly in experiments without further purification. Terephthalic acid ($C_6H_4(CO_2H)_2$, 99%), *1*,*2*,*4*,*5*-benzenetetracarboxylic acid ($C_{10}H_6O_8$, 96%), 2,5-Dihydroxyterephthalic acid ($C_8H_7NO_4$, 99%), sodium bicarbonate ($NaHCO_3$, 99%), deuterium oxide ($D_2O$, 99% atom D), and formic acid ($CH_2O_2$, 98-100%) were purchased from Sigma Aldrich. Zirconium chloride ($ZnCl_4$, 98%), *1*-butanol ($C_4H_{10}O$, 99%, extra pure), *n*-butyric acid ($C_4H_{18}O_2$, 99%, extra pure), butyl butyrate (98%, Acros Organics), heptane ($C_7H_{16}$, HPLC grade) and *1*-octanol ($C_8H_{18}O$, 99%, pure), were purchased from Acros Organics. *N*,*N*-dimethylformamide (DMF, Analytical reagent grade), and dichloromethane (DCM, Analytical reagent grade) were purchased from Fisher Scientific.

b. Powder X-Ray Diffraction (PXRD)

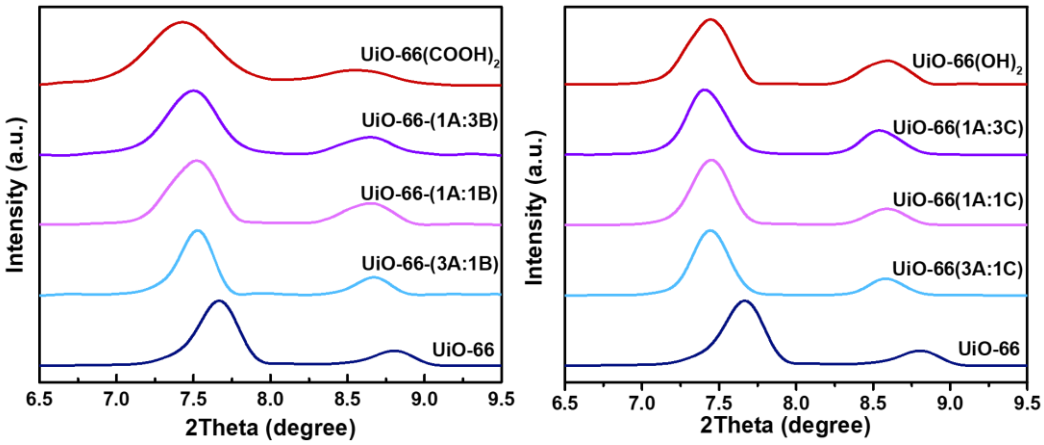


**Figure S11:** A narrow 2theta range of the PXRD patterns of the MTV-MOFs showing the shift in peaks towards a lower angle with the increase in incorporation of the functionalized linkers

c. [1]H-NMR results

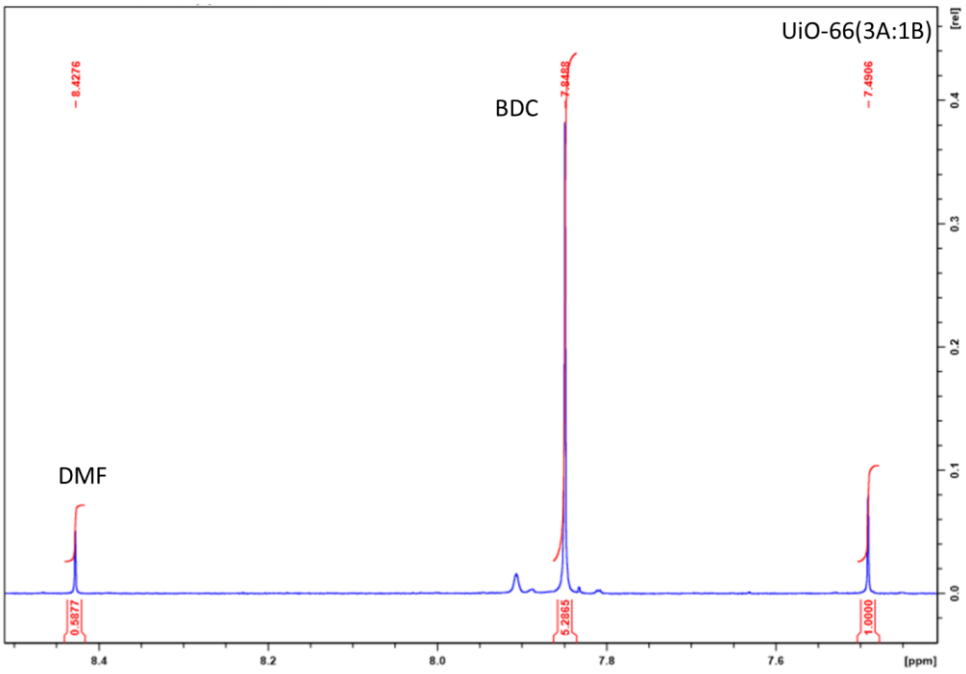


**Figure S12:** [1]H-NMR spectra of UiO-66(3A:1B)

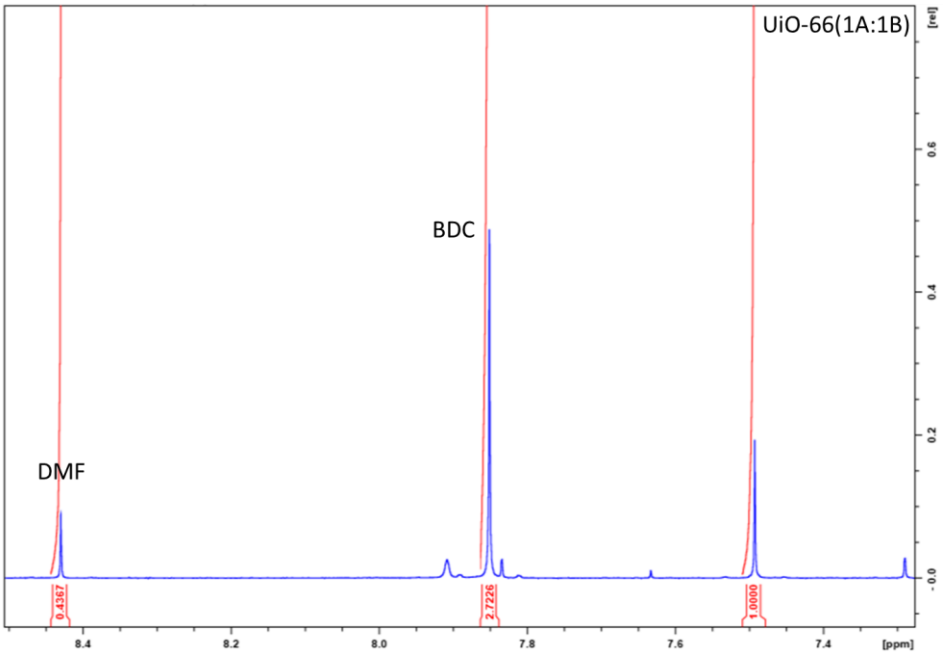


**Figure S13:** [1]H-NMR spectra of UiO-66(1A:1B)

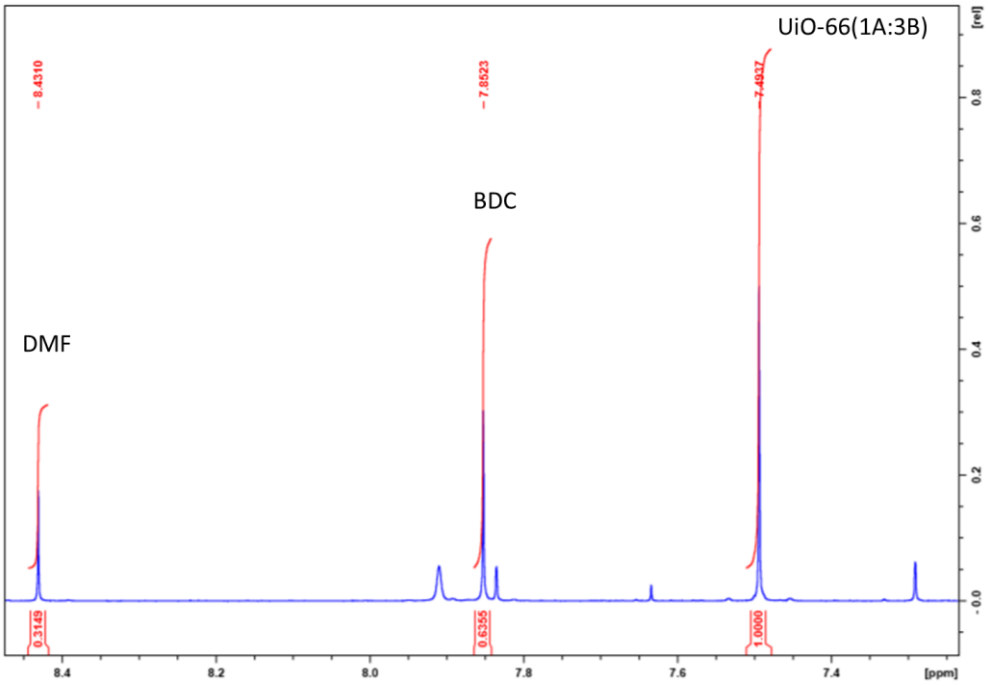


**Figure S14:** 1H-NMR spectra of UiO-66(1A:3B)

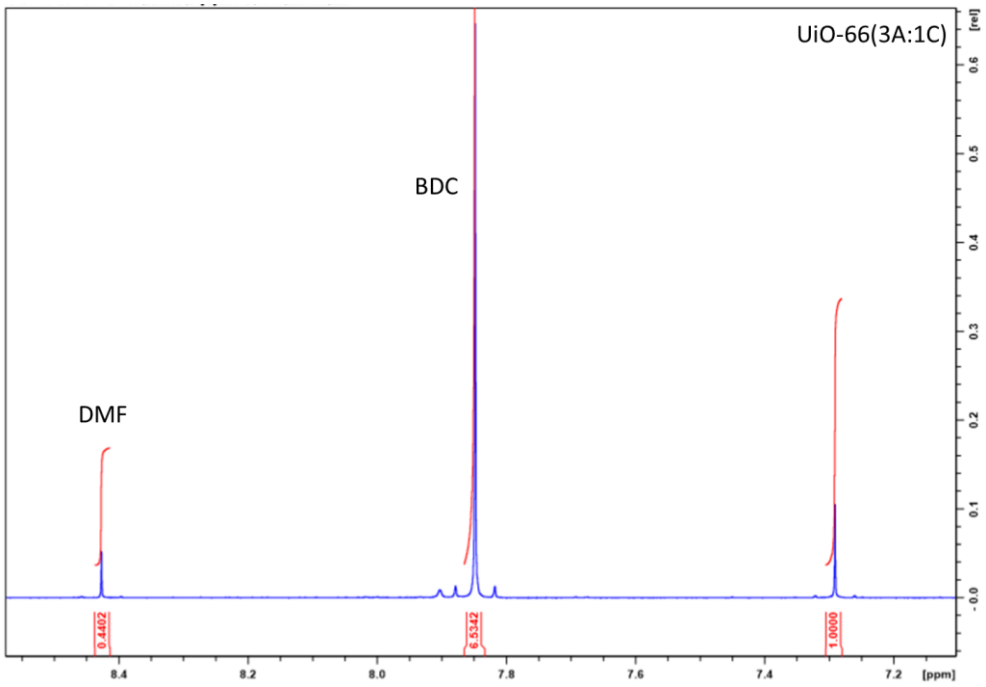


**Figure S15:** [1]H-NMR spectra of UiO-66(3A:1C)

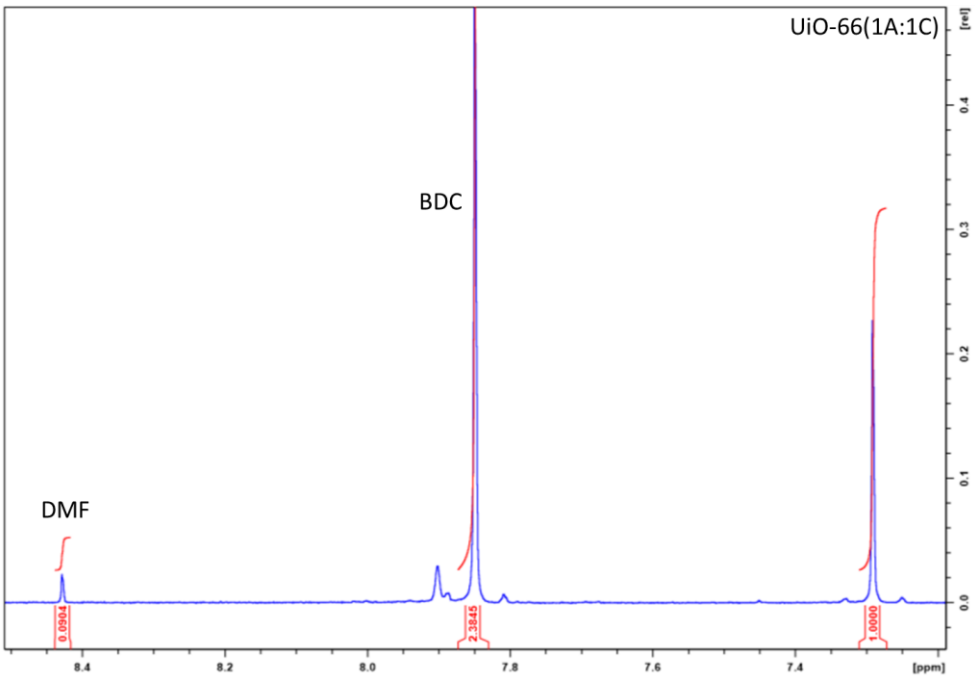


**Figure S16:** $^{1}$H-NMR spectra of UiO-66(1A:1C)

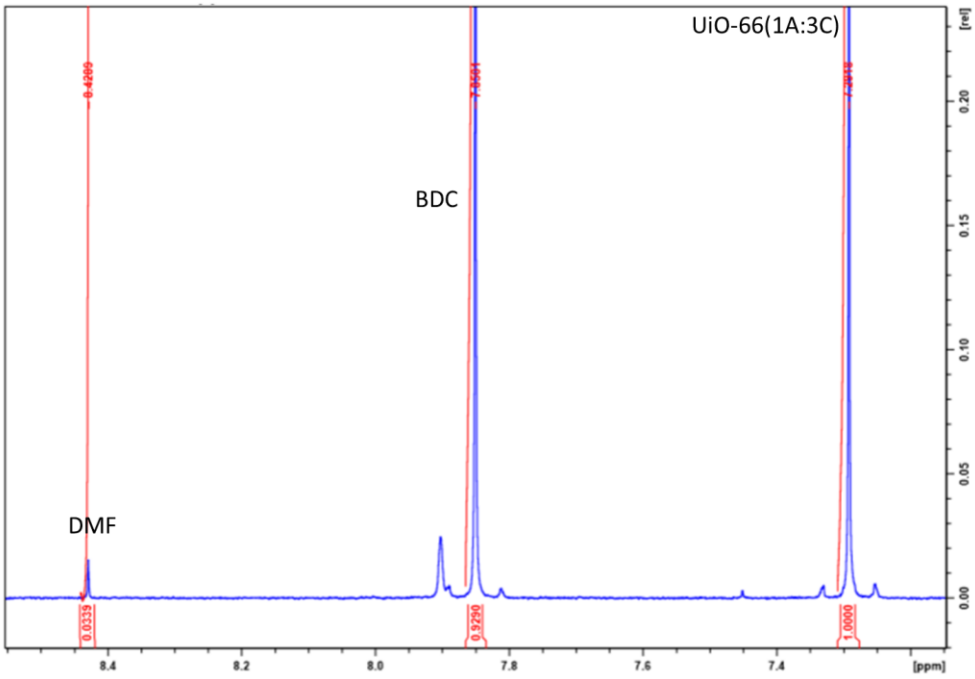


**Figure S17:** $^{1}$H-NMR spectra of UiO-66(1A:3C)

d. Regression model supplementary data

**Table S3:** parameters used to build the regression model

| MOF | Defects Number | Surface Area | Catalyst Loading | % T | %A | % C | Conversion | Reference |
|---|---|---|---|---|---|---|---|---|
| **UiO-66** | 1.39 | 1052 | 5 | 1 | 0 | 0 | 83.4 | [143] |
| **UiO-66(COOH)2** | 1.32 | 284 | 5 | 0 | 0 | 1 | 90.2 | [143] |
| **UiO-66(NH)2** | 1.72 | 801 | 5 | 0 | 1 | 0 | 74.7 | [143] |
| **UiO-66** | 1.39 | 1052 | 2 | 1 | 0 | 0 | 75.4 | [143] |
| **UiO-66(COOH)2** | 1.32 | 284 | 2 | 0 | 0 | 1 | 81.5 | [143] |
| **UiO-66(NH)2** | 1.72 | 801 | 2 | 0 | 1 | 0 | 67.7 | [143] |
| **UiO-66** | 1.39 | 1052 | 1 | 1 | 0 | 0 | 69.9 | [143] |
| **UiO-66(COOH)2** | 1.32 | 284 | 1 | 0 | 0 | 1 | 75.4 | [143] |
| **UiO-66(NH)2** | 1.72 | 801 | 1 | 0 | 1 | 0 | 60.15 | [143] |
| **TB** | 1.36 | 1049 | 2 | 1 | 0 | 0 | 57.2 | [121] |
| **T1AA** | 1.5 | 1490 | 2 | 1 | 0 | 0 | 70.4 | [121] |
| **T2AA** | 1.53 | 1593 | 2 | 1 | 0 | 0 | 78.1 | [121] |
| **T1FA** | 1.72 | 1695 | 2 | 1 | 0 | 0 | 83.6 | [121] |
| **T2FA** | 1.86 | 1813 | 2 | 1 | 0 | 0 | 89.1 | [121] |
| **CB** | 0.88 | 51 | 2 | 0 | 0 | 1 | 63.3 | [121] |
| **C1AA** | 1.38 | 268 | 2 | 0 | 0 | 1 | 77.4 | [121] |
| **C2AA** | 1.44 | 376 | 2 | 0 | 0 | 1 | 81.5 | [121] |
| **C1FA** | 1.9 | 517 | 2 | 0 | 0 | 1 | 88.2 | [121] |
| **C2FA** | 1.93 | 522 | 2 | 0 | 0 | 1 | 91.5 | [121] |
| **AB** | 1.5 | 1016 | 2 | 0 | 1 | 0 | 64.2 | [121] |
| **A1AA** | 1.67 | 1294 | 2 | 0 | 1 | 0 | 69.6 | [121] |
| **A2AA** | 1.73 | 1434 | 2 | 0 | 1 | 0 | 77.2 | [121] |
| **A1FA** | 1.87 | 1570 | 2 | 0 | 1 | 0 | 80.3 | [121] |
| **A2FA** | 2.02 | 1723 | 2 | 0 | 1 | 0 | 84.7 | [121] |
| **T2FA (1%)** | 1.87 | 1812 | 1 | 1 | 0 | 0 | 75 | This study |
| **C2FA (1%)** | 1.93 | 522 | 1 | 0 | 0 | 1 | 76.4 | This study |
| **UiO-66(OH)2** | 1.51 | 602 | 1 | 0 | 0 | 0 | 80.4 | This study |
| **UiO-66(3A:1B)** | 1.83 | 773 | 1 | 0.84 | 0 | 0.16 | 70.3 | This study |
| **UiO-66(1A:1B)** | 2.14 | 657 | 1 | 0.73 | 0 | 0.27 | 85.3 | This study |

| | | | | | | | | |
|---|---|---|---|---|---|---|---|---|
| **UiO-66(1A:3B)** | 1.98 | 609 | 1 | 0.39 | 0 | 0.61 | 88.8 | This study |
| **UiO-66(3A:1C)** | 1.33 | 1290 | 1 | 0.87 | 0 | 0 | 72.5 | This study |
| **UiO-66(1A:1C)** | 1.73 | 947 | 1 | 0.74 | 0 | 0 | 86.5 | This study |
| **UiO-66(1A:3C)** | 1.9 | 761 | 1 | 0.48 | 0 | 0 | 82.2 | This study |

**Table S4:** Normalazied parameters used to build the regression model

| MOF | Defects Number | Surface Area | Catalyst Loading | % T | %A | % C | Conversion | Reference |
|---|---|---|---|---|---|---|---|---|
| **UiO-66** | 0.40 | 0.57 | 1.00 | 1.00 | 0.00 | 0.00 | 83.4 | [143] |
| **UiO-66(COOH)$_2$** | 0.35 | 0.13 | 1.00 | 0.00 | 0.00 | 1.00 | 90.2 | [143] |
| **UiO-66(NH)$_2$** | 0.67 | 0.43 | 1.00 | 0.00 | 1.00 | 0.00 | 74.7 | [143] |
| **UiO-66** | 0.40 | 0.57 | 0.25 | 1.00 | 0.00 | 0.00 | 75.4 | [143] |
| **UiO-66(COOH)$_2$** | 0.35 | 0.13 | 0.25 | 0.00 | 0.00 | 1.00 | 81.5 | [143] |
| **UiO-66(NH)$_2$** | 0.67 | 0.43 | 0.25 | 0.00 | 1.00 | 0.00 | 67.7 | [143] |
| **UiO-66** | 0.40 | 0.57 | 0.00 | 1.00 | 0.00 | 0.00 | 69.9 | [143] |
| **UiO-66(COOH)$_2$** | 0.35 | 0.13 | 0.00 | 0.00 | 0.00 | 1.00 | 75.4 | [143] |
| **UiO-66(NH)$_2$** | 0.67 | 0.43 | 0.00 | 0.00 | 1.00 | 0.00 | 60.15 | [143] |
| **TB** | 0.38 | 0.57 | 0.25 | 1.00 | 0.00 | 0.00 | 57.2 | [121] |
| **T1AA** | 0.49 | 0.82 | 0.25 | 1.00 | 0.00 | 0.00 | 70.4 | [121] |
| **T2AA** | 0.52 | 0.88 | 0.25 | 1.00 | 0.00 | 0.00 | 78.1 | [121] |
| **T1FA** | 0.67 | 0.93 | 0.25 | 1.00 | 0.00 | 0.00 | 83.6 | [121] |
| **T2FA** | 0.78 | 1.00 | 0.25 | 1.00 | 0.00 | 0.00 | 89.1 | [121] |
| **CB** | 0.00 | 0.00 | 0.25 | 0.00 | 0.00 | 1.00 | 63.3 | [121] |
| **C1AA** | 0.40 | 0.12 | 0.25 | 0.00 | 0.00 | 1.00 | 77.4 | [121] |
| **C2AA** | 0.44 | 0.18 | 0.25 | 0.00 | 0.00 | 1.00 | 81.5 | [121] |
| **C1FA** | 0.81 | 0.26 | 0.25 | 0.00 | 0.00 | 1.00 | 88.2 | [121] |
| **C2FA** | 0.83 | 0.27 | 0.25 | 0.00 | 0.00 | 1.00 | 91.5 | [121] |
| **AB** | 0.49 | 0.55 | 0.25 | 0.00 | 1.00 | 0.00 | 64.2 | [121] |
| **A1AA** | 0.63 | 0.71 | 0.25 | 0.00 | 1.00 | 0.00 | 69.6 | [121] |
| **A2AA** | 0.67 | 0.78 | 0.25 | 0.00 | 1.00 | 0.00 | 77.2 | [121] |
| **A1FA** | 0.79 | 0.86 | 0.25 | 0.00 | 1.00 | 0.00 | 80.3 | [121] |
| **A2FA** | 0.90 | 0.95 | 0.25 | 0.00 | 1.00 | 0.00 | 84.7 | [121] |
| **T2FA (1%)** | 0.79 | 1.00 | 0.00 | 1.00 | 0.00 | 0.00 | 75 | This study |
| **C2FA (1%)** | 0.83 | 0.27 | 0.00 | 0.00 | 0.00 | 1.00 | 76.4 | This study |
| **UiO-66(OH)$_2$** | 0.50 | 0.31 | 0.00 | 0.00 | 0.00 | 0.00 | 80.4 | This study |
| **UiO-66(3A:1B)** | 0.75 | 0.41 | 0.00 | 0.84 | 0.00 | 0.16 | 70.3 | This study |

| | | | | | | | | |
|---|---|---|---|---|---|---|---|---|
| **UiO-66(1A:1B)** | 1.00 | 0.34 | 0.00 | 0.73 | 0.00 | 0.27 | 85.3 | This study |
| **UiO-66(1A:3B)** | 0.87 | 0.32 | 0.00 | 0.39 | 0.00 | 0.61 | 88.8 | This study |
| **UiO-66(3A:1C)** | 0.36 | 0.70 | 0.00 | 0.87 | 0.00 | 0.00 | 72.5 | This study |
| **UiO-66(1A:1C)** | 0.67 | 0.51 | 0.00 | 0.74 | 0.00 | 0.00 | 86.5 | This study |
| **UiO-66(1A:3C)** | 0.81 | 0.40 | 0.00 | 0.48 | 0.00 | 0.00 | 82.2 | This study |

**Table S*5*:** The parameters suggested for the model along with their corresponding regression coefficients and p-values

| Independent Variables | Coefficients | P-value |
|---|---|---|
| **Cst** | 39.95 | 1.82E-08 |
| **% A** | 6.87 | 1.10E-02 |
| **% B** | 21.94 | 3.98E-06 |
| **%C** | 25.25 | 1.18E-04 |
| **DN** | 25.07 | 1.57E-05 |
| **SA** | 16.19 | 1.12E-02 |
| **CL** | 15.38 | 2.75E-04 |

**Table S6:** The regression model statistics summary

| Model Evaluation Parameter | Value |
|---|---|
| **Multiple R** | 0.850 |
| **$R^2$** | 0.723 |
| **Adjusted $R^2$** | 0.659 |
| **Standard Error** | 5.191 |
| **Observations** | 33 |
| **Significance F** | 3.286E-06 |

**Table S7:** Model-predicted vs. experimentally obtained conversion to butyl butyrate and the average error between the two for the set of experiments done

| Observation | MOF | $Conv_{mod}$ | $Conv_{exp}$ | *Residuals* |
|---|---|---|---|---|
| **1** | UiO-66 | 81.6 | 83.4 | 1.84 |
| **2** | UiO-66$(COOH)_2$ | 88.2 | 90.2 | 2.03 |
| **3** | UiO-66$(NH)_2$ | 78.9 | 74.7 | -4.24 |
| **4** | UiO-66 | 70.0 | 75.4 | 5.39 |
| **5** | UiO-66$(COOH)_2$ | 76.6 | 81.5 | 4.87 |
| **6** | UiO-66$(NH)_2$ | 67.4 | 67.7 | 0.30 |
| **7** | UiO-66 | 66.2 | 69.9 | 3.73 |
| **8** | UiO-66$(COOH)_2$ | 72.8 | 75.4 | 2.62 |
| **9** | UiO-66$(NH)_2$ | 63.6 | 60.15 | -3.41 |
| **10** | TB | 69.4 | 57 | -12.19 |
| **11** | T1AA | 76.2 | 70.4 | -5.83 |
| **12** | T2AA | 77.8 | 78.1 | 0.33 |
| **13** | T1FA | 82.5 | 83.6 | 1.11 |
| **14** | T2FA | 86.4 | 89.1 | 2.74 |
| **15** | CB | 65.7 | 63.3 | -2.43 |
| **16** | C1AA | 77.7 | 77.4 | -0.28 |
| **17** | C2AA | 79.9 | 81.5 | 1.64 |
| **18** | C1FA | 90.3 | 88.2 | -2.11 |
| **19** | C2FA | 91.0 | 91.5 | 0.55 |
| **20** | AB | 65.0 | 64.2 | -0.80 |
| **21** | A1AA | 70.9 | 69.6 | -1.34 |
| **22** | A2AA | 73.4 | 77.2 | 3.78 |
| **23** | A1FA | 77.4 | 80.3 | 2.85 |
| **24** | A2FA | 81.8 | 84.7 | 2.86 |
| **25** | T2FA (1%) | 82.7 | 75 | -7.70 |
| **26** | C2FA (1%) | 87.1 | 76.4 | -10.71 |
| **27** | UiO-66$(OH)_2$ | 82.8 | 80.4 | -2.40 |
| **28** | UiO-66(3A:1B) | 74.8 | 70.3 | -4.47 |
| **29** | UiO-66(1A:1B) | 81.53 | 85.3 | 3.77 |
| **30** | UiO-66(1A:3B) | 83.03 | 88.8 | 5.77 |
| **31** | UiO-66(3A:1C) | 69.55 | 72.5 | 2.95 |
| **32** | UiO-66(1A:1C) | 76.75 | 86.5 | 9.75 |
| **33** | UiO-66(1A:3C) | 83.20 | 82.2 | -1.00 |

# BIBLIOGRAPHY


1. *BP energy outlook* 2019, British Petroleum.
2. Sirsam, R., D. Hansora, and G.A. Usmani, *A Mini-Review on Solid Acid Catalysts for Esterification Reactions.* Journal of The Institution of Engineers (India): Series E : Chemical and Textile Engineering, 2016. **97**(2): p. 167-181.
3. Hailian, L. and Eddaoudi, *Design and synthesis of an exceptionally stable and highly porous metal-organic framework.* Nature, 1999. **402**(6759).
4. Hers, J.S., B.C.C.v.d. Zwaan, and J. Bollen, *An Integrated Assessment of Climate Change, Air Pollution, and Energy Security Policy*. 2010, Petten: ECN.
5. Agarwal, A.K., *Biofuels (alcohols and biodiesel) applications as fuels for internal combustion engines.* Progress in Energy and Combustion Science, 2007. **33**(3): p. 233-271.
6. Klevas, V., et al., *Measures for increasing demand of solar energy.* Renewable and Sustainable Energy Reviews, 2013. **27**: p. 55-64.
7. Demirbas, A., *Competitive liquid biofuels from biomass.* Applied Energy, 2011. **88**(1): p. 17-28.
8. Sjöblom, M., et al., *In situ biocatalytic synthesis of butyl butyrate in diesel and engine evaluations.* ChemCatChem, 2017: p. 4529-4537.
9. Jenkins, R.W., et al., *Potential renewable oxygenated biofuels for the aviation and road transport sectors.* Fuel, 2013. **103**(4): p. 593-599.
10. Severini, F., J.J. Leahy, and W. Kwapinski, *Heterogeneous Char Based Solid Acid Catalysts from Brown Bin Waste to Create a Green Process for the Production of Butyl Butyrate.* Waste Biomass Valor Waste and Biomass Valorization, 2017. **8**(7): p. 2431-2441.
11. Hoydonckx, H.E., et al., *Esterification and Transesterification of Renewable Chemicals.* Topics in Catalysis, 2004. **27**(1-4): p. 83-96.
12. Trejda, M., A. Nurwita, and D. Kryszak, *Synthesis of solid acid catalysts for esterification with the assistance of elevated pressure.* Microporous and Mesoporous Materials, 2019. **278**: p. 115-120.
13. Li, C. and Y. Liu. *Bridging heterogeneous and homogeneous catalysis : concepts, strategies, and applications*. 2014.
14. Severini, F., et al., *Development of heterogeneous acid catalysts produced from the carbonization of Miscanthus x giganteus for the esterification of butyric acid to butyl butyrate with n-butanol.* JCTB Journal of Chemical Technology & Biotechnology, 2016. **91**(7): p. 2076-2084.
15. Sharma, Y.C., B. Singh, and J. Korstad, *Advancements in solid acid catalysts for ecofriendly and economically viable synthesis of biodiesel.* BBB Biofuels, Bioproducts and Biorefining, 2011. **5**(1): p. 69-92.
16. Guldhe, A., et al., *Biodiesel synthesis from microalgal lipids using tungstated zirconia as a heterogeneous acid catalyst and its comparison with homogeneous acid and enzyme catalysts.* Fuel, 2017. **187**(Supplement C): p. 180-188.
17. Sejidov, F.T., Y. Mansoori, and N. Goodarzi, *Esterification reaction using solid heterogeneous acid catalysts under solvent-less condition.* Journal of Molecular Catalysis. A, Chemical, 2005. **240**(1): p. 186-190.
18. Ma, Y., et al., *Zeolite-catalyzed esterification I. Synthesis of acetates, benzoates and phthalates.* Applied Catalysis A, General, 1996. **139**(1): p. 51-57.

19. Perot, G. and M. Guisnet, *Advantages and disadvantages of zeolites as catalysts in organic chemistry.* Journal of Molecular Catalysis, 1990. **61**(2): p. 173-196.
20. Yang, D. and B.C. Gates, *Catalysis by Metal Organic Frameworks: Perspective and Suggestions for Future Research.* ACS Catal. ACS Catalysis, 2019: p. 1779-1798.
21. Van Vu, T., et al., *Selective hydroformylation of olefins over the rhodium supported large porous metal–organic framework MIL-101.* Applied Catalysis A: General, 2013. **468**: p. 410-417.
22. Khder, A.E.R.S., H.M.A. Hassan, and M.S. El-Shall, *Metal-organic frameworks with high tungstophosphoric acid loading as heterogeneous acid catalysts.* Applied Catalysis A: General, 2014. **487**: p. 110-118.
23. Babu, R., et al., *Aqueous microwave-assisted synthesis of non-interpenetrated metal-organic framework for room temperature cycloaddition of CO2 and epoxides.* Applied Catalysis A: General, 2017. **544**: p. 126-136.
24. Pu, M., et al., *Synthesis of iron-based metal-organic framework MIL-53 as an efficient catalyst to activate persulfate for the degradation of Orange G in aqueous solution.* Applied Catalysis A: General, 2018. **549**: p. 82-92.
25. Bakuru, V.R., et al., *Exploring the Brønsted acidity of UiO-66 (Zr, Ce, Hf) metal–organic frameworks for efficient solketal synthesis from glycerol acetalization.* Dalton Transactions: An International Journal of Inorganic Chemistry, 2019. **48**(3).
26. Qin, J.S., et al., *Stable metal-organic frameworks as a host platform for catalysis and biomimetics.* Chemical communications (Cambridge, England), 2018. **54**(34): p. 4231-4249.
27. Liu, J., et al., *Applications of metal-organic frameworks in heterogeneous supramolecular catalysis.* Chemical Society reviews, 2014. **43**(16): p. 6011-61.
28. Wang, B., et al., *Nanoparticles@nanoscale metal-organic framework composites as highly efficient heterogeneous catalysts for size- and shape-selective reactions.* Nano Research, 2017. **10**(11): p. 3826-3835.
29. Zhang, F., et al., *Polyoxometalates confined in the mesoporous cages of metal–organic framework MIL-100(Fe): Efficient heterogeneous catalysts for esterification and acetalization reactions.* Chemical Engineering Journal, 2015. **269**(Supplement C): p. 236-244.
30. Yılmaz, E., E. Sert, and F.S. Atalay, *Synthesis and sulfation of titanium based metal organic framework; MIL-125 and usage as catalyst in esterification reactions.* Catalysis Communications, 2017. **100**(Supplement C): p. 48-51.
31. Chalvatzis, K.J., *Electricity generation development of Eastern Europe: A carbon technology management case study for Poland.* Renewable and Sustainable Energy Reviews, 2009. **13**(6): p. 1606-1612.
32. Martínez, D.M. and B.W. Ebenhack, *Understanding the role of energy consumption in human development through the use of saturation phenomena.* Energy Policy, 2008. **36**(4): p. 1430-1435.
33. Chalvatzis, K.J. and A. Ioannidis, *Energy supply security in the EU: Benchmarking diversity and dependence of primary energy.* Applied Energy, 2017. **207**: p. 465-476.
34. *Key World Energy Statistics* 2018. DOI: https://doi.org/10.1007/978-81-322-3577-4.

35. Ringsmuth, A.K., M.J. Landsberg, and B. Hankamer, *Can photosynthesis enable a global transition from fossil fuels to solar fuels, to mitigate climate change and fuel-supply limitations?* Renewable and Sustainable Energy Reviews, 2016. **62**: p. 134-163.
36. *BP statistical review of world energy*. 2018, BP.
37. *Climate change 2014: impacts, adaptation and vulnerability*. 2014: Intergovernmental Panel on Climate Change.
38. Wood, N. and K. Roelich, *Tensions, capabilities, and justice in climate change mitigation of fossil fuels.* Energy Research & Social Science, 2019. **52**: p. 114-122.
39. Leonard, M.D., E.E. Michaelides, and D.N. Michaelides, *Energy storage needs for the substitution of fossil fuel power plants with renewables.* Renewable Energy, 2020. **145**: p. 951-962.
40. *BP Energy Outlook.* Tendernews.com, 2017.
41. Fivga, A., et al., *A review on the current state of the art for the production of advanced liquid biofuels.* AIMS Energy, 2019. **7**(1): p. 46-76.
42. World Energy, C., C. Conservation, and C. World Energy. *World energy resources, 1985-2020 : executive summaries of reports on resources, conservation and demand to the Conservation Commission of the World Energy Conference*. Guildford [England]; New York: Published for the WEC by IPC Science and Technology Press.
43. *Global Energy Transformation: A RoadMap to 2050*. 2018.
44. Thangavelu, S.K., A.S. Ahmed, and F.N. Ani, *Review on bioethanol as alternative fuel for spark ignition engines*, S.U.o.T.F.o. Engineering., Editor. 2016, Pergamon Press.
45. Kumar, S., et al., *Advances in diesel-alcohol blends and their effects on the performance and emissions of diesel engines.* Renewable and Sustainable Energy Reviews, 2013. **22**: p. 46-72.
46. García, V.n., et al., *Challenges in biobutanol production: How to improve the efficiency?* Renewable and Sustainable Energy Reviews, 2011. **15**(2): p. 964-980.
47. *Fenaroli's Handbook of Flavor Ingredients, Sixth Edition*. 2009; Available from: http://www.myilibrary.com?id=234423.
48. Ezeji, T.C., N. Qureshi, and H.P. Blaschek, *Bioproduction of butanol from biomass: from genes to bioreactors.* Current opinion in biotechnology, 2007. **18**(3): p. 220-7.
49. Aschenbrenner, E.M., C.K. Weiss, and K. Landfester, *Enzymatic Esterification in Aqueous Miniemulsions.* Chemistry - A European Journal, 2009. **15**(10): p. 2434-2444.
50. Pereira, G.N., et al., *Solvent-Free Production of Ethylene Glycol Monostearate through Enzymatic Esterification.* Industrial & Engineering Chemistry Research, 2018. **57**(19).
51. Intergovernmental Panel on Climate, C., et al. *Climate change 2014 : mitigation of climate change : Working Group III contribution to the Fifth assessment report of the Intergovernmental Panel on Climate Change*. 2015; Available from: http://dx.doi.org/10.1017/CBO9781107415416.
52. Cirujano, F.G., A. Corma, and F.X. Llabrés i Xamena, *Conversion of levulinic acid into chemicals: Synthesis of biomass derived levulinate esters over Zr-*

*containing MOFs.* Chemical Engineering Science, 2015. **124**(Supplement C): p. 52-60.
53. Cirujano, F.G., A. Corma, and F.X. Llabrés i Xamena, *Zirconium-containing metal organic frameworks as solid acid catalysts for the esterification of free fatty acids: Synthesis of biodiesel and other compounds of interest.* Catalysis Today, 2015. **257**(Part 2): p. 213-220.
54. Ngo, H.L., et al., *Mesoporous Silica-Supported Diarylammonium Catalysts for Esterification of Free Fatty Acids in Greases.* Journal of the American Oil Chemists' Society, 2010. **87**(4): p. 445-452.
55. Engin, A., H. Haluk, and K. Gurkan, *Production of lactic acid esters catalyzed by heteropoly acid supported over ion-exchange resins.* Green Chemistry, 2003. **5**(4): p. 460-466.
56. Mello, V.M., et al., *Metal oxides as heterogeneous catalysts for esterification of fatty acids obtained from soybean oil.* Fuel Processing Technology, 2011. **92**(1): p. 53-57.
57. Opanasenko, M., *Catalytic behavior of metal-organic frameworks and zeolites: Rationalization and comparative analysis.* Catalysis Today, 2015. **243**(C): p. 2-9.
58. Corma, A., *From microporous to mesoporous molecular sieve materials and their use in catalysis.* Chemical Reviews, 1997. **97**(6).
59. Chen, N.Y., W.E. Garwood, and F.G. Dwyer, *Shape selective catalysis in industrial applications*. 1989, New York: M. Dekker.
60. Eddaoudi, M., et al., *Modular chemistry: secondary building units as a basis for the design of highly porous and robust metal-organic carboxylate frameworks.* Accounts of chemical research, 2001. **34**(4): p. 319-30.
61. Dhakshinamoorthy, A., et al., *Metal Organic Frameworks as Solid Catalysts in Condensation Reactions of Carbonyl Groups.* ADSC Advanced Synthesis & Catalysis, 2013. **355**(2-3): p. 247-268.
62. Hoskins, B.F. and R. Robson, *Infinite polymeric frameworks consisting of three dimensionally linked rod-like segments.* Journal of the American Chemical Society, 1989. **111**(15): p. 5962-5964.
63. Furukawa, H., et al., *The Chemistry and Applications of Metal-Organic Frameworks.* Science, 2013. **341**(6149): p. 1230444-1230444.
64. Yaghi, O.M., G. Li, and H. Li, *Selective binding and removal of guests in a microporous metal–organic framework.* Nature, 1995. **378**(6558): p. 703-706.
65. Kondo, M., et al., *Three-Dimensional Framework with Channeling Cavities for Small Molecules: {[M2(4, 4'-bpy)3(NO3)4]·xH2O}n (M □ Co, Ni, Zn).* Angewandte Chemie International Edition in English, 1997. **36**(16): p. 1725-1727.
66. Chui, S.S., et al., *A chemically functionalizable nanoporous material.* Science, 1999. **283**(5405): p. 1148-50.
67. Farha, O.K., et al., *Metal-organic framework materials with ultrahigh surface areas: is the sky the limit?* Journal of the American Chemical Society, 2012. **134**(36): p. 15016-21.
68. Yuan, S., et al., *Stable Metal-Organic Frameworks with Group 4 Metals: Current Status and Trends.* ACS central science, 2018. **4**(4): p. 440-450.

69. Chughtai, A.H., et al., *Metalorganic frameworks: versatile heterogeneous catalysts for efficient catalytic organic transformations.* Chemical Society Reviews, 2015. **44**(19): p. 6804-6849.
70. Hu, Y.H. and L. Zhang, *Hydrogen Storage in Metal-Organic Frameworks.* ADMA Advanced Materials, 2010. **22**(20): p. E117-E130.
71. Barea, E., C. Montoro, and J.A.R. Navarro, *Toxic gas removal - metal-organic frameworks for the capture and degradation of toxic gases and vapours.* Chemical Society Reviews, 2014. **43**(16): p. 5419-5430.
72. Atallah, H., et al., *A highly stable indium based metal organic framework for efficient arsenic removal from water.* Dalton Transactions: An International Journal of Inorganic Chemistry, 2018. **47**(3): p. 799-806.
73. Della Rocca, J., D. Liu, and W. Lin, *Nanoscale metal-organic frameworks for biomedical imaging and drug delivery.* Accounts of chemical research, 2011. **44**(10): p. 957-68.
74. Mortada, B., et al., *Postmetalated Zirconium Metal Organic Frameworks as a Highly Potent Bactericide.* Inorg. Chem. Inorganic Chemistry, 2017. **56**(8): p. 4739-4744.
75. Kreno, L.E., et al., *Metal-Organic Framework Materials as Chemical Sensors.* Chemical Reviews, 2012. **112**(2): p. 1105-1125.
76. Valvekens, P., F. Vermoortele, and D. De Vos, *Metalorganic frameworks as catalysts: the role of metal active sites.* Catal. Sci. Technol. Catalysis Science & Technology, 2013. **3**(6): p. 1435.
77. Amrita Chatterjee, X.H., Frank Leung-Yuk Lam, *Towards a recyclable MOF catalyst for efficient production of furfural.* Catalysis Today, 2018. **314**: p. 129-136.
78. Jaluddin, S.N., K. Kassim, and W.N.W. Ibrahim, *Mixed Linker Metal Organic Framework as an Efficient and Reusable Catalyst for Suzuki Miyaura Coupling Reaction.* PROCHE Procedia Chemistry, 2015. **16**: p. 8-14.
79. Shearer, G.C., et al., *Defect Engineering: Tuning the Porosity and Composition of the Metal-Organic Framework UiO-66 via Modulated Synthesis.* Chemistry of Materials, 2016. **28**(11): p. 3749-3761.
80. Kleist, W., et al., *Mixed-Linker Metal-Organic Frameworks as Catalysts for the Synthesis of Propylene Carbonate from Propylene Oxide and $CO_2$.* European Journal of Inorganic Chemistry, 2009. **2009**(24): p. 3552-3561.
81. Deng, H., et al., *Multiple Functional Groups of Varying Ratios in Metal-Organic Frameworks.* Science, 2010. **327**(5967): p. 846-850.
82. Laboratory, S.N.A., *Large-Pore Apertures in a Series of Metal-Organic Frameworks.* Science 336: 1018-1023, 2012, 2014.
83. Fujita, M., et al., *Preparation, Clathration Ability, and Catalysis of a Two-Dimensional Square Network Material Composed of Cadmium(II) and 4,4'-Bipyridine.* Journal of the American Chemical Society, 1994. **116**(3): p. 1151-1152.
84. Zhu, L., et al., *Metal-Organic Frameworks for Heterogeneous Basic Catalysis.* Chemical reviews, 2017. **117**(12): p. 8129-8176.
85. Xu, C., et al., *Functional metal-organic frameworks for catalytic applications.* Coordination chemistry reviews, 2019. **388**: p. 268-292.

86. Schaate, A., et al., *Modulated Synthesis of Zr-Based Metal-Organic Frameworks: From Nano to Single Crystals.* CHEM Chemistry - A European Journal, 2011. **17**(24): p. 6643-6651.
87. Zahn, G., et al., *Insight into the mechanism of modulated syntheses: in situ synchrotron diffraction studies on the formation of Zr-fumarate MOF*. CrystEngComm, 2014. **16**(39).
88. Wißmann, G., et al., *Modulated synthesis of Zr-fumarate MOF.* Microporous and Mesoporous Materials, 2012. **152**: p. 64-70.
89. Vermoortele, F., et al., *Synthesis Modulation as a Tool To Increase the Catalytic Activity of Metal–Organic Frameworks: The Unique Case of UiO-66(Zr).* Journal of the American Chemical Society, 2013. **135**(31): p. 11465-11468.
90. Atzori, C., et al., *Effect of Benzoic Acid as a Modulator in the Structure of UiO-66: An Experimental and Computational Study.* Journal of Physical Chemistry C, 2017. **121**(17): p. 9312-9324.
91. Lee, J., et al., *Metal-organic framework materials as catalysts.* Chemical Society reviews, 2009. **38**(5): p. 1450-9.
92. Férey, G., *Hybrid porous solids: past, present, future.* Chemical Society Reviews, 2008. **37**(1): p. 191-214.
93. Cavka, J.H., et al., *A new zirconium inorganic building brick forming metal organic frameworks with exceptional stability.* Journal of the American Chemical Society, 2008. **130**(42): p. 13850-1.
94. DeCoste, J.B., et al., *Stability and degradation mechanisms of metal–organic frameworks containing the Zr6O4(OH)4 secondary building unit.* Journal of Materials Chemistry A, 2013. **1**(18): p. 5642.
95. Xi, W., et al., *Direct and post-synthesis incorporation of chiral metallosalen catalysts into metal-organic frameworks for asymmetric organic transformations.* Chemistry (Weinheim an der Bergstrasse, Germany), 2015. **21**(36): p. 12581-5.
96. Bakuru, V.R. and S.B. Kalidindi, *Synergistic Hydrogenation over Palladium through the Assembly of MIL-101(Fe) MOF over Palladium Nanocubes.* Chemistry - A European Journal, 2017. **23**(65): p. 16456-16459.
97. Dhakshinamoorthy, A., M. Alvaro, and H. Garcia, *Metal-organic frameworks as heterogeneous catalysts for oxidation reactions.* Catalysis Science and Technology, 2011. **1**(6): p. 856-867.
98. Guo, Q., et al., *A Chromium Hydroxide/MIL-101(Cr) MOF Composite Catalyst and Its Use for the Selective Isomerization of Glucose to Fructose.* Angewandte Chemie, 2018. **130**(18).
99. Hasan, Z., J.W. Jun, and S.H. Jhung, *Sulfonic acid-functionalized MIL-101(Cr): An efficient catalyst for esterification of oleic acid and vapor-phase dehydration of butanol.* Chemical Engineering Journal, 2015. **278**(Supplement C): p. 265-271.
100. Panchenko, Timofeeva, and Jhung, *Acid-base properties and catalytic activity of metal-organic frameworks: A view from spectroscopic and semiempirical methods.* Catalysis Reviews, 2016. **58**(2): p. 209-307.
101. Li, H., et al., *Establishing Microporosity in Open Metal−Organic Frameworks: Gas Sorption Isotherms for Zn(BDC) (BDC = 1,4-Benzenedicarboxylate).* Journal of the American Chemical Society, 1998. **120**(33): p. 8571-8572.

102. Canivet, J., M. Vandichel, and D. Farrusseng, *Origin of highly active metalorganic framework catalysts: defects? Defects!* DT Dalton Transactions, 2016. **45**(10): p. 4090-4099.
103. Yang, Q., et al., *A Water Stable Metal-Organic Framework with Optimal Features for CO2 Capture.* Angewandte Chemie International Edition, 2013. **52**(39): p. 10506–10510.
104. Zhou, et al., *Zirconium-containing UiO-66 as an efficient and reusable catalyst for transesterification of triglyceride with methanol.* JECHEM Journal of Energy Chemistry, 2016. **25**(5): p. 874-879.
105. Caratelli, C., et al., *Nature of active sites on UiO-66 and beneficial influence of water in the catalysis of Fischer esterification.* Journal of Catalysis, 2017. **352**: p. 401-414.
106. Ren, J., et al., *Structural defects in metal-organic frameworks (MOFs): Formation, detection and control towards practices of interests.* CCR Coordination Chemistry Reviews, 2017. **349**: p. 169-197.
107. Trickett, C.A., et al., *Definitive molecular level characterization of defects in UiO-66 crystals.* Angewandte Chemie (International ed. in English), 2015. **54**(38): p. 11162-7.
108. Taddei, M., *When defects turn into virtues: The curious case of zirconium-based metal-organic frameworks.* CCR Coordination Chemistry Reviews, 2017. **343**: p. 1-24.
109. Wu, H., et al., *Unusual and highly tunable missing-linker defects in zirconium metal-organic framework UiO-66 and their important effects on gas adsorption.* Journal of the American Chemical Society, 2013. **135**(28): p. 10525-32.
110. Chaemchuen, S., et al., *Defect formation in metal-organic frameworks initiated by the crystal growth-rate and effect on catalytic performance.* YJCAT Journal of Catalysis, 2017. **354**: p. 84-91.
111. Shearer, G.C., et al., *Tuned to Perfection: Ironing Out the Defects in MetalOrganic Framework UiO-66.* Chem. Mater. Chemistry of Materials, 2014. **26**(14): p. 4068-4071.
112. Nouar, F., et al., *Tuning the properties of the UiO-66 metal organic framework by Ce substitution.* Chemical communications (Cambridge, England), 2015. **51**(77): p. 14458-61.
113. Wei, R., et al., *Tuning the properties of Zr6O8 nodes in the metal organic framework UiO-66 by selection of node-bound ligands and linkers.* Chem. Mater. Chemistry of Materials, 2019.
114. Chen, S., et al., *Hydrogen storage properties of the novel crosslinked UiO-66-(OH)2.* HE International Journal of Hydrogen Energy, 2018. **43**(32): p. 15370-15377.
115. Issa, R., et al., *Controlled growth and composition of multivariate metal-organic frameworks-199 via a reaction-diffusion process.* Nano Research, 2020.
116. Burrows, A.D., *Mixed-component metal–organic frameworks (MC-MOFs): enhancing functionality through solid solution formation and surface modifications.* CrystEngComm, 2011. **13**(11): p. 3623.
117. Burrows, A.D., et al., *Post-Synthetic Modification of Tagged Metal-Organic Frameworks.* Angewandte Chemie International Edition, 2008. **47**(44): p. 8482-8486.

118. Taddei, M., et al., *Mixed-linker UiO-66: structure-property relationships revealed by a combination of high-resolution powder X-ray diffraction and density functional theory calculations.* Physical chemistry chemical physics : PCCP, 2017. **19**(2): p. 1551-1559.
119. Kim, M., et al., *Postsynthetic modification at orthogonal reactive sites on mixed, bifunctional metal-organic frameworks.* Chemical communications (Cambridge, England), 2011. **47**(27): p. 7629-31.
120. Bunck, D.N. and W.R. Dichtel, *Mixed Linker Strategies for Organic Framework Functionalization.* Chemistry - A European Journal, 2013. **19**(3): p. 818-827.
121. Jrad, A., et al., *Structural engineering of Zr-based metal-organic framework catalysts for optimized biofuel additives production.* Chemical Engineering Journal, 2020. **382**: p. 122793.
122. Milina, M., S. Mitchell, and J. Pérez-Ramírez, *Prospectives for bio-oil upgrading via esterification over zeolite catalysts.* Catalysis Today, 2014. **235**(Supplement C): p. 176-183.
123. Long, J., et al., *Amine-functionalized zirconium metal-organic framework as efficient visible-light photocatalyst for aerobic organic transformations.* Chemical communications (Cambridge, England), 2012. **48**(95): p. 11656-8.
124. Han, X. and L. Zhou, *Optimization of process variables in the synthesis of butyl butyrate using acid ionic liquid as catalyst.* Chemical Engineering Journal, 2011. **172**(1): p. 459-466.
125. Ju, I.B., et al., *Kinetic study of catalytic esterification of butyric acid and n-butanol over Dowex 50Wx8-400.* CEJ Chemical Engineering Journal, 2011. **168**(1): p. 293-302.
126. Valenzano, L., et al., *Disclosing the complex structure of UiO-66 metal organic framework: A synergic combination of experiment and theory.* Chem. Mater. Chemistry of Materials, 2011. **23**(7): p. 1700-1718.
127. Shearer, G.C., et al., *In Situ Infrared Spectroscopic and Gravimetric Characterisation of the Solvent Removal and Dehydroxylation of the Metal Organic Frameworks UiO-66 and UiO-67.* Top Catal Topics in Catalysis, 2013. **56**(9-10): p. 770-782.
128. Molavi, H., et al., *Enhancing CO2/N2 adsorption selectivity via post-synthetic modification of NH2-UiO-66(Zr).* Microporous and Mesoporous Materials, 2018. **257**: p. 193-201.
129. Luan, Y., et al., *Synthesis of a flower-like Zr-based metalorganic framework and study of its catalytic performance in the Mannich reaction.* RSC Adv. RSC Adv., 2015. **5**(25): p. 19273-19278.
130. Van De Voorde, B., et al., *Improving the mechanical stability of zirconium-based metal-organic frameworks by incorporation of acidic modulators.* J. Mater. Chem. A Journal of Materials Chemistry A, 2015. **3**(4): p. 1737-1742.
131. Zuoxiang, Z., et al., *Recent Developments on the Mechanism and Kinetics of Esterification Reaction Promoted by Various Catalysts*. 2012: INTECH Open Access Publisher.
132. Zeng, Z., et al., *Recent Developments on the Mechanism and Kinetics of Esterification Reaction Promoted by Various Catalysts.* 2012.
133. Fogler, H.S., *Elements of chemical reaction engineering*. 2006, Prentice Hall PTR: Upper Saddle River, NJ.

134. Dhakshinamoorthy, A., et al., *Intracrystalline diffusion in Metal Organic Framework during heterogeneous catalysis: Influence of particle size on the activity of MIL-100 (Fe) for oxidation reactions.* Dalton Trans. Dalton Transactions, 2011. **40**(40): p. 10719-10724.
135. Katz, M.J., et al., *A facile synthesis of UiO-66, UiO-67 and their derivatives.* Chemical communications (Cambridge, England), 2013. **49**(82): p. 9449-51.
136. Biswas, S., et al., *Enhanced selectivity of CO2 over CH4 in sulphonate-, carboxylate- and iodo-functionalized UiO-66 frameworks.* Dalton Trans. Dalton Transactions, 2013. **42**(13): p. 4730-4737.
137. Orellana-Tavra, C., et al., *Amorphous metal-organic frameworks for drug delivery.* Chemical communications (Cambridge, England), 2015. **51**(73): p. 13878-81.
138. Bennett, T.D. and A.K. Cheetham, *Amorphous metal-organic frameworks.* Accounts of chemical research, 2014. **47**(5): p. 1555-62.
139. Han, Y., et al., *Facile synthesis of morphology and size-controlled zirconium metalorganic framework UiO-66: the role of hydrofluoric acid in crystallization.* CrystEngComm, 2015. **17**(33).
140. Chen, Z., et al., *Scalable, room temperature, and water-based synthesis of functionalized zirconium-based metal–organic frameworks for toxic chemical removal.* CrystEngComm, 2019. **21**(14).
141. Das, A., et al., *A dual functional MOF-based fluorescent sensor for intracellular phosphate and extracellular 4-nitrobenzaldehyde.* Dalton Transactions: An International Journal of Inorganic Chemistry, 2019. **48**(4).
142. Díaz-García, M., et al., *Nanoscaled M-MOF-74 Materials Prepared at Room Temperature.* Crystal Growth & Design Crystal Growth & Design, 2014. **14**(5): p. 2479-2487.
143. Jrad, A., et al., *Tuning acidity in zirconium-based metal organic frameworks catalysts for enhanced production of butyl butyrate.* APCATA Applied Catalysis A, General, 2019. **570**: p. 31-41.
144. Zhigang, H., et al., *Modulator Effects on the Water-Based Synthesis of Zr/Hf Metal-Organic Frameworks: Quantitative Relationship Studies between Modulator, Synthetic Condition, and Performance.* Crystal Growth & Design, 2016. **16**(4).
145. Marx, S., et al., *Tuning functional sites and thermal stability of mixed-linker MOFs based on MIL-53(Al).* Dalton Transactions, 2010. **39**(16): p. 3795-3798.
146. Taddei, M., et al., *Mixed-linker UiO-66: structure–property relationships revealed by a combination of high-resolution powder X-ray diffraction and density functional theory calculations.* Physical Chemistry Chemical Physics, 2017. **19**(2): p. 1551-1559.
147. Yan, X. and X.G. Su, *Linear Regression Analysis: Theory and Computing*. 2009: World Scientific Publishing Co., Inc.
148. Trinh, H., S. Yusup, and Y. Uemura, *Optimization and kinetic study of ultrasonic assisted esterification process from rubber seed oil.* Bioresource Technology, 2018. **247**(Supplement C): p. 51-57.
149. *Kinetics of Modified Zirconia-catalyzed Heterogeneous Esterification Reaction for Biodiesel Production*. 2010; Available from: http://docsdrive.com/pdfs/ansinet/jas/2010/2584-2589.pdf.